TU Delft

Exploring the limits of traditional L-flange connection v/s C1 wedge connection

Pratyaksh Gupta

MSc Thesis

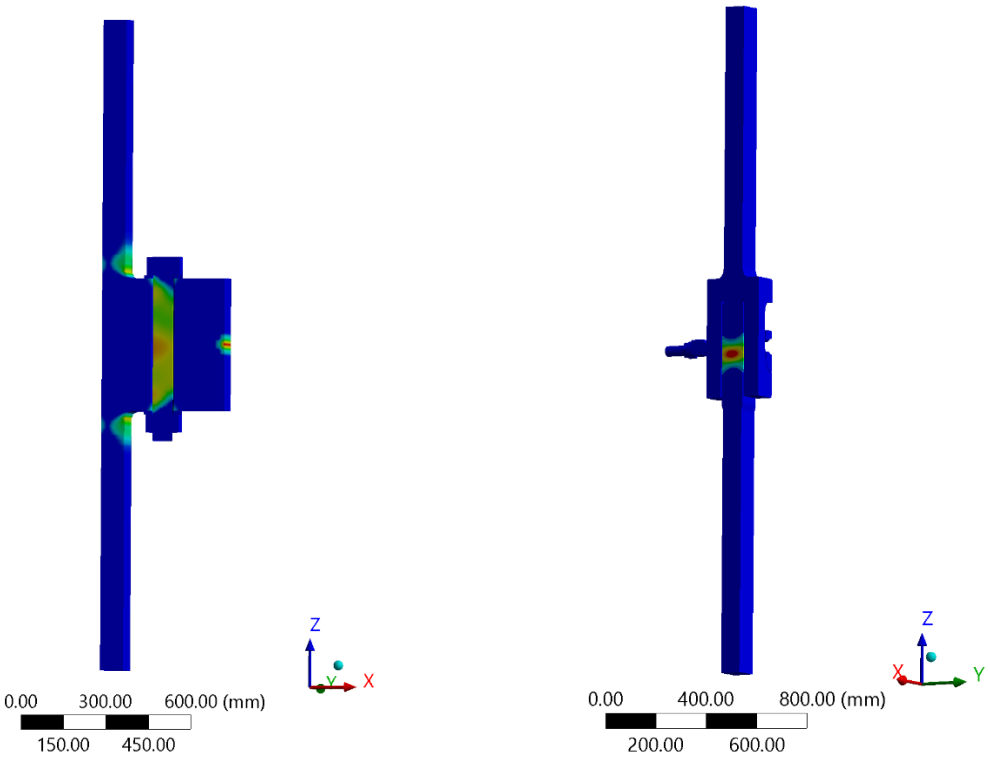

Exploring the limits of traditional L-flange connection v/s C1 wedge connection

by

Pratyaksh Gupta

In partial fulfilment of the requirement for the degree of

Master of Science

In Civil Engineering

at the Delft University of Technology,

to be defended publicly on Thursday September 28,2023 at 16:00

Faculty:	Civil Engineering and Geosciences	
Degree:	MSc. Civil Engineering	
Track:	Structural Enginnering	
Student number:	5040795	
Project Duration:	November 23rd, 2022 – September 28th, 2023	
Thesis Committee:	Prof.dr. M. (Milan) Veljkovic,	TU Delft (Chair)
	Ir. H. (Hagar) El Bamby,	TU Delft
	Dr. Peter Meijers,	TU Delft
	Ir. Koen Creusen,	C1 connections
	Ir. Jasper Winkes,	C1 connections

TU Delft

C1 CONNECTIONS

Preface

This thesis is the final chapter of my journey at Faculty of Civil Engineering and Geosciences, TU Delft. A lot was learnt while pursuing masters programme in civil engineering and I am incredibily grateful for that. The journey was full of endeavours, excitement and fallbacks. But at the end, everything worked out for the best.

I am incredibaly grateful to Prof. Milan whose umpteen guidance and critical questions helped me refine and develop the thesis. Hagar, my daily supervisor at TU Delft, who was always available at the click of moment for the silliest doubts and the assurance she provided was highly motivating. I would like to thank Peter, who stood by the project at all times and provided critical observations. Moreover, I would like to thank everyone at C1 connections.

I would like to express my sincere gratitude to Jasper, who believed in me to carry the project. His ideas and expertise was greatly contributed to the development of the thesis. I would also like to thank Koen and George, who helped me throughtout the thesis and made sure I was moving ahead in the right direction.

I would like to thank all the teachers and Professors for their knowledge with which I will call myself a structural engineer. It was them which made the field of structural engineering fascinating and interesting for me.

I would also thank my friends here in Delft and back in India, who providied constant support and encouragement. Thanks for bearing with me in my difficult times. Your frienship means a lot to me.

To Mumma, I wish you were here with us. The great memories with you have kept me going ahead and I hope you keep on guiding me from wherever you are. To Papa, Jee, Nishtha di and Trapti, I am grateful for the unconditional love and support I have received throughout the life from you all. I want to thank my nephews Shray, Shrut and Arin who have brighten our lives with joy and happiness. Words cannot describe what you all mean to me. I hope I have the same love and support for the future endeavours.

Abstract

The increase in demand for renewable energy has resulted in higher demand for wind energy. To meet this requirement, the wind turbine sizes are increasing rapidly, and this results in increasing load on the connections between MP-TP and the segments of the tower.

This research focuses on traditional L-flange connection and novel C1 wedge connection, former the most widely used in the offshore industry and other being new to the offshore industry. The objective of this thesis is to evaluate the limits of the L-flange and C1 wedge connection. The design of the L-flange connection carried out on the basis of Petersen's theory[1]. It is designed to have higher ULS resistance with steel mass as low as possible. This analytical designed is then compared to finite element analysis (FEA). Previous study of Cheng[2] is used to validate the setup and methodology for FEM in Ansys.

For the same overturning moment, C1 wedge connection is designed using the design tool provided by C1 Connections. The design check for flanges is carried out. The design is then compared to finite element analysis (FEA). Fatigue limit state was verified for both the connections.

Based on the study, the following conclusions are made. Firstly, L-flange connection has around 30% higher ULS resistance compared to design overturning moment of 609MNm whereas C1 wedge connection has 55% higher ULS resistance. Secondly, L-flange connection has higher meridional deformation at the same elevation in the shell as compared to C1 wedge connection. The gap opening at the interface of the flanges is studied and it is observed that C1 wedge connection opens after the loss of contact force at the interface which is generated more efficiently through the pretension of stud whereas L-flange connection being an eccentric connection starts opening without full loss of contact force at the interface and the secondary path of load transfer is activated. This results in the lower meridional rigidity provided by the L-flange connection as compared to the C1 wedge connection. Lastly, C1 wedge connection provided an opportunity for several optimizations to have the same ULS resistance as that of L-flange connection. The mass of steel reduced for these optimizations. The L-flange connection weighed 53.72 tonnes for both ULS and FLS criterion whereas C1 wedge connection weights 20.8 tonnes for ULS criterion and 28.8 tonnes for FLS criterion.

Table of Contents

List of figures

List of tables

1 Introduction

1.1 Background

In recent decades, there has been a heightened consciousness regarding climate change, the limitations of fossil fuels, and the imperative for transitioning to renewable energy sources. Among these sources, wind energy, categorized as a second-generation renewable technology, has served various purposes throughout history, including milling grain and water pumping. Since the late 19th century, it has also been utilized to generate electricity. Initially, the focus was primarily on onshore wind farms for approximately a century. However, technological progress over the past few decades has propelled the development of offshore wind energy, unlocking its increasing potential and driving substantial growth in production.

The escalating potential of offshore wind power has garnered substantial attention and unprecedented investments in offshore wind projects in recent times. A staggering €26 billion has been allocated for the establishment of novel offshore wind farms in Europe, aimed at financing the creation of 7.1GW of fresh offshore power capacity[3]. This surge in investment underscores the growing demand for higher capacity and more efficient offshore wind turbines (OWTs). Simultaneously, there is an observable necessity to augment the dimensions of the supportive frameworks for the next generation of OWTs.

Supportive structures for OWTs commonly consist of tubular towers and substructures. To facilitate transportation, the tubular towers are segmented into shorter units. The interconnections between these adjoining segments play a pivotal role in ensuring the robustness and stability of OWT structures.

The integral components of an offshore wind turbine consist of the tower, transition piece (TP), and foundation. The tower structure, shared with most onshore wind turbines featuring a steel tower, incorporates bolted ring-flange connections to link various tower segments. An exclusive feature of offshore wind turbines is the presence of the TP and foundation, serving as a link between the tower's lower end positioned several meters above the highest attainable sea-water level and the seabed as shown in Figure 1.1. Collectively, the TP and foundation are denoted as the substructure of the offshore wind turbine.

While multiple substructure designs are available, the prevailing options in the market are monopile and jackets, accounting for 81.9% and 6.6% of the installed capacity in 2018, respectively[4]. In both jacket and monopile substructures, the bolted ring-flange connection remains the prevalent means of linking the tower and substructure. For monopile substructures, the connection between transition piece and monopile was executed using grouted connection but the increasing capacity of growing wind turbines have led to innovative connections such as C1 wedge connection.

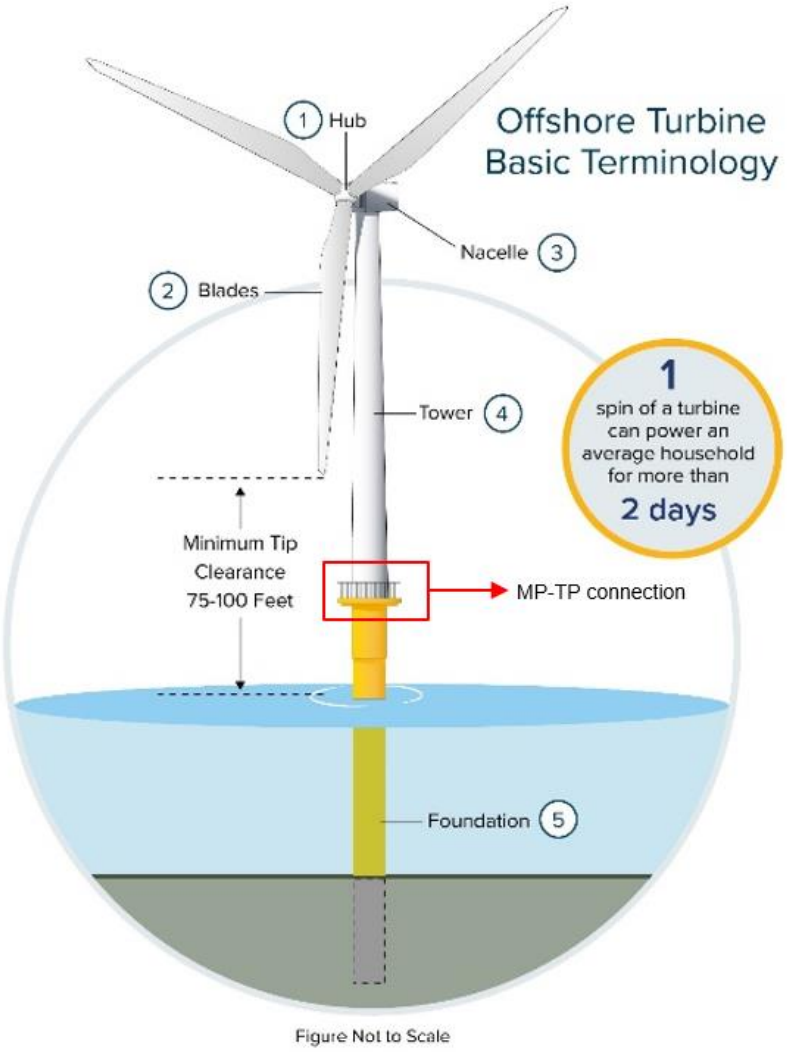

Figure 1.1: Offshore turbine terminology

1.1.1 Traditional ring flange connection

Steel tubular towers for wind turbines are fabricated in three-four different sections due to limitations of transport. These sections are mostly connection using ring flange connection techniques. For both monopile (MP) and transition piece (TP) and tower segments, bolted ring flange connection is the most widely used connection type[5]. Figure 1.2 represents the locations for MP-TP and towers segments that are connected using ring flange connections. This connection consists of two L shaped flanges machined from the forged ring and connected using preloaded bolts.

The performance of ring flange connections is impacted by several factors, including the rigidity of the ring flanges, imperfections in fabrication or execution, the methodology and arrangement of welding in the ring flange/segment junction, the type of bolts and their preloading method, and the management of achieved bolt preloading force.

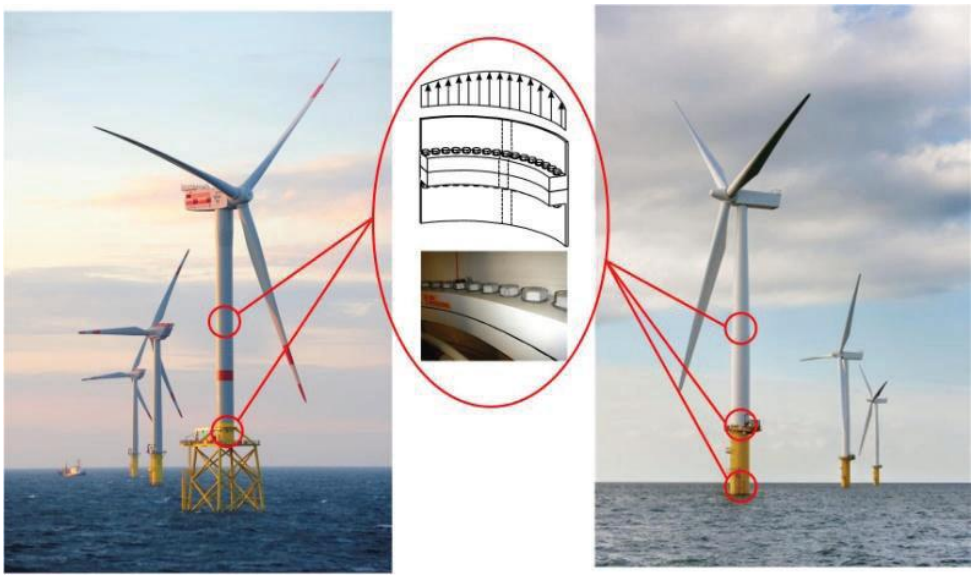

Figure 1.2: Locations for bolted ring-flange connections foo offshore wind towers[6]

1.1.2 C1 wedge connection

The escalating forces exerted on the connections of offshore towers supporting wind turbines have introduced complexities in designing the traditional bolted L-flange connections. Moreover, the substantial weight of components and equipment has added challenges to installation from a safety standpoint. A solution in this context is the symmetrical C1 Wedge Connection[7], designed for tubular sections. This connection comprises a cylindrical lower flange and an upper flange with a fork-like shape that slides over the lower flange. Radially elongated holes are present along the perimeters of both flanges, enabling C1 fasteners to draw them together. The fastener assembly utilizes a small horizontally positioned bolt to bring two wedges into contact. These wedges then amplify the force from the horizontal bolt, generating greater preload between the flanges by pulling them together. The arrangement of the bolt in the fastener minimizes significant load fluctuations due to external forces.

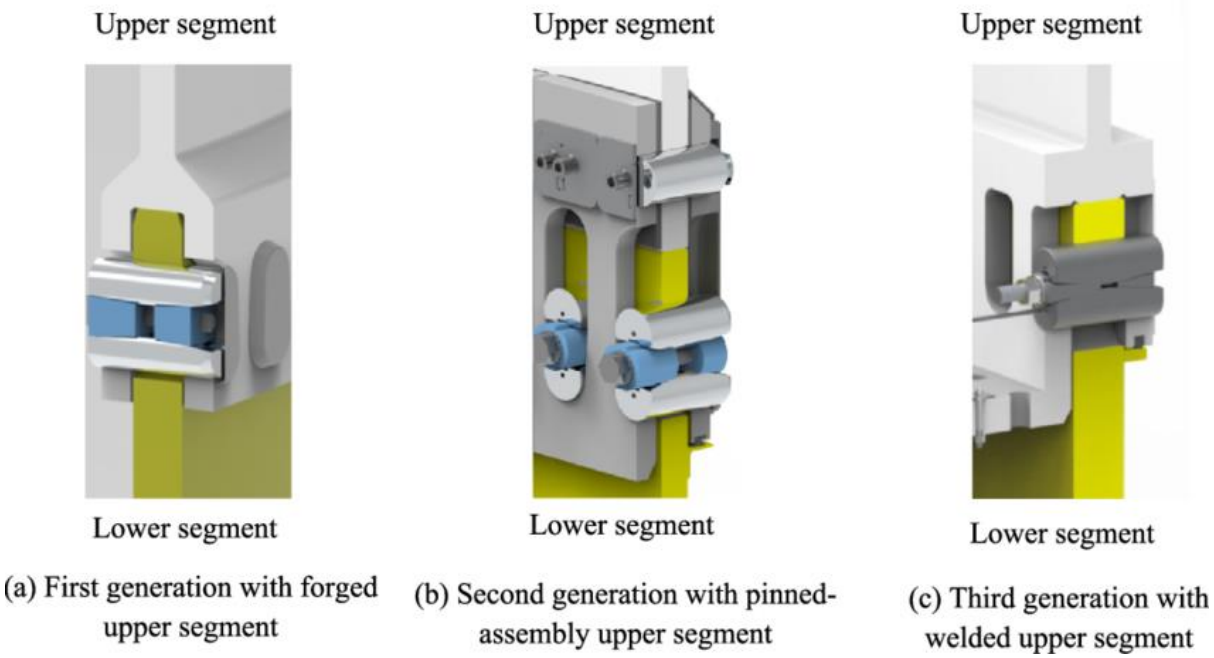

Figure 1.3: Representation of three generations of C1 wedge connection[8]

Unlike the bolted L-flange, the C1 Wedge Connection demonstrates higher resilience against preload loss[7]. This quality eliminates the necessity for regular maintenance and inspections. The adaptability of the C1 Wedge Connection renders it suitable for higher loads, which becomes increasingly relevant with the growing dimensions of wind turbines. Particularly, it proves advantageous in demanding settings such as hurricane and seismic-prone areas, or locations exposed to substantial dynamic loads arising from extreme wave conditions or floating foundations[7].

1.2 Problem definition

Current generation of wind turbines have capacity of 9.5MW to 11.0MW and the rotor diameter in range of 164m to 200m[9]. For the same, the shell diameter required for the tubular towers is around 6500mm. With next generation turbines, it is expected to capacity of about 14MW with 236m of diameter of rotor and 8000mm of diameter of shells[9]. This would increase the overturning moment on the tubular tower, therefore, the diameter of the shell would increase as well and in turn the connection has to scaled accordingly. These increasing dimensions generate a problem that must be overcome for the design of a safe and reliable OWT's.

One of the challenges here arises is the connection between TP-MP and the connection of tower segments. With increased wind turbines, connections are loaded with higher loads. The limitation of number of bolts and the maximum size of the bolts that could be placed on the circumference of the complete ring arises due to adequate spacing required for torquing tool. This in turn limit the capacity of the ring flange connection. Health and safety issues also start to arise as with M72 bolt already peaking to the allowable lifting weights, the torque tools required to tension these bolts are at par with the allowable limits[10].

Also, ring flange connection is an asymmetric connection which has the eccentricity for the bolt forces. This reduces the Ultimate limit state capacity of the connection. With increasing dimensions for the ring flange connection, the increase in steel used increases and it impacts the cost of the wind energy.

The design of wind turbine tubular towers is primarily dependent on the fatigue life of the bolted connection[11]. For higher bolt dimensions, a reduction factor is taken into consideration which ultimately reduces the fatigue life of the connection significantly[12, 13]. With rapidly increasing wind turbines capacity, current generation of OWT's requires ring flange connection with thicker flanges and higher bolt diameter which is a major problem to be dealt with.

Following the above problem defined with traditional flange connections, a novel C1 wedge connection was developed in 2017[14]. The design has undergone several modifications since then and at present third generation of C1 wedge connection is in place. Unlike traditional L-flange connection, C1 wedge connection is a symmetric connection which can be installed from one side of the connection[7].

As the traditional ring flange connection is believed to peak its limits with the upcoming next generations of wind turbines, the C1 wedge connection is promising connection for the TP-MP and tower segments. Therefore, it is necessary to evaluate the limits of both the connections with same tower dimensions and loading capacity.

1.3 Research objective

Problems discussed above with the traditional ring flange connection makes it necessary to test the limits of the connection and make a comparison with the C1 wedge connection. The objective of this thesis is to make a clear comparison between the two types of connections, namely traditional ring flange connection and C1 wedge connection. This will be done by answering the following main research question:

"How do the higher overturning moment influence the design of the traditional L-flange connection vs the C1 wedge connection?"

This research question will be answered by splitting the problem in two parts. One part focusses on the ULS limit of the connections. An analytical and numerical study will be done to design the traditional ring flange connection and C1 wedge connection for the ULS overturning moment. This study will be able to answer the following sub-questions:

"What are the ULS capacity for the connections?"

"How can be the C1 wedge connection be optimized to get the same ULS capacity as that of ring flange connection?"

The second component of this research would focus on the FLS criteria of the connections. Fatigue damage is calculated for the critical locations of both the connections and following questions could be answered at the end of the study:

"What are the FLS capacity of the connections?"

"Is FLS or ULS governing criteria for traditional ring flange connection?"

"Is FLS or ULS governing criteria for the C1 wedge connection?"

1.4 Thesis outline

In this thesis, symmetric ring flange connection, without presence of imperfections are considered. It is defined as symmetric ring flange connection as it can be translated to a single segment and the symmetry boundary conditions can be applied for the continuity of the segment in full ring flange connection. The ring flange connection is translated to a segment loaded with tension load. Torsion moment and self-weight of the components are not considered. Assumptions are made with diameter of shells of the tower and the bolt size used. Analytical study is performed to finalize the preliminary design of the L-flange connection based on the ULS capacity of the segment and the weight of the components(flanges) required (Chapter 3).

After the design is finalized, numerical study is performed in Ansys workbench and mechanical to evaluate the ULS capacity of the connection(Chapter 5). For the same design load that the L-flange connection is designed for, the C1 wedge connection is designed(Chapter 7), and numerical study is performed evaluate the ULS capacity(Chapter 8).

Furthermore, Optimization of C1 wedge connection is carried out to ensure that the webs and the flange of the C1 wedge connection have the same ULS capacity(Chapter 9). This ensures the savings in cost without compromise in the ULS capacity. Second optimization is performed to design the C1 wedge connection as of ULS capacity of L-flange connection to make a better comparison between two connections.

At last, FLS verifications are performed for both the connections and the governing criteria is indicated. FLS calculations are performed using Markov matrix theory(Chapter 10).

2 Literature review

In this chapter, relevant information for this research is discussed. The state of the art for bolted ring flange connections represents the relevant procedure to design a L-flange segment for the ultimate limit state. Further, the methodology to design the novel C1 wedge connection for ultimate limit state is discussed. Fatigue limit state is discussed for the connections which are verified for the ultimate limit state(ULS).

2.1 L-flange connection

Currently, tubular sections of OWT's are connected using bolted ring flange connections mostly[15]. For the design purpose, it is assumed that the resistance of the ring connection which is subjected in overturning moment can be translated to the single bolt segment[16]. The segment width c is equivalent to the arc length between two bolt holes. Layout of the ring flange connection is shown in Figure 2.1.

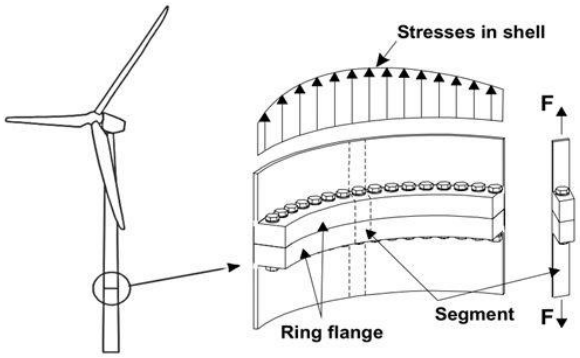

Figure 2.1: Ring flange connection in OWT's[17]

The Ultimate limit state (ULS) is the capacity of the connection at failure. For a safe and reliable OWT's, it is vital to ensure that the connections have resistance against ULS failure mechanism. Peterson[1] developed three failure mechanisms which are of importance for L-flange connection, namely failure mode A, B and C. Figure 2.2 represents failure modes of L-flange connection according to Petersen. Later, Seidel[16], proposed a theory to replace failure mode C with failure modes D and E. Figure 2.3 represents Seidel's theory for failure mode C. He proposed that location of yielding for failure mode C can occur in the flange at the centre of bolt hole or in the flange at the centre of washer thickness. These mechanisms can be defined as:

A: Failure of the bolt

B: Failure of the bolt and plastic hinge in the shell

C: Plastic hinge in the flange and shell, according to Seidel, it can be separated into two mechanisms:

- D: Plastic hinge in the flange at bolt hole centre and shell
- E: Plastic hinge in flange at mid washer and shell

Tobinaga and Ishihara[18] studied the L-flange segment behaviour with different a/b ratios and came to conclusion: if flanges have ratio for a/b higher than 1.25, the location of the equivalent reaction force point moves outward from the inner edge of the flange by elastic deformation when the bolt reaches its ultimate capacity. This implies that further bolt lengthening is required to develop full plastic resistance, in which the reaction force acts at the

inner edge of the flange and the plastic hinge in the tower all has developed. For this reason, the ratio a/b for this research is limited to 1.25[19].

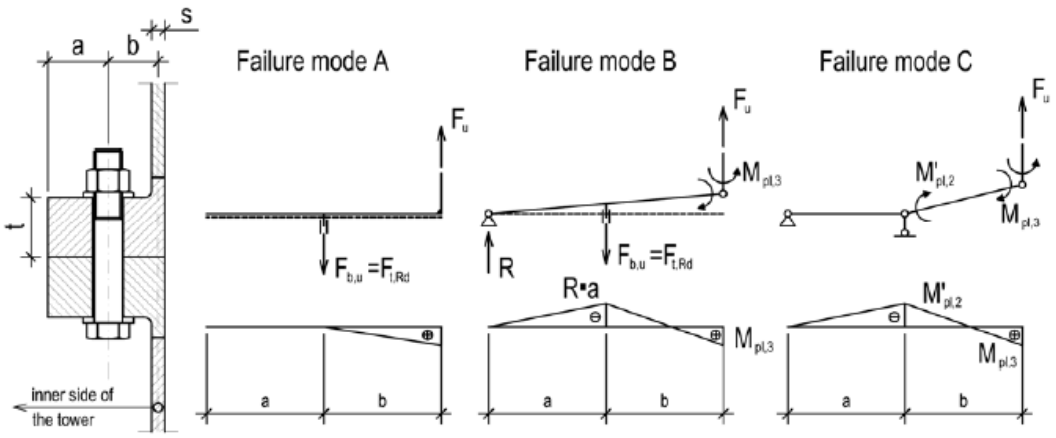

Figure 2.2: Petersen's failure mechanisms for ring flange connection[1]

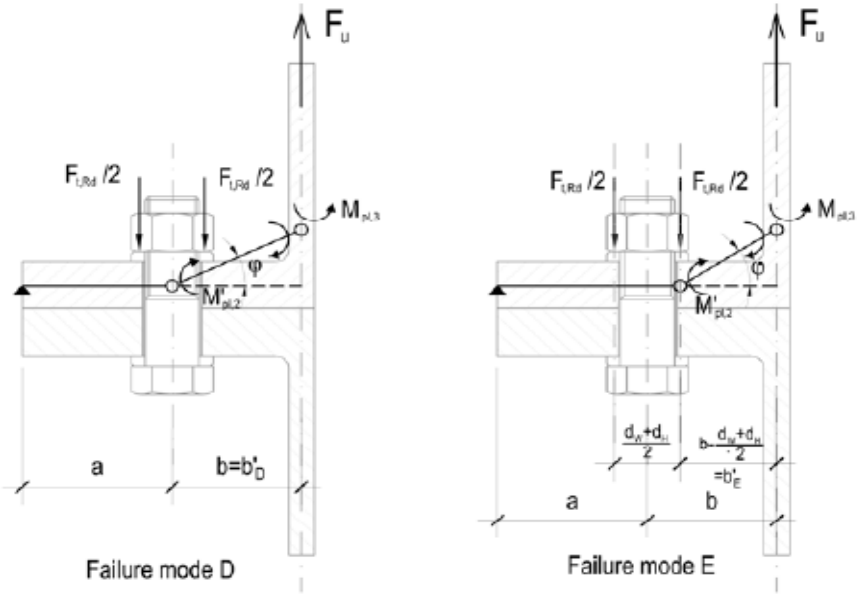

Figure 2.3: Seidel's refined mechanisms in place for failure mode C[16]

2.1.1 Failure modes

- Failure mode A: It is the failure of the bolt. When the bolt force is reaches the tension resistance of the bolt, the fracture in the bolt occurs. The tensile resistance of the bolt $F_{t,Rd}$ [20] is the ultimate resistance for failure mode A and it is obtained as:

$$F_{u,A} = F_{t,Rd} = \frac{0.9 f_{ub} A_s}{\gamma_{M2}}$$

- Failure mode B: This is the combination of fracture of the bolt and plastic hinge development in the flange to shell interface. The ultimate resistance of the connection for failure mode B can be calculated as:

$$F_{u,B} = \frac{(F_{t,Rd} * a + M_{pl,3})}{a + b}$$

Distances a is the distance from free end of the flange to the bolt axis and distance b is the distance from bolt axis to centre of the shell. This is represented in Figure 2.2. The bending moment in the shell $M_{pl,3}$ is the bending resistance considering the M-N and M-V interaction of the segment.

$$M_{pl,3} = \min\{M_{pl,N,sh}, M_{pl,V,fl}\}$$

Where

$$M_{pl,N,sh} = \left[1 - \left(\frac{N}{N_{pl,sh}}\right)^2\right] * M_{pl,sh} = \left[1 - \left(\frac{F_u}{C_w * s * f_{y,sh}}\right)^2\right] * \frac{C_w * s^2}{4} * f_{y,sh}$$

$$M_{pl,V,fl} = \left[\sqrt{1 - \left(\frac{V}{V_{pl,fl}}\right)^2}\right] * M_{pl,fl} = \left[1 - \left(\frac{F_u}{c * t * f_{y,fl}/\sqrt{3}}\right)^2\right] * \frac{c * t^2}{4} * f_{y,fl}$$

- Failure mode C: It is the formation of plastic hinge in the flange at the bolt axis and plastic hinge in the flange to shell junction. The mechanism can be calculated as:

$$F_{u,C} = \frac{M'_{pl,2} + M_{pl,3}}{b}$$

Where

$$M'_{pl,2} = \frac{c' * t^2}{4} * f_y$$

- Failure mode D: This failure is one of the two sub mechanisms proposed by Seidel[16]. In this failure mode, formation of plastic hinge in the flange at the bolt axis and flange to shell interface. The resistance for failure mode D can be calculated as:

$$F_{u,D} = \frac{M'_{pl,2} + \Delta M_{pl,2} + M_{pl,3}}{b'_D}$$

Where:

$$\Delta M_{pl,2} = \frac{F_{t,Rd}}{2} * \frac{d_W + d_B}{4}$$

For failure mode D to be considered, the following conditions must be satisfied:

$$\left(\frac{F_{t,Rd}}{2} - F_{u,D}\right) * \left(\frac{d_W + d_B}{4}\right) \leq M_{pl,2} - M'_{pl,2}$$

$$r = \frac{M'_{pl,2} + \Delta M_{pl,2}}{F_{t,Rd} - F_u} \leq a$$

- Failure mode E: The last failure mode is the second sub mechanism developed by Seidel. This failure mode observes formation of plastic hinge at mid washer axis and flange to shell junction. The resistance can be calculated as:

$$F_{u,E} = \frac{M_{pl,2} + M_{pl,3}}{b'_E}$$

Where

$$M_{pl,2} = \frac{c * t^2}{4} * f_y$$

For failure mode E to be considered, the following conditions must be satisfied:

$$\left(\frac{F_{t,Rd}}{2} - F_{u,E}\right) * \left(\frac{d_W + d_B}{4}\right) \geq M_{pl,2} - M'_{pl,2}$$

$$r = \frac{M'_{pl,2} + 2 * \Delta M_{pl,2}}{F_{t,Rd} - F_u} - \frac{d_W + d_B}{4} \leq a$$

2.2 C1 wedge connection

The C1 wedge connection was designed and proposed for tubular structures but can be used for other types of structures as well[7]. The main geometry consists of three main components namely upper flange with fork like cross-section, lower flange and C1 fastener as shown in Figure 2.4. The flanges have elongated holes designed particularly to predefine the contacts.

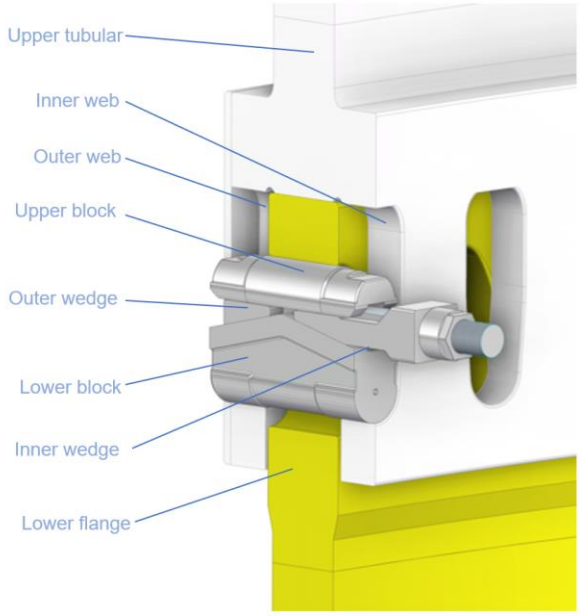

Figure 2.4: Components of the C1 wedge connection[7]

2.2.1 Components of C1 wedge connection

- Upper flanges
  The upper flange takes the form of a ring that exhibits a cross-section resembling a fork, as depicted in Figure 2.5. The vertical components of this fork-shaped structure are referred to as webs, and their mechanical behaviour closely resembles that of the web found in an I-beam design[7]. Perpendicular holes are machined within these webs, designed to accommodate the C1 fastener. These holes possess a curvature at their base that mirrors the radius of the C1 fastener. Notably, these holes are machines in a manner that ensures a direct line of sight to the interface connecting the upper and lower flanges. In terms of dimensions, the width of these holes exceeds the diameter of the C1 fastener. This sizing choice serves to permit a certain degree of tilting movement for the C1 fastener, particularly in the event of minor tangential misalignment scenarios.

- Lower flange

The lower flange is constructed as a tubular steel element featuring elongated holes arranged radially. At the top position of holes, they share the same radius as the C1 fastener's radius. Notably, the width of these holes is more than the diameter of the C1 fastener. This particular dimensioning choice has been made to enable the potential tilting movement of the C1 fastener, particularly when faced with slight tangential misalignment scenarios[7].

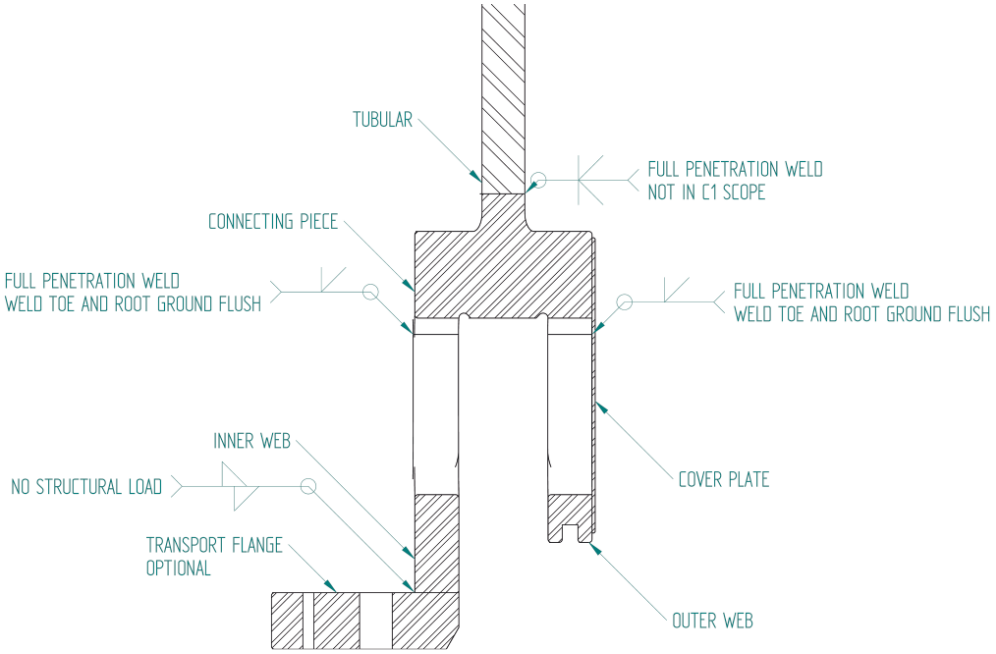

Figure 2.5 : Cross-section of welded upper flange[7]

- C1 fastener
  The C1 fastener is comprised of five primary steel elements: an upper block, a lower block, an inner wedge, an outer wedge, and a bolt (or a stud and nut combination), as illustrated in Figure 2.6. The lower block is positioned within the hole of the upper flange, and upon installation, the upper block comes into contact with the hole of the lower flange. The wedges are inserted between these blocks and are linked together using the bolt.

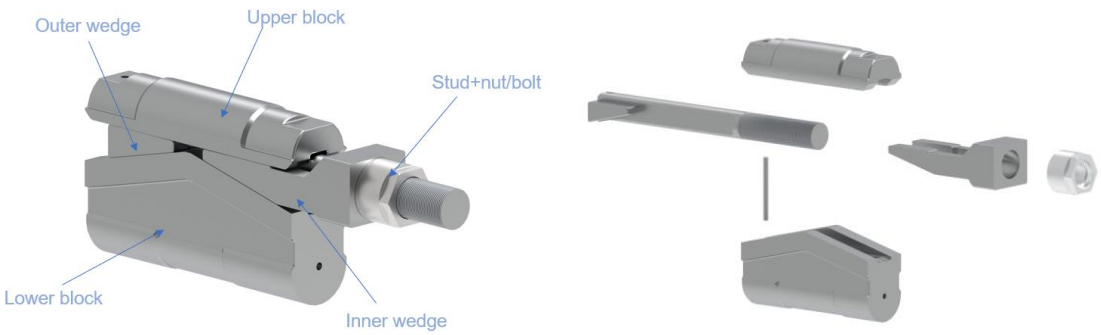

Figure 2.6: C1 wedge connection fastener[7]

2.2.2 Preload mechanism

Applying a preload to the bolt (or stud) causes the wedges within the C1 fastener to be drawn together. This is achieved by the horizontal force exerted by the head of the bolt on the inner wedge, alongside the equivalent force exerted by the threads on the outer wedge. As a result, both wedges bear an equivalent load. To ascertain the resultant vertical preload, the analysis involves employing a free body diagram (FBD), as depicted in Figure 2.7. Within this framework, each wedge is presumed to contribute half of the vertical preload denoted as F_{pre}. The equilibrium of horizontal forces acting on the inner wedge can be considered as follows:

Considering the equilibrium of the inner wedge in z-direction:

$$\Sigma F_z = 0$$

$$F_{N,z} - F_{friction,2,z} - \frac{F_{pre}}{2} = 0$$

$$F_N * \cos(\beta) - \mu * F_N * \sin(\beta) = \frac{F_{pre}}{2}$$

$$\frac{F_{pre}}{2} = F_N * (\cos(\beta) - \mu \sin(\beta))$$

$$F_N = \frac{F_{pre}}{2} * \left(\frac{1}{\cos(\beta) - \mu \sin(\beta)}\right) \tag{2.1}$$

Considering equilibrium of the inner wedge in x-direction:

$$\Sigma F_x = 0$$

$$F_{friction,1} + F_{friction,2,x} + F_{N,x} - F_{stud} = 0$$

$$F_{stud} = \mu * \frac{F_{pre}}{2} + F_N * \mu * \cos(\beta) + F_N * \sin(\beta) \tag{2.2}$$

Combining eq. (2.1) with (2.2):

$$F_{stud} = \mu * \frac{F_{pre}}{2} + \frac{F_{pre}}{2} * \left(\frac{1}{\cos(\beta) - \mu \sin(\beta)}\right) * (\sin(\beta) + \mu * \cos(\beta))$$

$$F_{stud} = F_{pre} * \frac{1}{2} * \left(\mu + \left(\frac{\sin(\beta) + \mu * \cos(\beta)}{\cos(\beta) - \mu * \sin(\beta)}\right)\right) \tag{2.3}$$

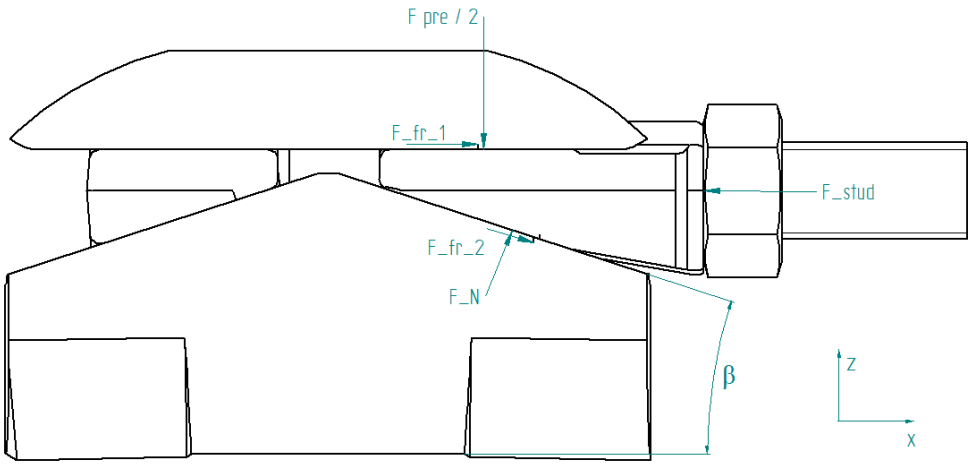

Figure 2.7: Free body diagram of C1 fastener

2.2.3 ULS resistance

The structural integrity under Ultimate Limit State (ULS) conditions in the C1 Wedge Connection is predominantly influenced by the thickness of the lower flange and the vertical webs of the upper flange. This evaluation takes into account two key factors: the net stress existing between the holes and the pressure exerted within these holes due to contact. For the purpose of design, the highest tensile load per individual section of the connection is commonly employed. The overturning moment on the OWT's is converted to the maximum tensile load per segment[7]:

$$Q_d = \frac{4\,M_d}{\pi D^2}\left[\frac{MN}{m}\right]$$

$$F_{seg,d} = Q_d * l_{seg} = Q_d * \frac{\pi D}{N_{segments}} = \frac{4M_d}{D * N_{segments}}$$

Where:

Q_{seg} = design line load(MN/m)
L_{seg} = segment length
M_d = design overturning moment (MNm)
D = structural diameter(m)
N_{seg} = number of segments
The net stress design criteria is obtained from EN 1993-1-8[20]:

$$\sigma_{net,d} \leq \frac{f_y}{\gamma_{M,1}}$$

With $\gamma_{M,1}$= 1.1[21]

$$\sigma_{net,d} = \frac{F_{seg,d}}{t * (l_{seg} - D_{hole})}$$

The design criteria for contact pressure:

$$P_{contact} \leq \frac{f_y}{\gamma_{M,2}}$$

With $\gamma_{M,2}$= 1.25[21];

$$P_{contact} = \frac{F_{seg,d}}{t * (D_{fastener})}$$

2.2.4 Number of segments

For an optimized design, utilization of net stress and contact pressure should be equal:

$$\frac{\sigma_{net,d}}{\frac{f_y}{\gamma_{M,1}}} = \frac{\rho_{contact}}{\frac{f_y}{\gamma_{M,2}}}$$

Therefore,

$$\frac{\sigma_{net,d}}{\rho_{contact}} = \frac{\gamma_{M,2}}{\gamma_{M,1}} = \frac{1.25}{1.1} = 1.14$$

Manufacturing and installation tolerances are taken into account by considering D_{hole} = 1.15*$D_{fastener}$. Considering, the net stress equation:

$$\sigma_{net,d} = \frac{F_{seg,d}}{t * (l_{seg} - 1.15 * D_{fastener})}$$

The equation can be rewritten as:

$$\frac{\left(\frac{F_{seg,d}}{t * (l_{seg} - 1.15 * D_{fastener})}\right)}{\left(\frac{F_{seg,d}}{t * (D_{fastener})}\right)} = 1.14$$

This simplifies to:

$$\frac{D_{fastener}}{l_{seg} - 1.15\, D_{fastener}} = 1.14$$

$$l_{seg} = 2.02 * D_{fastener}$$

This segment length will give the following number of fasteners:

$$N_{fasteners} = \frac{circumference}{l_{seg}}$$

3 Design of L-flange connection

In this chapter, design of L-flange segment for ULS resistance is discussed. Diameter of shell of the tower is assumed to be 8m and the bolt size of M80. References from literature review are taken for the relation between wall thickness and flange thickness. The aim of this chapter is to optimize the connection for ULS resistance with dimensions of components that lead to least steel mass. Therefore, comparison is carried out between steel mass and ULS resistance. The following dimensions are chosen for optimization as shown in Figure 3.1:

- Shell thickness(s)
- Distance centre of bolt to free end of flange(a)
- Distance centre of bolt to centre of shell(b)
- Flange thickness(t)

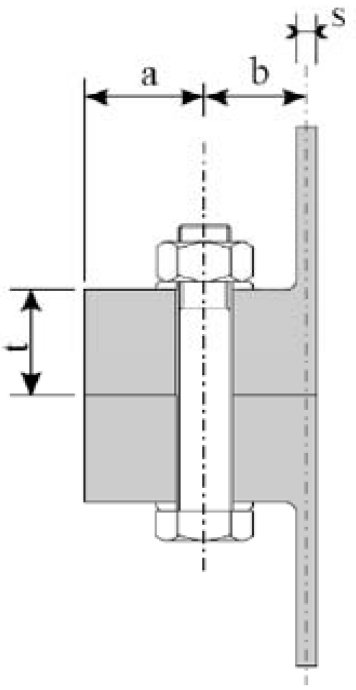

Figure 3.1: L-flange segment with abbreviations of dimensions

3.1 Flange and wall thickness relation

For ULS calculations, the flange dimensions play a vital role. For L-flange connections, increasing the flange dimensions would continuously increase the ULS resistance but the increase in the ULS resistance in comparison to steel mass of flange must be studied. For this, flange thickness and wall thickness of various ring flange bolted connection are considered from literature review and internal sources and extrapolated to get a linear relation between flange and wall thickness. Relation between the flange thickness and wall thickness for literature review and internal sources are shown in Figure 3.2 and Figure 3.3 [18],[2],[22],[23],[24].

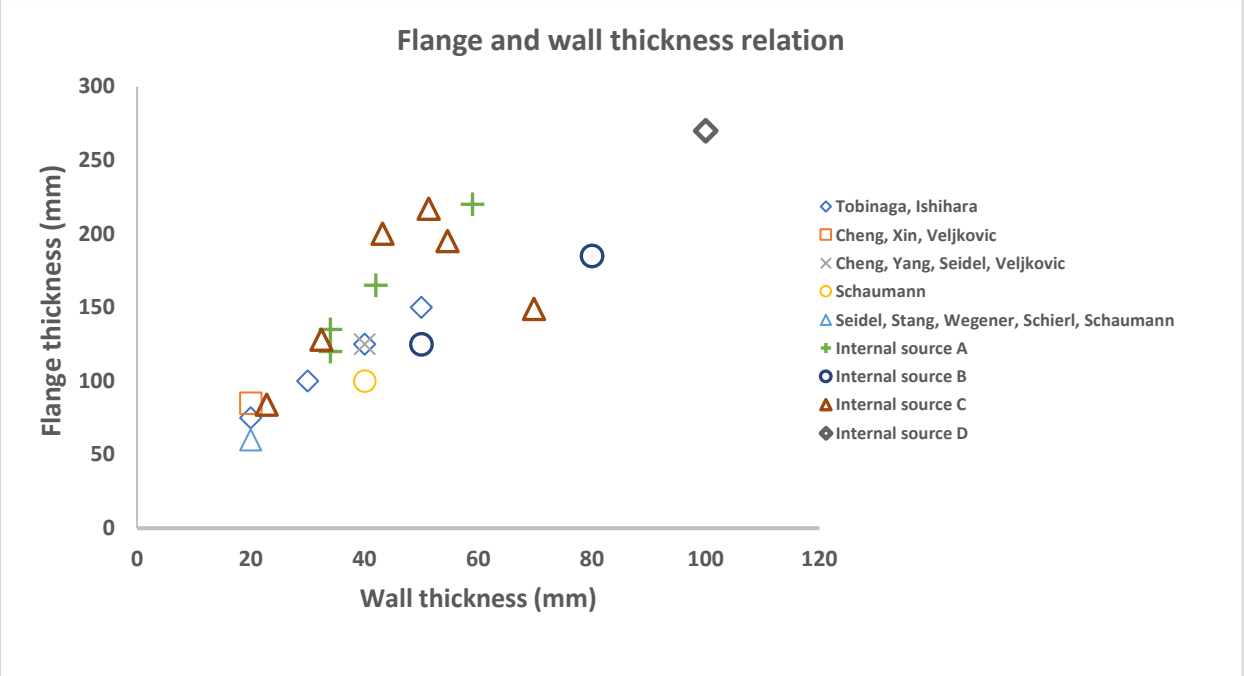

Figure 3.2: Flange and wall thicknesses for different L-flange connections

The values are linearly extrapolated to find the relation between the wall and flange thickness. The relation found is:

$$\text{Flange thickness} = 2.2285 * \text{wall thickness} + 44.458$$

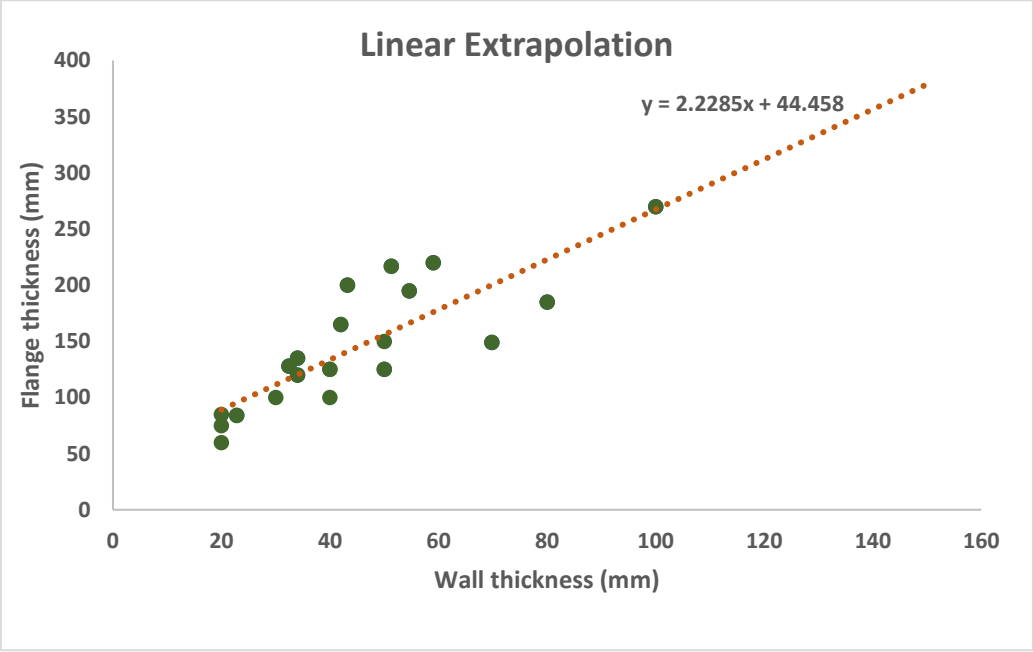

Figure 3.3: Linear extrapolation of flange and wall thickness

3.2 Distance a and b relation

For application of ULS theory by Peterson/Seidel[1],[16] , the ratio of a/b shall be limited to a/b<1.25[19]. IF the ratio is higher than 1.25, the location of the equivalent reaction force point moves outward from the inner edge of the flange by elastic deformation when the bolt first

reaches its ultimate capacity. This ultimate would results in lengthening of bolt required to develop the full plastic limit state, in which the reaction force acts at the inner edge of the flange and the hinge formation in the shell has developed[19],[18].

Therefore, the relation between a and b is:

$$a = 1.25b$$

3.3 Distance centre of bolt to centre of shell(b)

The distance between centre of bolt to centre of shell correspond to the eccentricity for the force that can applied to the connection. This force corresponds to the moment generated in the flange at bolt axis with lever arm as distance b, it is optimum to keep the distance between centre of bolt to centre of shell (b) as minimum. Therefore, the distance b is calculated considering the following dimensions/clearances:

- Size of the washer (140mm)
- Radius at the neck of the flange (25mm)
- Minimum clearance from the washer (45mm)
- Thickness of shell (s)

Distance b is calculated as sum of 0.5 times the washer size, neck radius for the weld, 0.5 times the wall thickness and 45mm as clearance. Therefore,

$$b = 0.5 * washer + 25 + 0.5 * wall\ thickness + 45$$

3.4 Segment width

The segment width is the width of the equivalent segment that corresponds to the complete ring flange connection. The segment width is dependent on several factors such as bolt size, number of bolts and bolt tensioner tool.

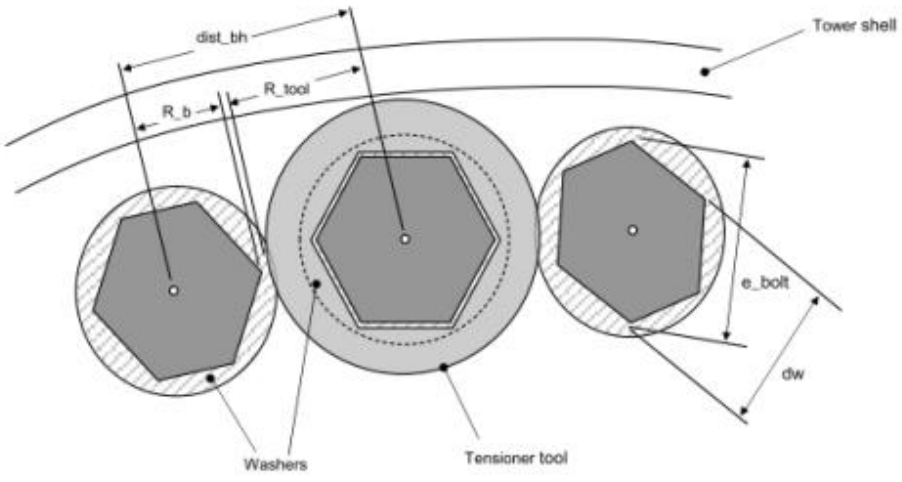

Figure 3.4: Representation of spacing required for bolt tensioner tool

As the connection is being designed for ULS, maximum number of bolts should be placed on the ring. Adequate spacing should be available for the bolt torque tool. For this, the specific fasteners were chosen from ITH[25]. Bolt tensioning tool diameter is extrapolated for M80 bolt size as shown in Figure 3.5.

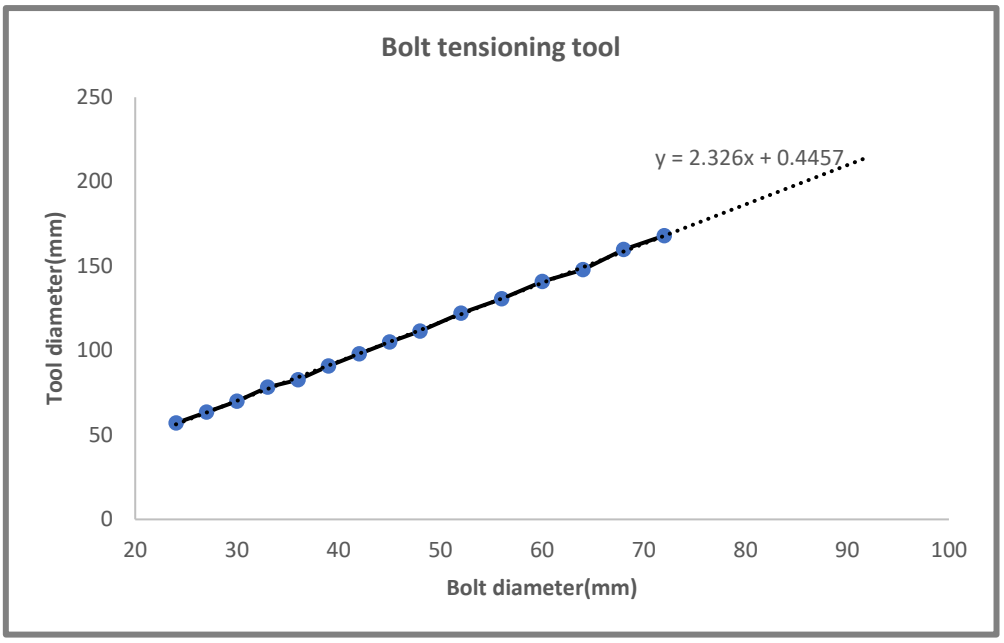

Figure 3.5: Bolt tensioning tool diameter relation

The diameter of the tool for M80 bolt size from Figure 3.5 is 187mm.

- Assumption of segment width of 2 times bolt diameter is done. Therefore, segment width(c)=160mm
- Diameter of the bolt head=127mm

- Spacing between the end of the bolt head to centre of adjacent bolt head = 160-127*0.5 = 33mm

- Total spacing for bolt tensioning tool available=160+33=193mm

3.5 Shell thickness v/s segment strength

Using equations in section 3.1, 3.2 and 3.3, input data from Table 1 and shell thickness of 50mm-150mm in increasing step sizes of 5mm, ULS calculations are performed to find the ULS load that the segment can withstand and respective gross weight of flange steel. Steel mass for gross flange(Figure 3.6) is considered for the calculations and design. The steel mass is equal to the thickness of flange*width of the flange*number of segments. Steel weight and ULS limits were plotted for bolt size M80 as depicted in Figure 3.7.

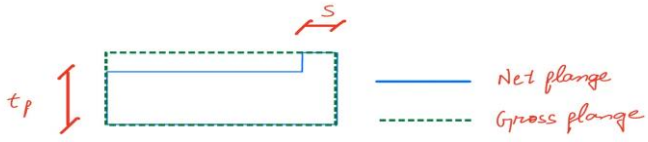

Figure 3.6: Steel mass for flange

INPUT		
Description	**Unit**	**Value**
Diameter of the shell(OD)	mm	8000
Bolt Size	mm	80
Bolts grade	-	10.9
Material partial factor(ULS)	-	1.1
Bolt partial safety factor(ULS)	-	1.25

Table 1: Input data for L-flange connection design

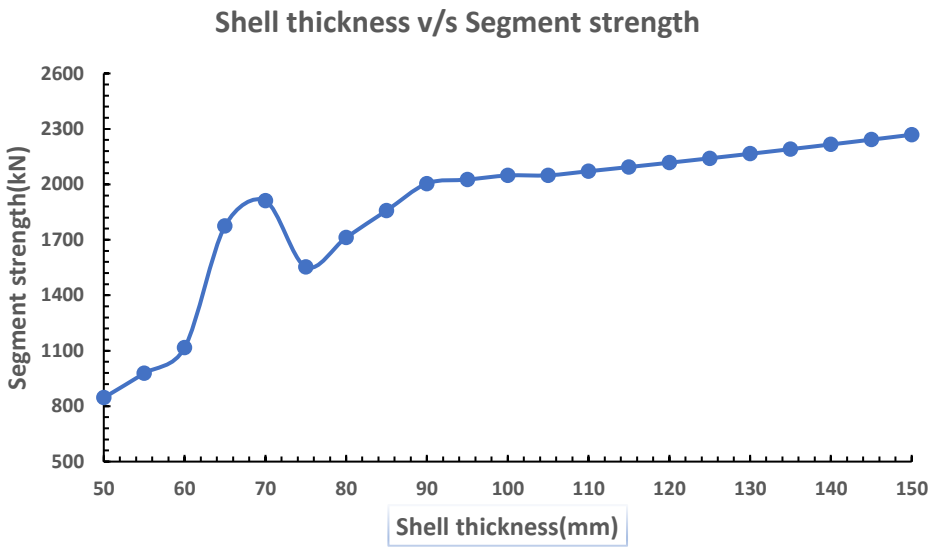

Figure 3.7: Wall thickness and segment strength relation with failure mode D and E

A peak can be observed at shell thickness of 65mm and 70mm. For these two wall thicknesses and their respective flange design, the conditions for mode D and E are fulfilled, hence the governing mode is either failure mode D or E. As the results from failure mode D and E are not consistent for the given range of wall thickness, Further analysis is done based on failure mode A, B and C. Figure 3.8 shows the relation of shell thickness to segment strength considering only Failure mode A, B and C.

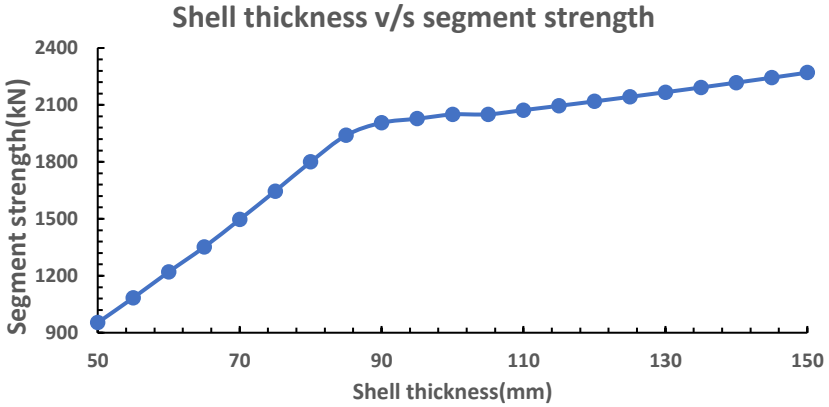

Figure 3.8: Wall thickness and segment strength relation considering failure mode C

It can be observed from Figure 3.8 that till about 85mm of shell thickness the segment strength increases linearly with a higher gradient than compared to the higher shell thickness. The increase in the segment strength is gradual as compared to the increase in the mass of the steel. Therefore, shell thickness of 85mm is considered for the design which is also the point for comparable segment strength and steel mass.

The final design parameters are presented in Table 2.

Description	Unit	Value
Diameter of the shell(OD)	mm	8000
Number of bolts	-	148
Bolt Size	mm	80
Bolts grade	-	10.9
Bolt circle diameter(BCD)	mm	7550
Wall thickness(s)	mm	85
Flange thickness	mm	233.9
Material partial factor(ULS)	-	1.1
Bolt partial safety factor(ULS)	-	1.25
Distance between centre of bolt to centre of wall(b)	mm	182.5
Distance between centre of bolt to free end of flange(a)	mm	228

Table 2: Final parameters for L-flange connection design

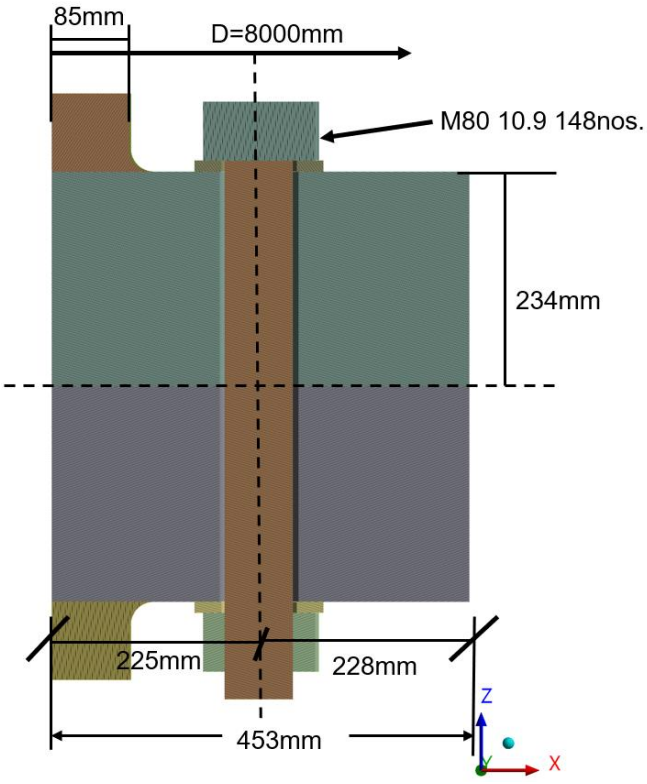

3.6 Mass of the connection

Mass of the L-flange connection is mostly composed from the mass of the flanges. The net flange mass constitutes of the flange mass prior to machining and cutting. The mass of the complete ring for both flanges is 53.72tonnes.

4 FEA: Methodology

In this chapter, the methodology, material models and boundary conditions for FEA are discussed. The relevant information is subsequently used later in the FEA of L-flange and C1 wedge connection. The FEM software used (Ansys) has been elaborated in detail for the methodology used and the characteristic details.

4.1 Contact elements

The contact pair in Ansys is defined using contact surface on one body and target surface on another body. The contact pair should be defined to properly capture the behaviour of the contact in terms of penetration. To do this, the stiffer part is defined as target surface.

CONTA174 element is used in Ansys for the contact surfaces and TARGE170 elements are used to represent target surfaces.

4.2 Mesh elements

For structural FEA, several element types are present to define the properties of components of structure. For both L-flange and C1-wedge connection solid elements are used. Solid elements have been chosen as they provide more accurate results.

One of the property of the elements is the degree of freedom(DOF) per node, geometry and number of nodes. Linear element type is used in ansys which has three degree of freedom at each node : translations in the nodal x, y, and z directions[26] as presented Figure 4.1.

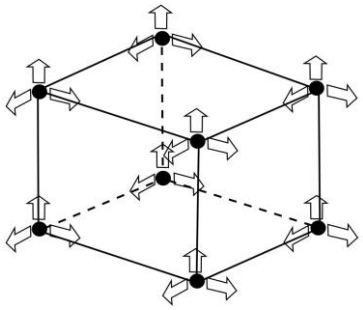

Figure 4.1: Linear element

4.3 Non-linear material model

EN 10025-3-2019 suggests the reduction of yield strength for S275NL, S355NL and S460NL material with increase in the thickness of the plates used. DNV[27] describes the development of true stress-true plastic strain curves.

For bolt grade 10.9 and fastener of C1 wedge connection, the material properties are defined multi-linear curve as shown in Figure 4.2 and Figure 4.3. The yield strength and ultinmate strength of bolt is described in The reduced yield strength for thicknesses of plates is shown in Table 4.

Bolt 10.9	Yield strength(MPa)	Ultimate strength(MPa)
	900	1000

Table 3: Bolt material strength

		-------EN-10025-3-------		
		S275N(L)	S355N(L)	S460N(L)
Thickness from	to (mm)			
0	16	275	355	460
17	25	265	345	440
26	40	265	345	440
41	50	255	335	430
51	63	255	335	430
64	80	245	325	410
81	100	235	315	400
101	120	225	295	380
121	150	225	295	380
151	200	215	285	370
201	250	205	275	370

Table 4: Reduced yield strength as per EN 10025-3:2019

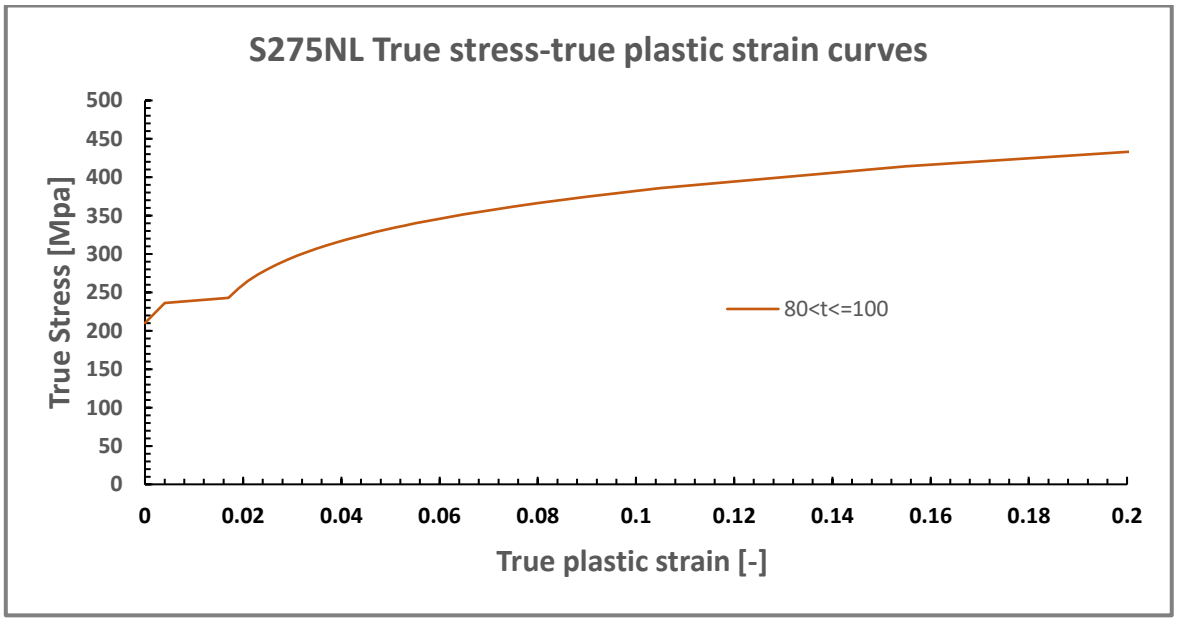

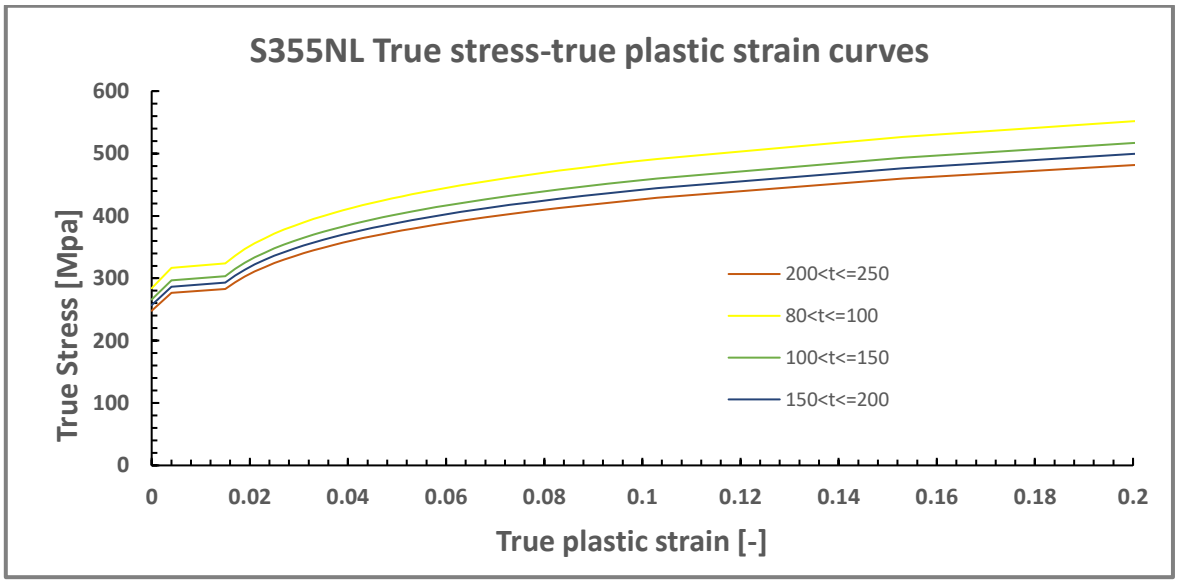

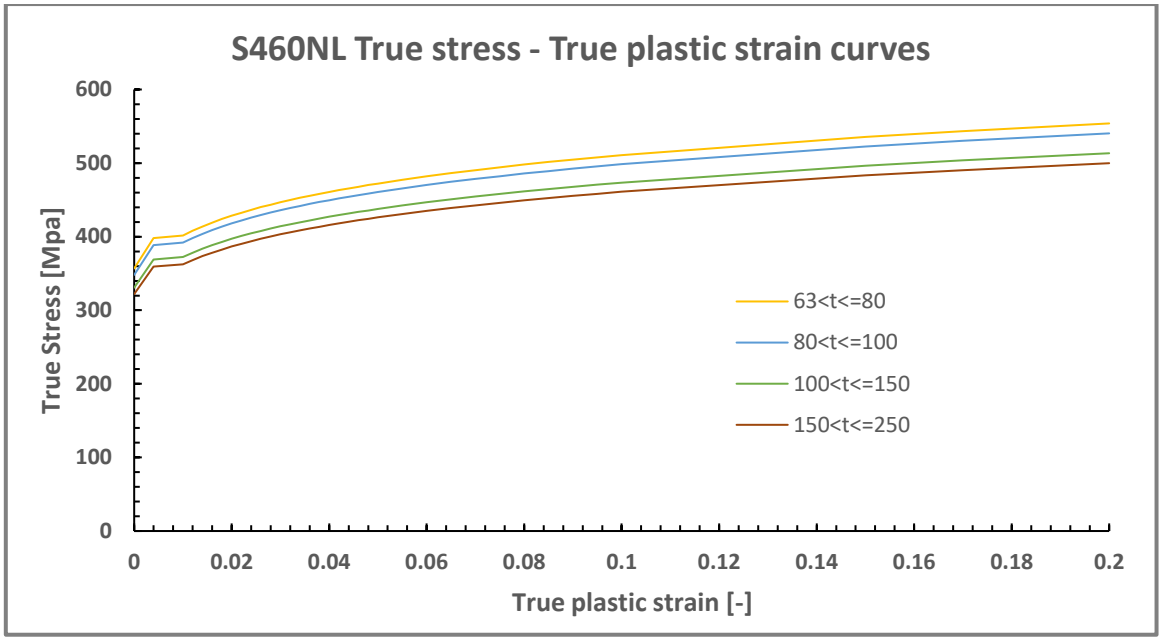

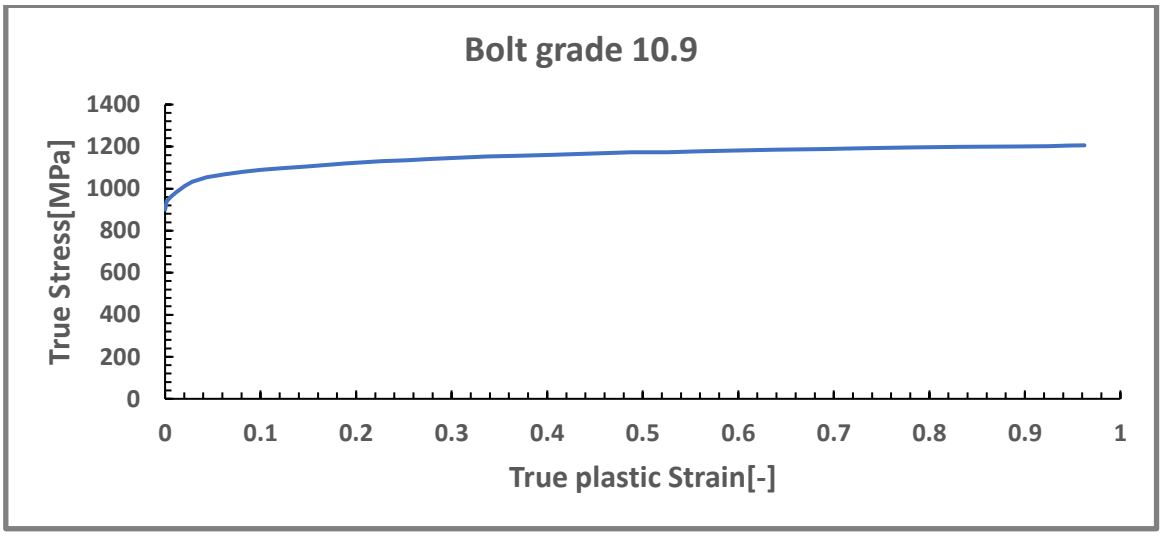

Figure 4.2: Bolt true stress-true plastic strain curve

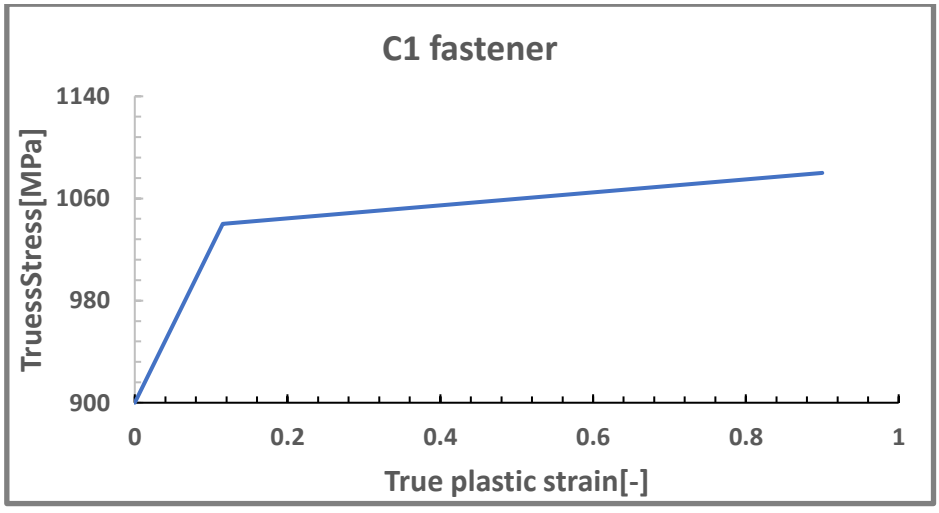

Figure 4.3: C1 fastener true stress-true plastic strain curve

5 FEA: L-flange connection

In this chapter, Cheng's study[2] on L-flange connection has been validated and the methodology used to validate the results have been implemented to obtain the results for M80 bolt single segment.

5.1 Validation of Cheng's[2] M48 bolt single segment

Cheng[2] modelled and analysed a single segment of L-flange connection with M48 bolt size[2]. The results were obtained using explicit solver but to reduce the computation cost the results were validated using static structural solver of Ansys. This would provide the further definitions for M80 bolt size design that could be analysed using same methodology. The design is shown in Figure 5.1. A representation of Cheng's[2] study and variable taken in this study are presented in Table 5.

Criterion	Cheng's[2] study	This study
Solver	Explicit	Static structural
Preloading mechanism	Turn of nut	Pretension lock
Mesh size	8mm	10mm
BC at bottom	Fixed support	Restrained in z-direction
Friction coefficient	0.13	0.13

Table 5: Comaprison of variables

5.1.1 Design and boundary conditions

To reduce the computation cost and time further, the bolt and nut in the modelled without threads as the criteria here is to find the ULS resistance which is independent of the threads.

The preloading is applied using bolt pretension in Ansys instead of turn of nut preloading.

Linear elements(SOLID185) of 10mm size were used to mesh all the components of the segment. Shell of the segment is S355NL and flanges are S275NL. Bolt grade used in 10.9. The study with fully threaded bolts with full contact is taken into account.

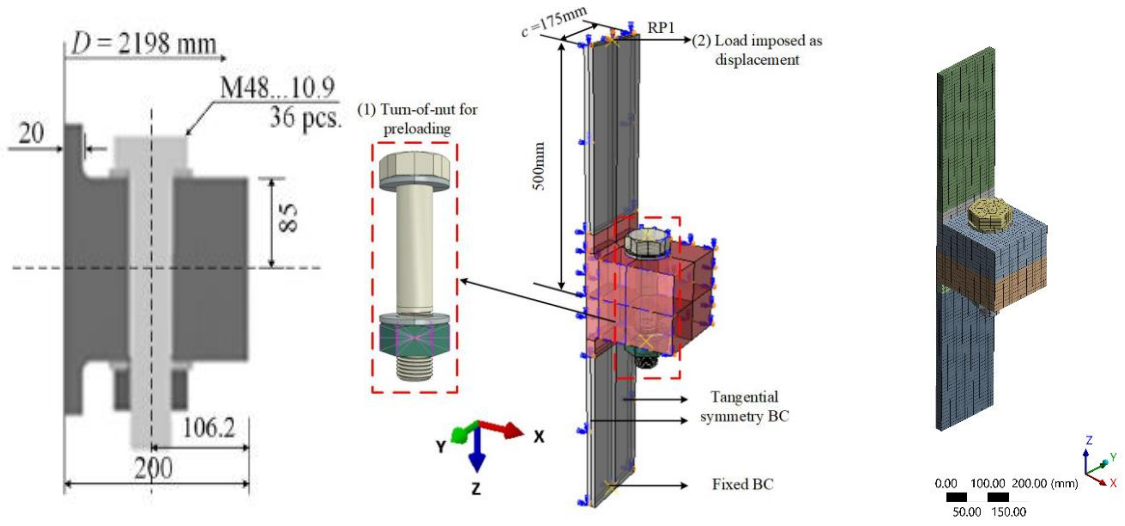

Figure 5.1: L-flange design for M48 bolt[2]

As the segment is a part of the ring flange connection and doesn't incur the curvature, symmetry conditions are applied on left and right side of the segment. The symmetry on both sides of the segment ensures that the stiffness from the complete ring is accounted for. The bottom end of the segment has the displacement in z-direction fixed to 0 to prevent rigid body movement as shown in Figure 5.2.

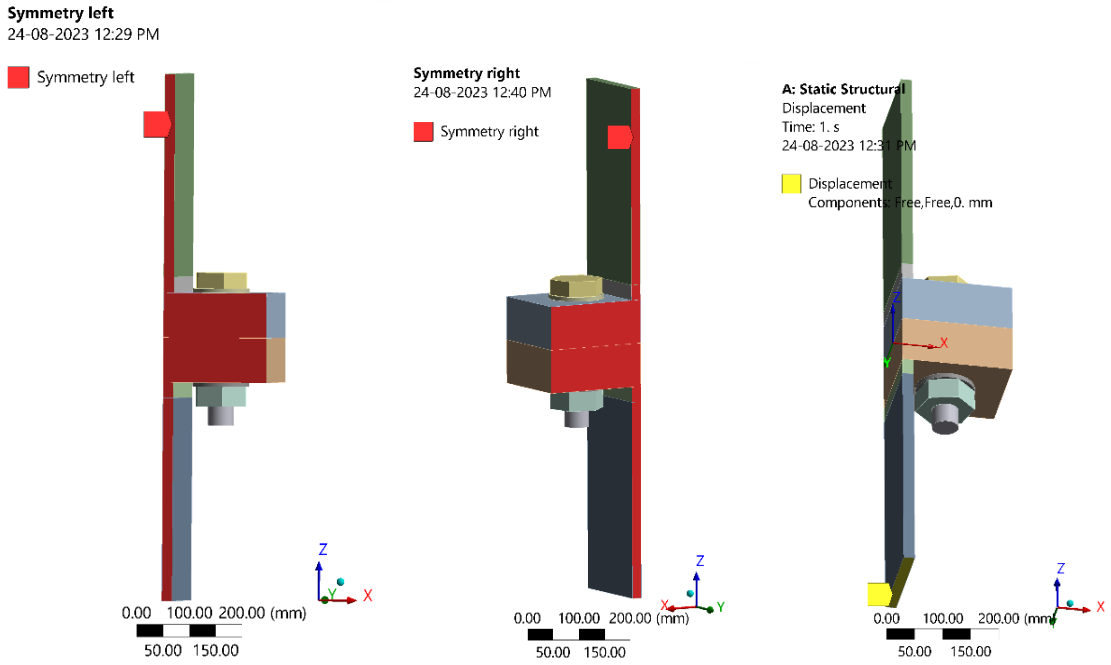

Figure 5.2: Boundary conditions

5.1.2 Contacts

Frictional contacts are defined for flange to flange, bolt to flange and washer to flanges. Frictional contact of μ=0.13 is used[2]. Bonded contacts are defined for the nut to bolt as the pretension is locked in Ansys in second substep which is the substep for application of external load. to lock the preload and restrict movement of bolt to generate pretension during preload. Bonded contacts are also used for washer to nut and washer to bolt head.

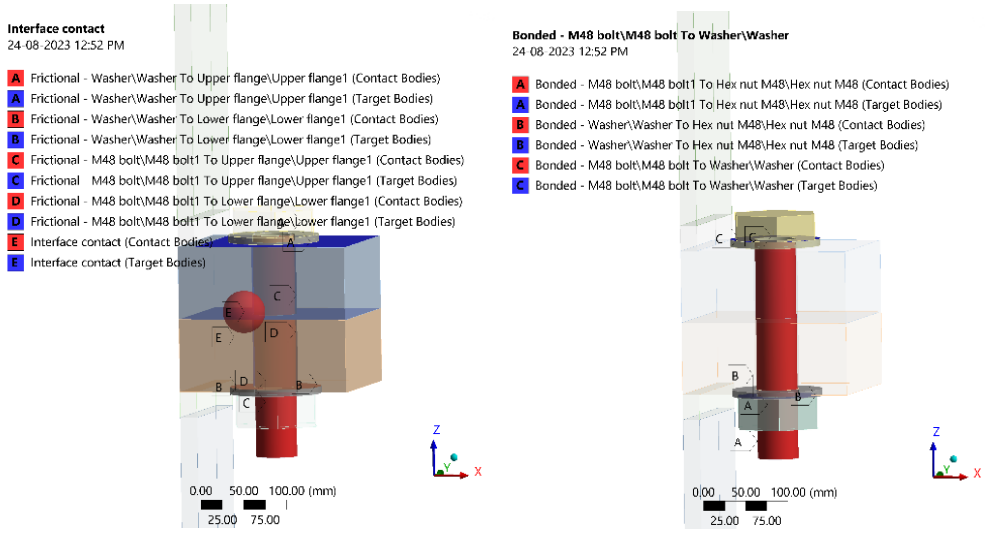

Figure 5.3: Contacts definition

5.1.3 Preload and force

Preload of 1082kN is applied as per Cheng's[2] study. Preloading of the bolt is done in first substep of the analysis using bolt pretension function of Ansys. The preload is applied to the shank of the bolt in z-direction. In second substep, this preload is locked with assumption of no preload loss during loading.

Force is applied in second substep of the analysis on the upper surface as surface load on shell of the segment as shown in Figure 5.4.

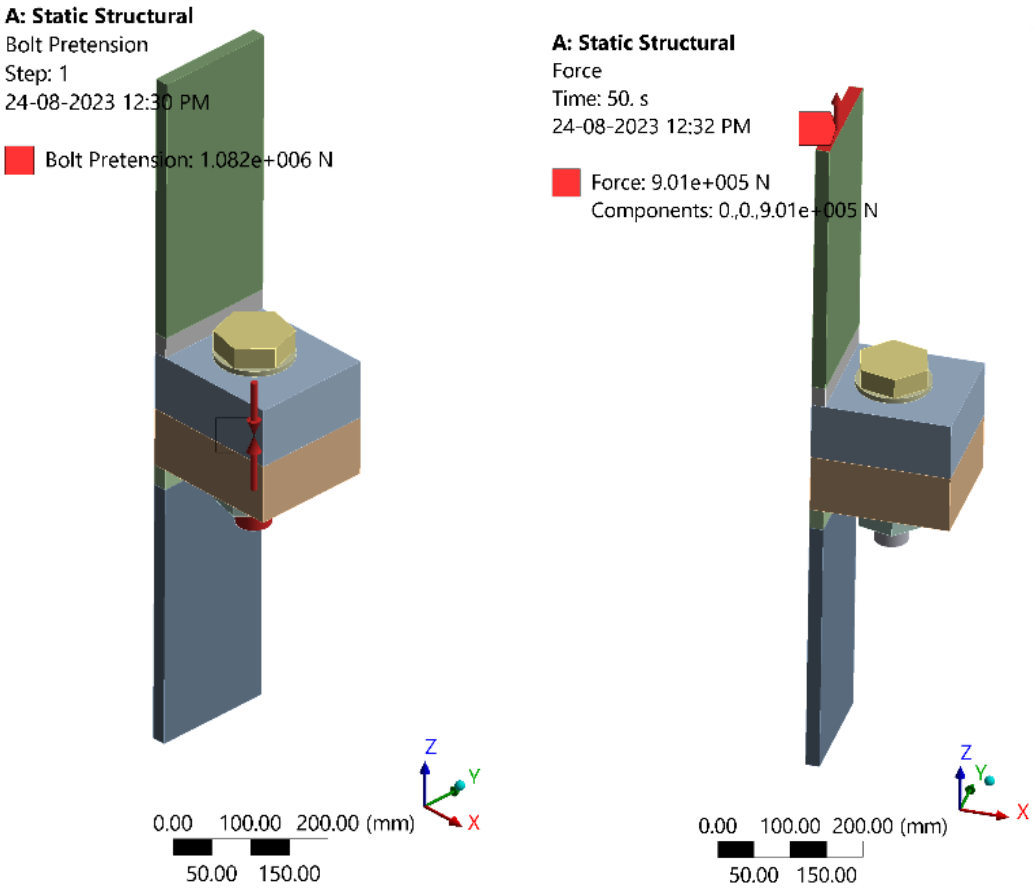

Figure 5.4: Preloading and Force application

5.1.4 Results

Failure at 5% plastic strain is observed and the corresponding applied load is equal 806kN which is in order with 835kN from Cheng's[2] results. The strain value also corresponds to start of the necking in the bolt.

Load displacement curve is plotted(Figure 5.5) and the maximum displacement at ULS failure the top of segment in z-direction is approximately 14mm which is in order with 13.5mm displacement at failure for Cheng's[2] results. The results of the study are presented in Appendix A.

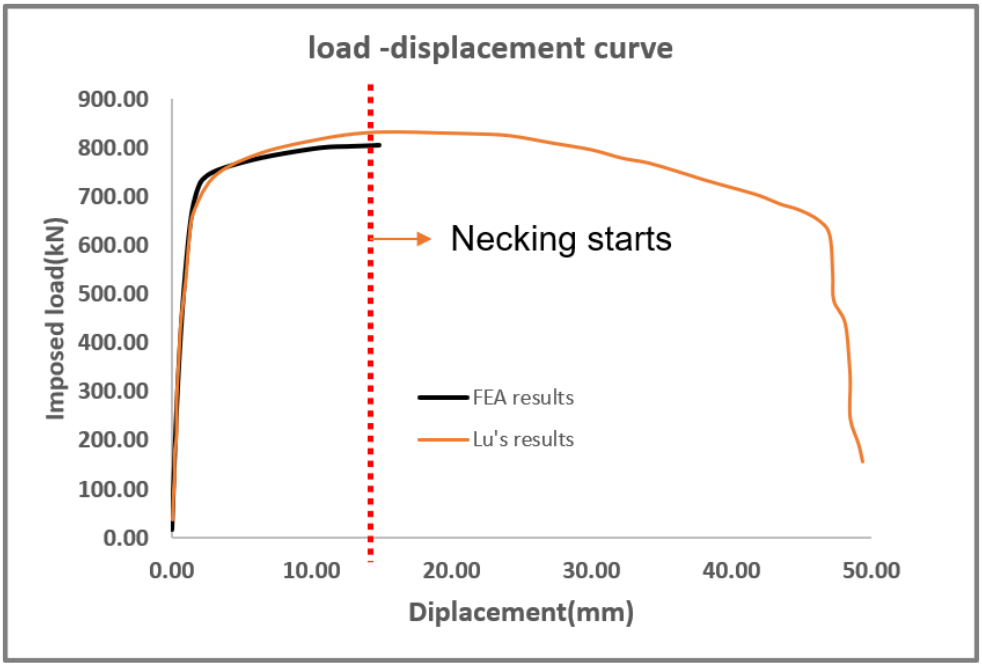

Figure 5.5: Load-dispacement curve

FEA shows(Figure 5.6) that yielding of the wall and failure of bolt is the governing criteria, therefore the result of failure mode B from Peterson's theory are compared. ULS failure load=806kN which is in order with 792kN from failure mode B resistance. The variation is 1% which is acceptable.

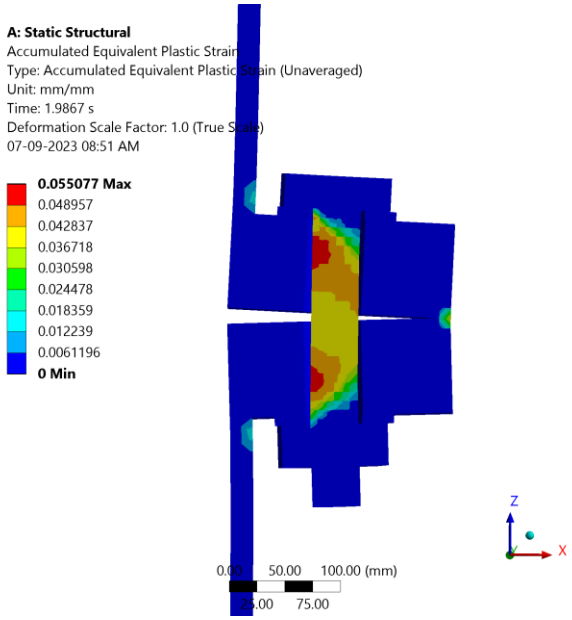

Figure 5.6: Plastic yielding and bolt failure at ULS

The gap opening at the shell location is also in order with the results from Cheng's[2] study as shown in Figure 5.7.

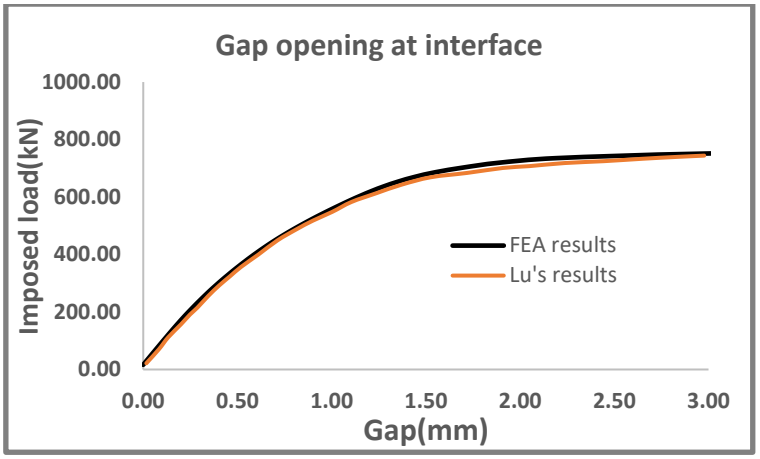

Figure 5.7: Gap opening at interface

5.2 M80 bolt

5.2.1 3D model

As per parameters finalized in Table 2, 3D geometry was modelled as shown in Figure 5.8. 148 M80 bolt segment are present in the complete ring flange connection. One curved segment would be imported to Ansys as the connection is symmetrical and assumption is made that no imperfections are present. As partial safety factors cannot be incorporated in Ansys, the analysis is done for ULS and the ULS resistance is calculated again for the Peterson's failure mode A, B and C without the consideration of partial safety factors.

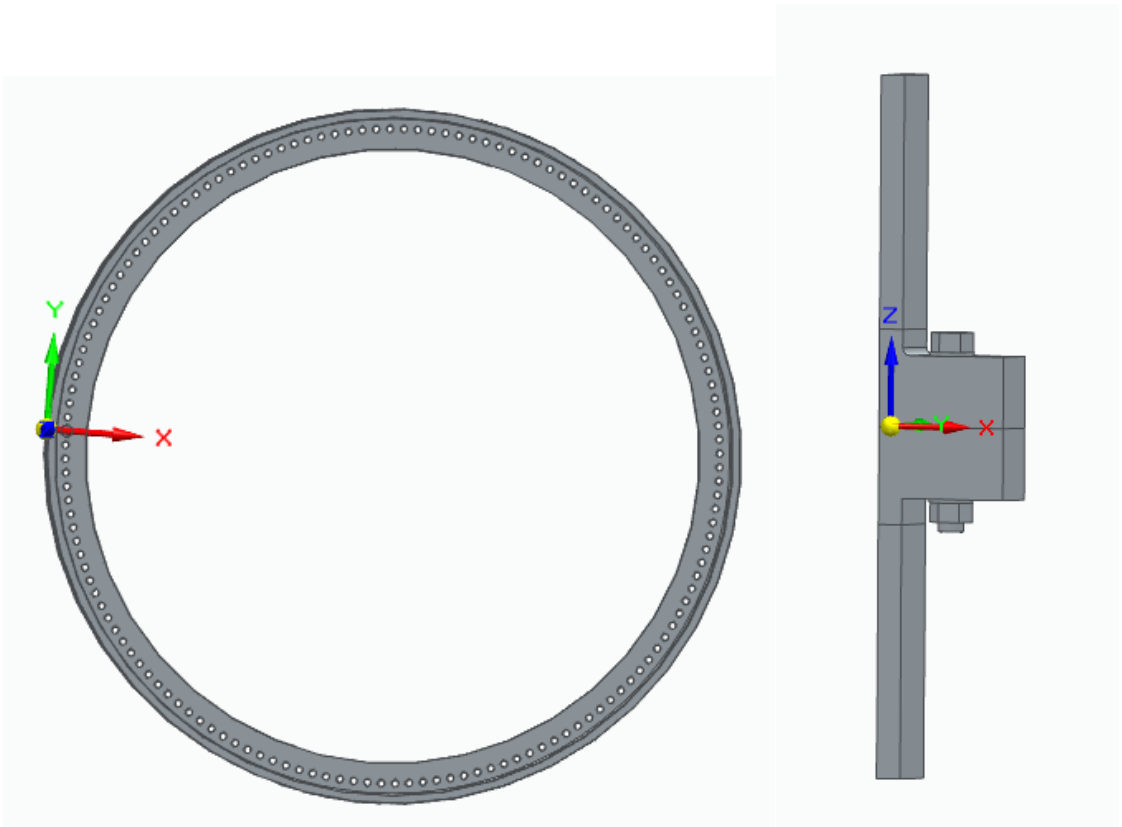

Figure 5.8: 3D model and segment

5.2.2 Material model and mesh

The dimensions for the components of the connection are taken from Table 2. Thicknesses of the components and reduced yield strength as per EN 10025-3:2019 are presented in Table 6. Initial modulus of elasticity of E=210GPa and poisson's ratio of 0.3 is used. The washer is modelled with elastic material whereas flanges, shell and bolts are modelled using elastic-plastic material. The true stress- plastic strain curves are presented in section 4.3.

Component	Thickness	Material	Reduced Yield strength [MPa]
Upper flange	234	S355NL	275
Lower flange	234	S355NL	275
Shell	85	S355NL	315

Table 6: Yield strength of M80 bolt segment components

Linear elements of size 20mm are used to mesh all the components of M80 bolt segment. As shown in Figure 5.9.

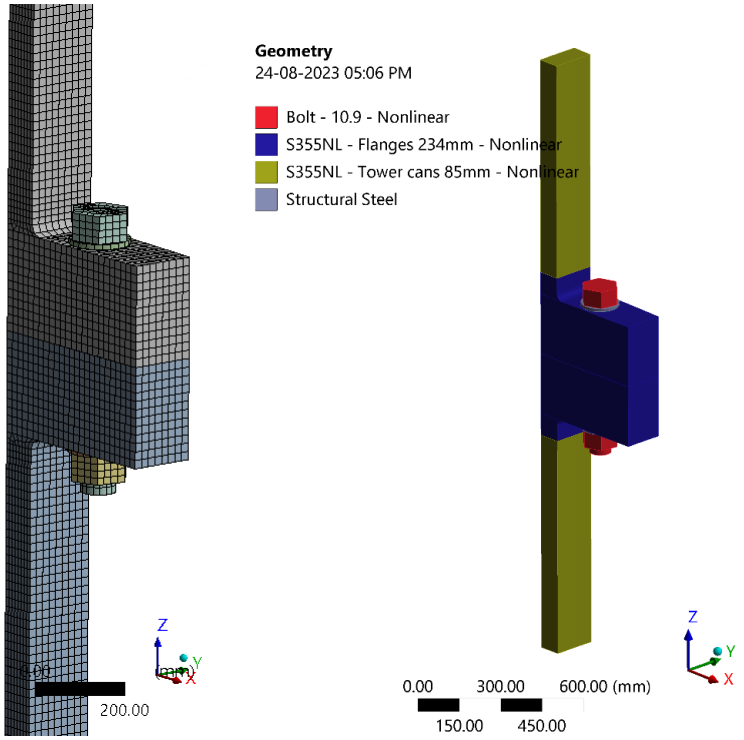

Figure 5.9: Mesh and material

5.2.3 Boundary conditions

As one of the 148 segments is cut from the geometry, the segment is analysed with the curvature of the ring flange. To account for the symmetry, left and right side of the segment are restricted to displace in the normal direction. Therefore, 0mm displacement is applied on all the surfaces of left and right side of the segment. The bottom of the segment is fixed in z-direction prevent rigid body movement. This is shown in Figure 5.10.

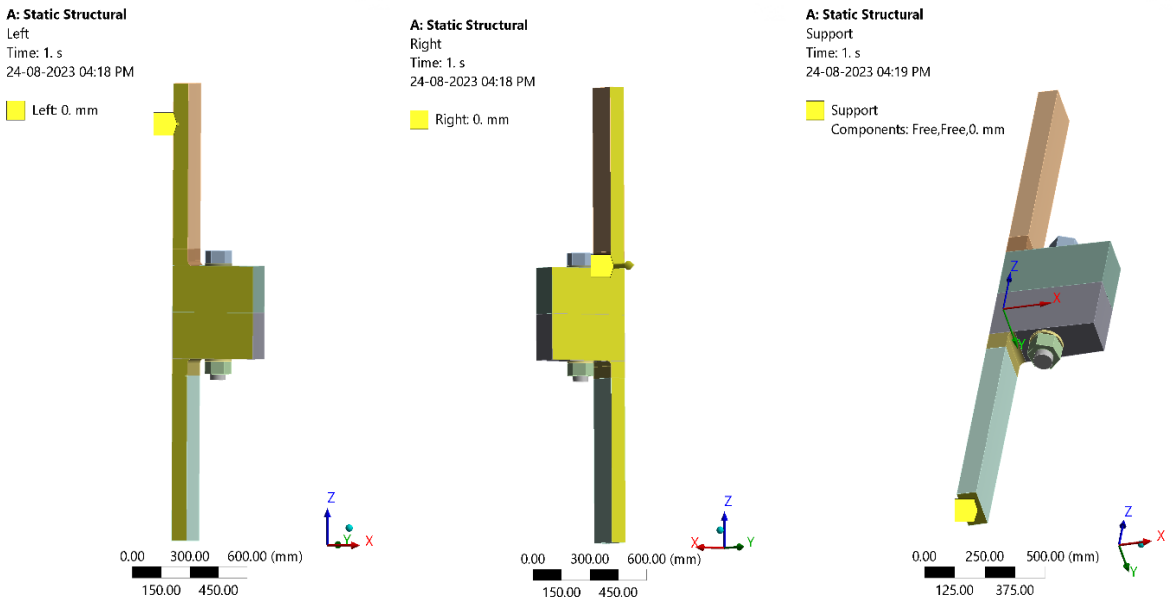

Figure 5.10: Boundary condition for M80 bolt segment

5.2.4 Contacts

Contacts are defined using the same methodology of M48 bolt segment. Frictional contacts are defined for flange to flange, washer to flange and bolt to flange as shown in Figure 5.11. Bonded contacts are defined for washer to nut and nut head and bolt to nut as shown in Figure 5.12.

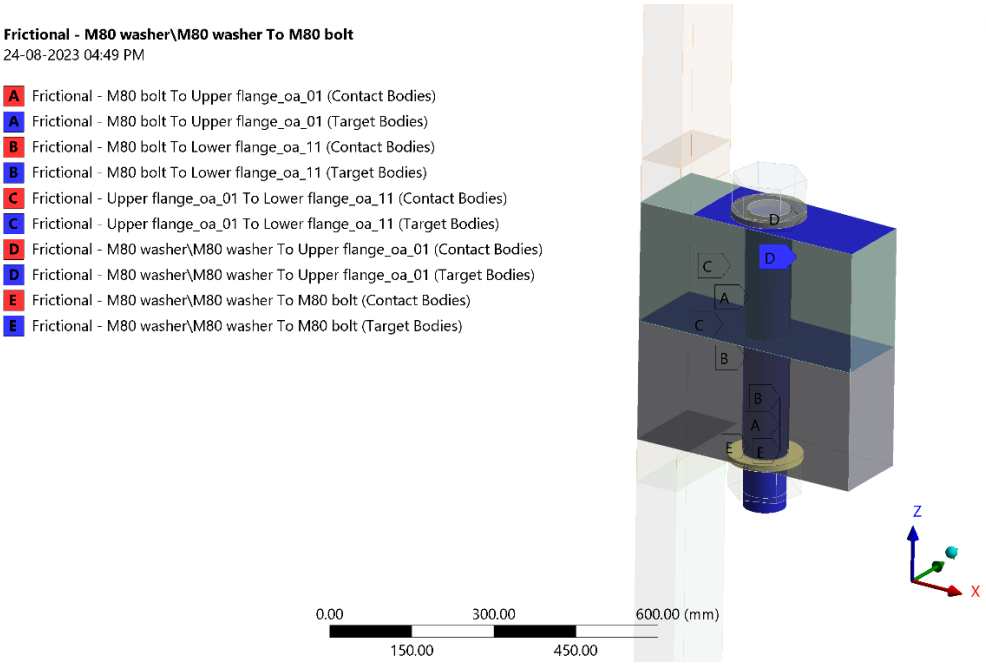

Figure 5.11: Frictional contacts in M80 bolt segment

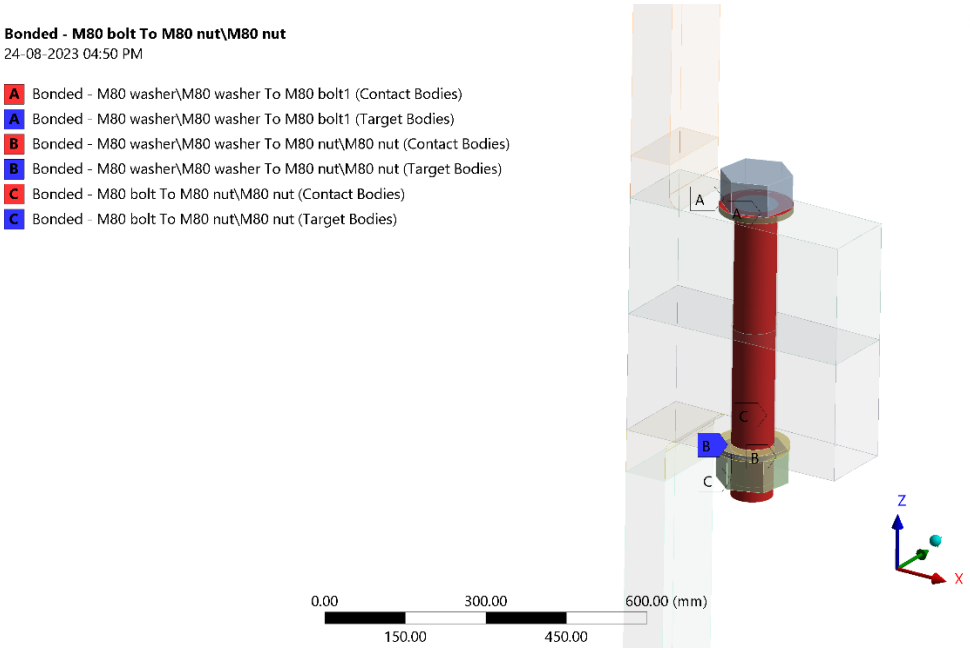

Figure 5.12: Bonded segments in M80 bolt segment

5.2.5 Preload and force

The preload is applied equal to the maximum allowable value (70% of the bolt tensile strength) according to EN 1993-1-8 as $0.7A_sf_u$. This equals to 3162kN. The preload is applied in the first substep on the shank of the bolt. In the second substep, the external load is applied on the top surface of shell of the segment as the surface load. This is shown in Figure 5.13.

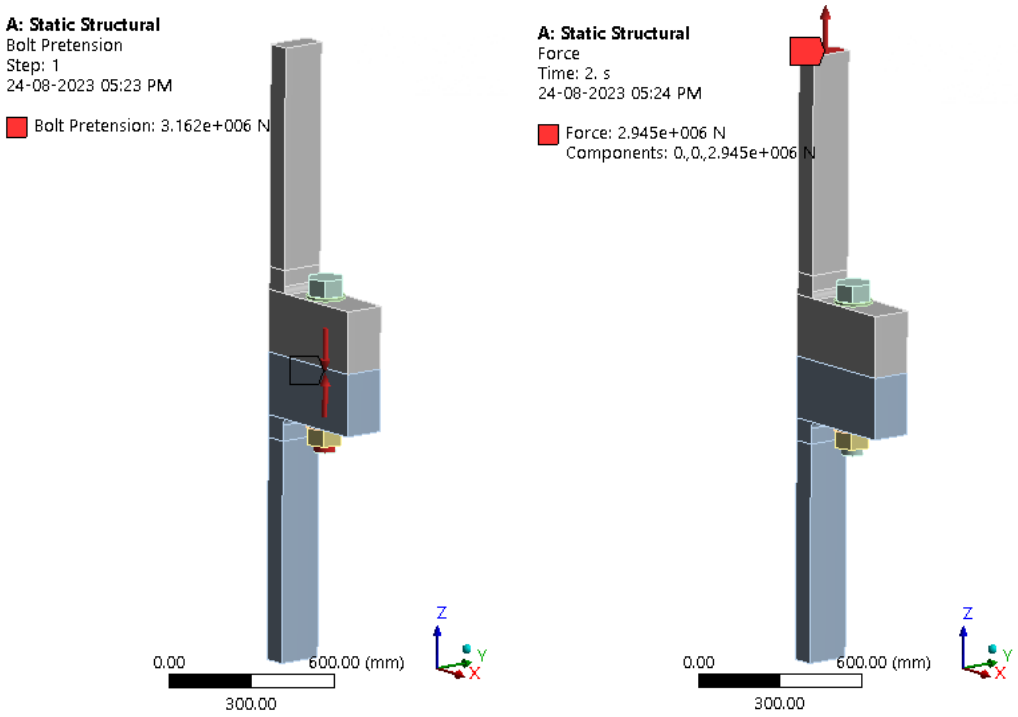

Figure 5.13: Bolt preload and external force

5.2.6 Results

Values of bolt preloading are obtained from interface between the flanges. The values are same as that of bolt preloading applied. Maximum principal stresses are obtained after preloading and contour plot is shown in Figure 5.14. The bolt preload is developed uniformly throughout the bolt.

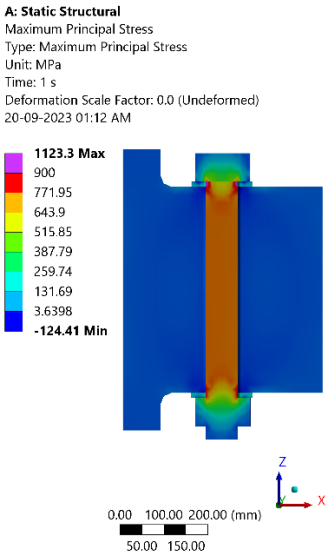

Figure 5.14: Maximum principal stress after preloading

5.2.6.1 ULS resistance

The ULS load is obtained at 5% plastic strain in the bolt. The 5% plastic strain corresponds to the limit state criterion as per EN 1993-1-5[28]. The load at this strain is 2506kN(787MNm).

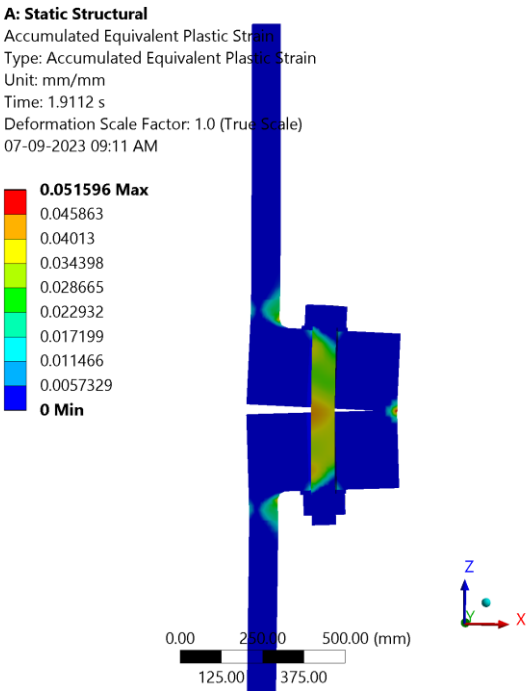

The ULS failure load without consideration of partial safety factors as per Peterson's theory and FEA are presented in Table 7.

Failure mode	Peterson's theory ULS(kN)	FEA(kN)
A	3906	2506
B	2327	
C	1924	

Table 7: Ultimate resistances from different approaches

As the plastic hinge formation in shell and failure of bolt can be visualized, the results of FEA are comparable with failure mode B of Petersen's theory. The variation in the results is 1%.

As the connection is designed considering partial factors as described in Table 1, the design load is 1940kN(609MNm) but the ULS resistance is 2506kN(787MNm) which is 30% more than the initial ULS load it is designed for. This difference can be justified as for the design, partial safety factors for bolt and other components are considered. This load translates to 609MNm of overturning moment at the connection level.

5.2.6.2 Load-displacement curve

Relationship between imposed external load and displacement in z-direction at 500mm above the interface of flanges(Figure 5.15) is obtained and plotted in Figure 5.16. It can be observed that the maximum deformation is 33mm at for ULS criteria..

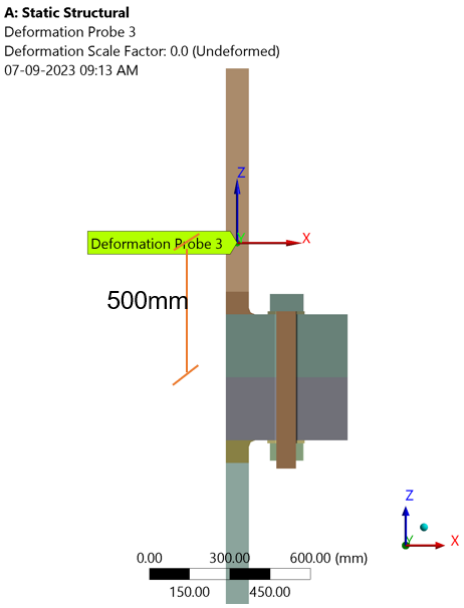

Figure 5.15: Location of the deformation probe

It can also be observed that displacement increases rapidly after the external load has exceeded 2100kN. To study this, plots for bolt force and contact force have been plotted in Figure 5.16.

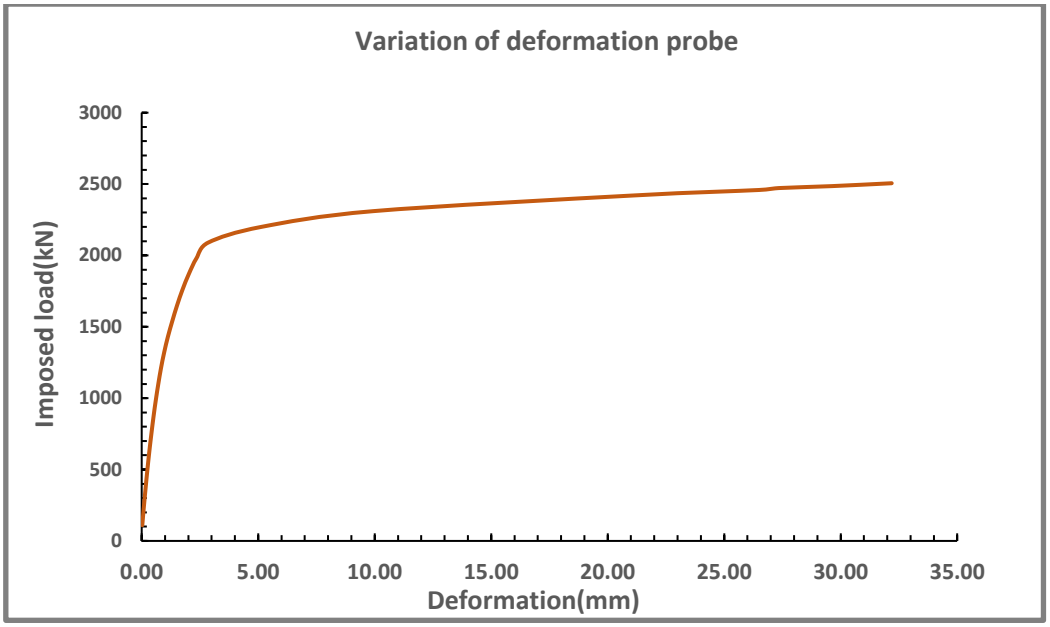

Figure 5.16: Load-displacement curve

5.2.6.3 Gap *opening*

As it is evident from the results, the gap opening and the displacement of the connection increases rapidly. This could be a problem for the bolt due to the environmental conditions. If the connection opens and the exposed to humidity or other hazardous environmental conditions, chances of corrosion are high. To account for this, the gap opening at bolt hole should be accounted for. No proper research is available at present. Various openings at bolt hole are assumed and the respective load for that opening is presented in Table 8. Different mesh sizes have been studied for this to verify the results of FEA.

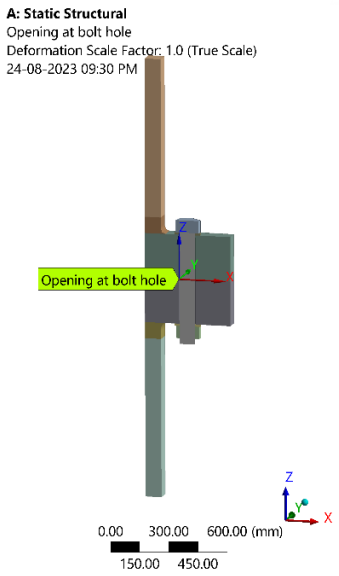

Figure 5.17: Location of probe for gap opening

		Gap opening(mm)		
		0.2	0.5	1
Mesh size(mm)	5	565kN	1137kN	1623kN
	10	559kN	1136kN	1620kN
	20	560kN	1148kN	1637kN

Table 8: Gap opening at bolt hole with different mesh sizes

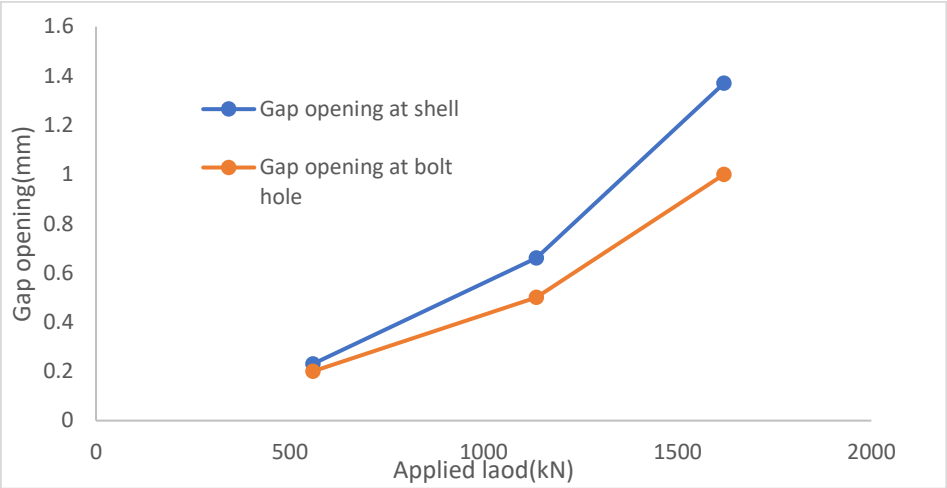

6 Validation of Cheng's[8] C1 wedge connection

In this chapter, results from Cheng's[8] study for C1 wedge connection for ULS criteria have been validated and discussed. The main aim of this chapter is to validate both experimental and FEA results of the second generation C1 wedge connection based on the yield strength obtained from the material certificate.

6.1 Design details

The design of second generation C1 wedge connection is shown in Figure 6.1. As the connection was tested experimentally for ULS and the net area for lower flange is less than that of the webs, the failure of lower flange in ULS is justified as observed from experiments[29].

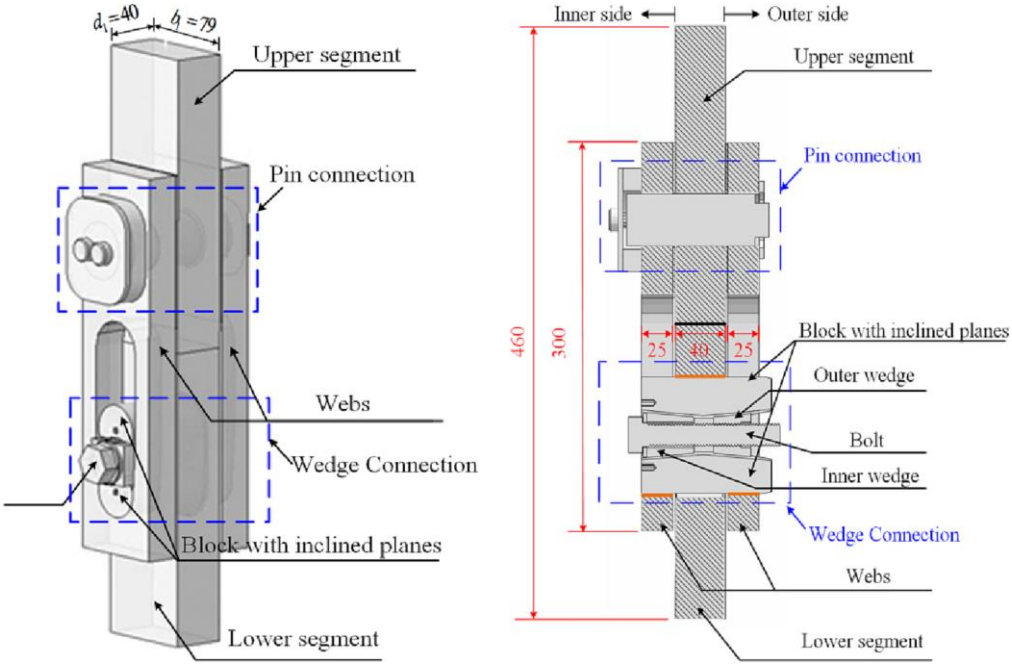

Figure 6.1: Illustration of C1 single segment(unit: mm)

Figure 6.2: Failed lower flange

6.2 Simplified design

The lower flange is the critical component of the C1 wedge connection. After the opening of the interface, the load transfers through the upper flange to the fastener and finally to the lower flange. The lower flange develops the highest net stress compared to the webs of the upper flange. Therefore, the lower flange failing in ULS is justified. For this reason, to validate the results, only lower flange and the upper block are modelled and analysed in Ansys(Figure 6.3). The connection is symmetrical; hence half segment is modelled with valid boundary conditions. Mesh size of 3mm with linear elements is used.

Lower block is used of S460NL material and upper block is used of 34CRNiMo6 steel.

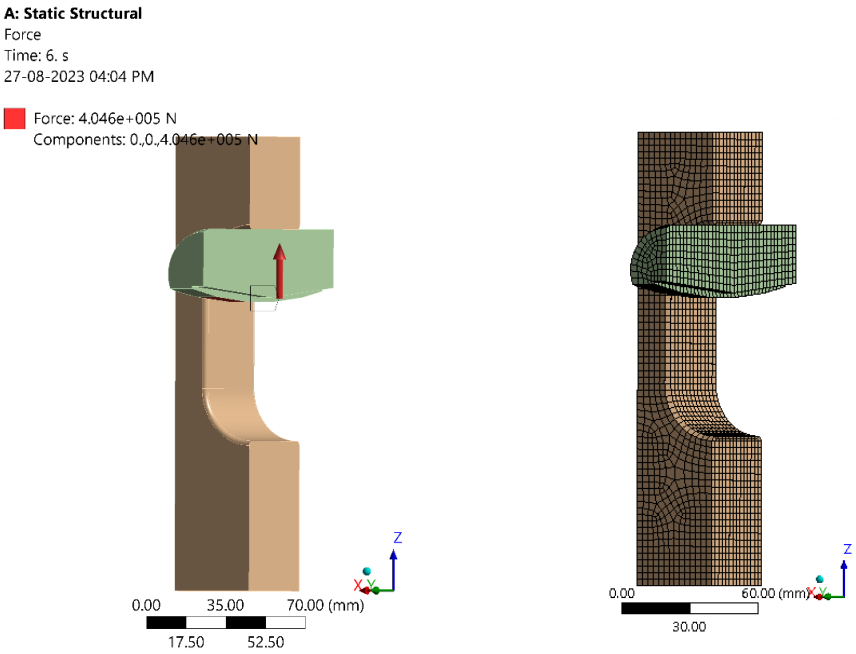

Figure 6.3: Illustration of simplified geometry

As the segment is validated compared to the experimental results, the boundary conditions on the block are applied. The block is allowed translational displacement in direction of applied load as shown in Figure 6.4.

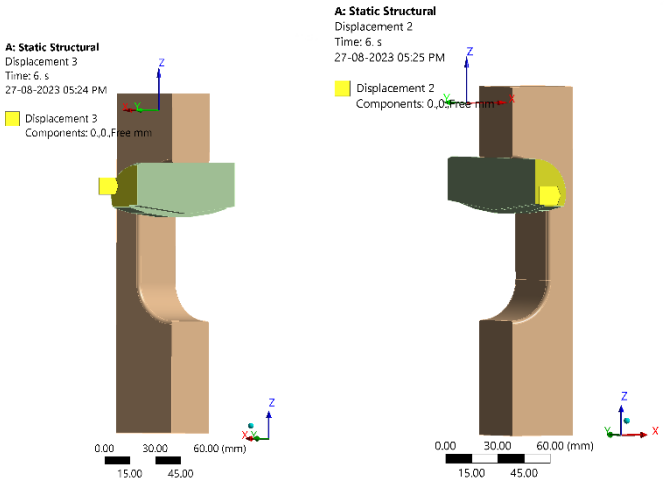

Figure 6.4: Boundary conditions for upper block

From the material certificate provided by C1 connections, the yield strength of 40mmx3000mm plate of S40NL grade is 485MPa. The material model for Ansys is generated based on this yield strength. The minimum elongation(plastic strain) at fracture is recorded as 23%.

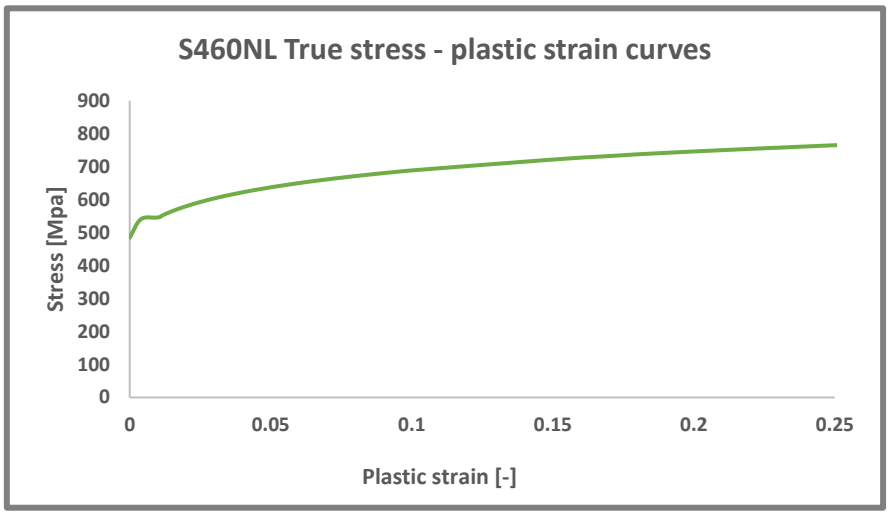

Figure 6.5: Stress strain curve for S460NL as per material certificate

6.3 Results

Analysis is expected to run till 23% plastic strain as per material certificate. Although, the damage material properties are not incorporated in Ansys, therefore the failure is considered at maximum plastic strain achievable. The relationship between applied load and plastic strain is presented in Figure 6.6. It can be observed that the plastic strain in the lower flange increases exponentially after application of around 800kN external load.

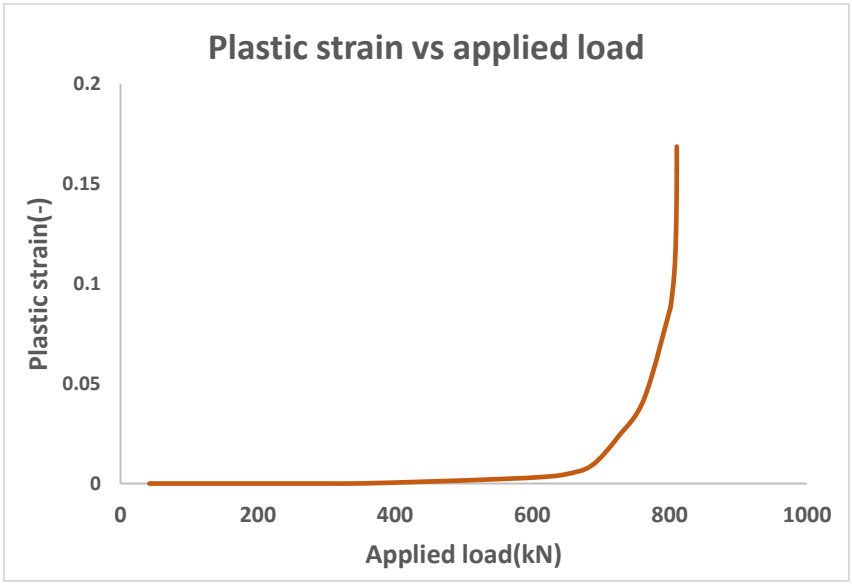

Figure 6.6: Relationship between applied load and plastic strain

Maximum achievable plastic strain is 16.8% as shown in Figure 6.7. ULS failure is considered at this plastic strain which equals 810.36kN. The results are comparable with Cheng's[8] result of 813kN for ULS failure. Experiment resulted in failure at 861kN. This variation can be explained with the material properties defined in Ansys. The results were validated and the

same methodology that has been used for this model could be applied to C1 wedge connection segment.

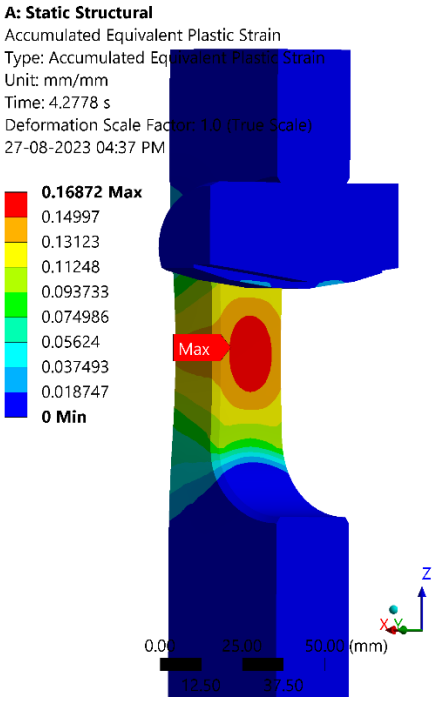

Figure 6.7: Maximum plastic strain in lower flange

7 Design of C1 wedge connection

In this chapter, design of C1 wedge connection for same overturning moment of 609MNm and 8m diameter of tower is discussed. Design tool provide by C1 connections is used to get the initial parameters for the components of the C1 wedge connection. Design tool is an automated tool developed to design the preliminary C1 wedge connection.

7.1 Nominal design

ULS resistance of C1 wedge connection is dependent on the wall thickness of the lower flange and the webs of the upper flange. As discussed in section 2.2.3, two factors are considered: the net stress between the holes and the contact pressure in the holes.

The input values for design tool to be entered are shown in Table 9 and the output dimensions and parameters are shown in Table 10.

Input			
ULS Load			
Description	**Symbol**	**Unit**	**Value**
Resulting design (factored) bending moment	$M_{res,d}$	MNm	609
Flange material grades			
Description			**Grade**
Upper and lower can material grade			S355NL
Lower flange material grade			S460NL
Upper flange webs material grade			S460NL
Upper flange crown material grade			S460NL
Upper can geometry			
Description	**Symbol**	**Unit**	**Value**
Upper can outer diameter	$D_{o,uc}$	mm	8000
Upper can nominal wall thickness	t_{uc}	mm	85
Lower can nominal wall thickness	t_{lc}	mm	85

Table 9: Input parameters for design of C1 wedge connection

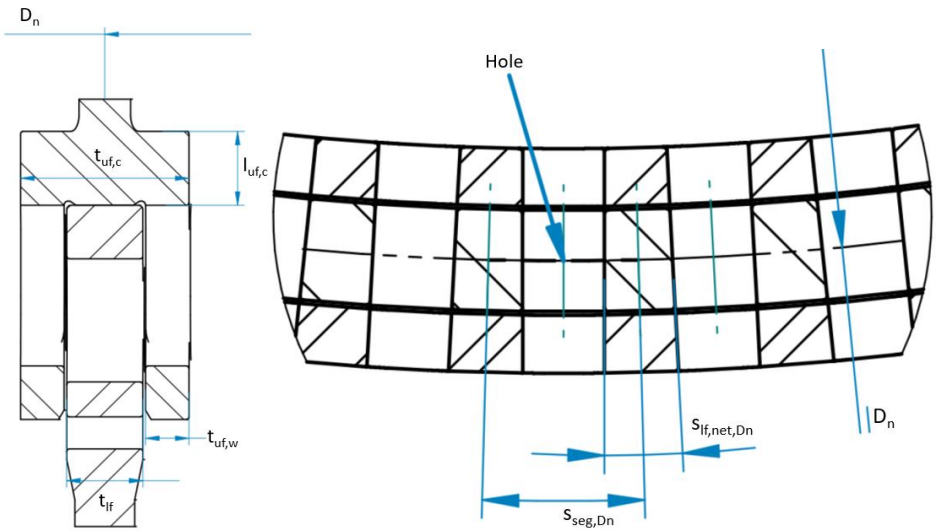

Figure 7.1: Parameters definition for C1 wedge connection

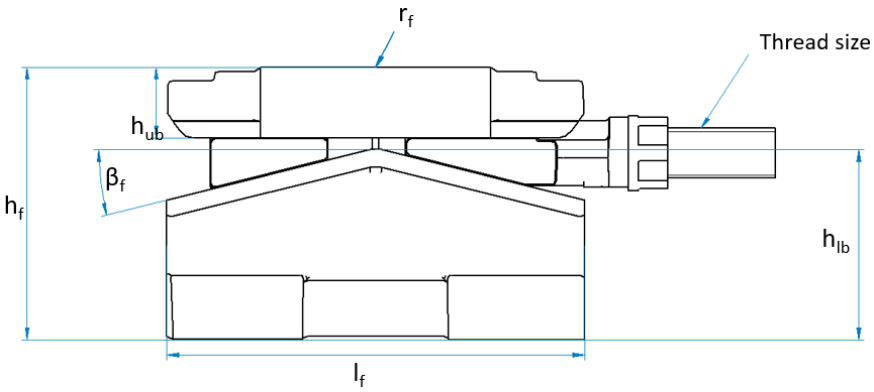

Figure 7.2: Parameters for C1 wedge fastener

Output			
Geometry			
Flange dimensions in radial direction			
Description	**Symbol**	**Unit**	**Value**
Neutral diameter of C1 Wedge Connection	D_n	mm	7915.0
Lower flange radial thickness	t_{lf}	mm	96
Upper flange single web radial thickness	$t_{uf,w}$	mm	67.0
Upper flange crown radial thickness	$t_{uf,c}$	mm	240
Flange dimensions in tangential direction			
Description	**Symbol**	**Unit**	**Value**
Segment arc length at neutral diameter	$s_{seg,Dn}$	mm	207
Net arc length between holes at neutral diameter	$s_{lf,net,Dn}$	mm	92
Flange dimensions in axial direction			
Description	**Symbol**	**Unit**	**Value**
Upper flange crown axial length	$l_{uf,c}$	mm	248
Fastener properties			
Description	**Symbol**	**Unit**	**Value**
Number of fasteners	n	-	120
Thread size	-	-	M42
Fastener radius	r_f	mm	50
Hole oversize for relative flange rotation	-	mm	15
Width of hole in flanges	s_{hole}	mm	115
Radius at edge of flange holes	$r_{hole\ edge}$	mm	5
Radius of alignment pin hole in LF	$r_{alignment\ pin}$	mm	30
Length of fastener	l_f	mm	240
Height of fastener	h_f	mm	180
Height of upper block	h_{ub}	mm	50
Height of lower block	h_{lb}	mm	120
Fastener slope beta	β_f	°	14
Material grade	-	-	30CrNiMo8

Table 10: Output from design tool

As discussed in section 2.2.4:

$$l_{seg} = 2.02 * D_{fastener} = 202\ mm$$

But to allow quick and alignment, the number of segments should be multiple of 6, therefore; number of segments=120 and l_{seg}= 207mm.

7.2 Segment load and preload

The design segment load based on $M_{res,d}$ of 609MNm is 2565kN. The nominal preload force to be generated using the fastener is 2565kN. As discussed in section 2.2.2,

$$F_{stud} = F_{pre} * \frac{1}{2} * \left(\mu + \left(\frac{\sin(\beta) + \mu * \cos(\beta)}{\cos(\beta) - \mu * \sin(\beta)} \right) \right)$$

$$F_{stud} = 0.165 * F_{pre}$$

$$F_{stud} = 434\text{kN}$$

Where $\beta = 0.244 radians, \mu = 0.04$

Fastener friction value is taken 0.04 based on testing with 34CrNiMo06 coated with ZnNi. As per VDI-2230-1, tightening factor, α_A = 1.05 is to be taken into account.

Therefore,

$$F_{stud,upper\ bound} = \frac{2 * F_{stud}}{1 + \frac{1}{1.05}} = 445\text{kN}$$

$$F_{pre,upper\ bound} = 2677kN$$

7.3 Design checks – flanges

Yield strength for plates based on thickness and EN 10025-3:2019 and yield strength and ultimate strength of fastener are given in Table 11.

Final material strength			
Description	**Symbol**	**Unit**	**Value**
Lower flange	$f_{y,lf}$	MPa	400
Upper flange web	$f_{y,uf,w}$	MPa	410
Upper flange crown	$f_{y,uf,c}$	MPa	370
Fastener - yield	$f_{y,f}$	MPa	900
Fastener - ultimate	$f_{ub,f}$	MPa	1040

Table 11: Material strength for components of C1 wedge connection

As per section 2.2.3, the design checks are performed and presented in tables below.

Interface between flanges - compression			
Description	**Symbol**	**Unit**	**Value**
Lower flange radial thickness final	t_{lf}	mm	96.0
Contact area between upper and lower flange	$A_{fl,contact}$	mm2	19893
Upper bound compressive load + highest preload	$F_{fl,contact,d}$	MN	5.242
Contact pressure	p_{fl}	MPa	263
Allowable pressure	$p_{fl,R}$	MPa	370

Design utilization		-	0.712
Lower flange design checks			
Contact pressure			
Description	**Symbol**	**Unit**	**Value**
Projected contact area	$A_{lf,proj}$	mm2	8600
Design contact pressure	$p_{lf,d}$	MPa	311
Material factor	$y_{M,p}$	-	1.25
Allowable pressure	$p_{lf,R}$	MPa	320
LF contact pressure design utilization		-	**0.973**
Net stress			
Description	**Symbol**	**Unit**	**Value**
Net area	$A_{lf,net}$	mm2	8853
Design load	$s_{lf,net}$	MPa	302
Material factor	$y_{M,net}$	-	1.1
Allowable stress	$s_{lf,R}$	MPa	364
LF net cross section design utilization		-	**0.832**

Upper flange			
Contact pressure			
Description	**Symbol**	**Unit**	**Value**
Projected contact area	$A_{ufw,proj}$	mm2	5700
Design contact pressure	$p_{ufw,d}$	MPa	235
Material factor	$y_{M,p}$	-	1.25
Allowable pressure	$p_{ufw,R}$	MPa	328
Design utilization		-	0.716
Net stress			
Description	**Symbol**	**Unit**	**Value**
Net area - both webs	$A_{uf,net}$	mm2	12357
Design load	$s_{uf,net}$	MPa	217
Material factor	$y_{M,net}$	-	1.1
Allowable stress	$s_{uf,R}$	MPa	336
Design utilization		-	0.644

8 FEA: C1 wedge connection

In this chapter, FEA for C1 wedge connection is discussed. C1 wedge connection designed in previous chapter has been modelled and analysed in Ansys. The purpose for this study is to get results for ULS criteria and make a comparison later with L-flange connection.

8.1 3D model

As per parameters finalized in previous section, 3D geometry was modelled as shown in Figure 8.1. 120 C1 wedge segments are present in the complete ring connection. One segment would be imported to Ansys as the connection is symmetrical and assumption is made that no imperfections are present.

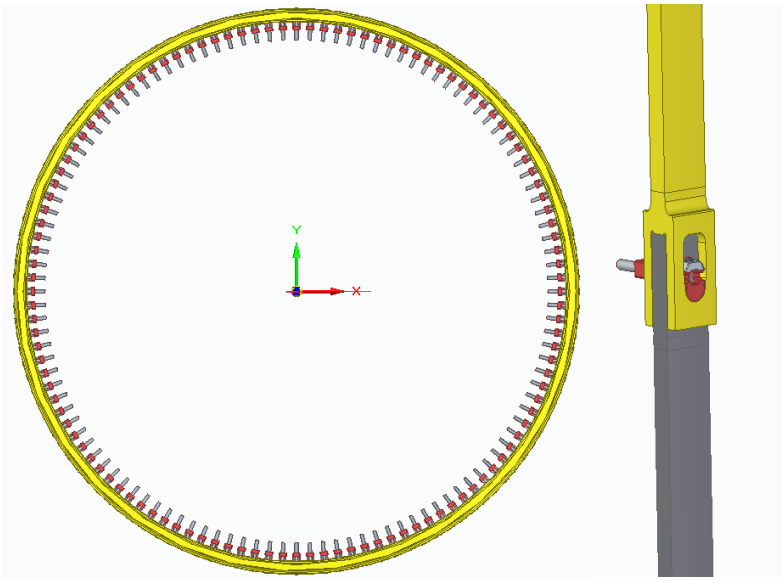

Figure 8.1: 3 D model and segment

8.2 Material model and mesh

The dimensions for the components of the connection are taken from Table 10. Thicknesses of the components and reduced yield strength as per EN 10025-3:2019 are presented in Table 11. Initial modulus of elasticity of E=210GPa and poisson's ratio of 0.3 is used. The washer is modelled with elastic material whereas flanges, shell and bolts are modelled using elastic-plastic material. As the segment is symmetric, half segment is analysed with appropriate boundary conditions to reduce computational time and cost.

Linear elements of size 10mm are used to mesh the components. Upper block and lower flange is meshed with 8mm elements, nut is meshed with 4mm elements and stud is meshed with 6mm elements.

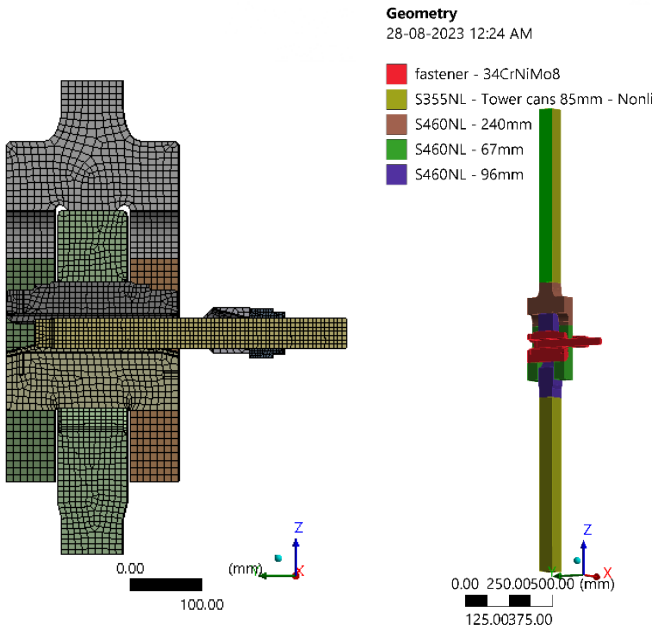

Figure 8.2: Mesh and material

8.3 Boundary conditions

As one of the 120 segments is cut from the geometry, the segment is analysed with the curvature of the ring. To account for the symmetry, left and right side of the half segment are restricted to displace in the normal direction. Therefore, 0mm displacement is applied on all the surfaces of left and right side of the half segment. The bottom of the segment is fixed to prevent rigid body movement. This is shown in Figure 8.3.

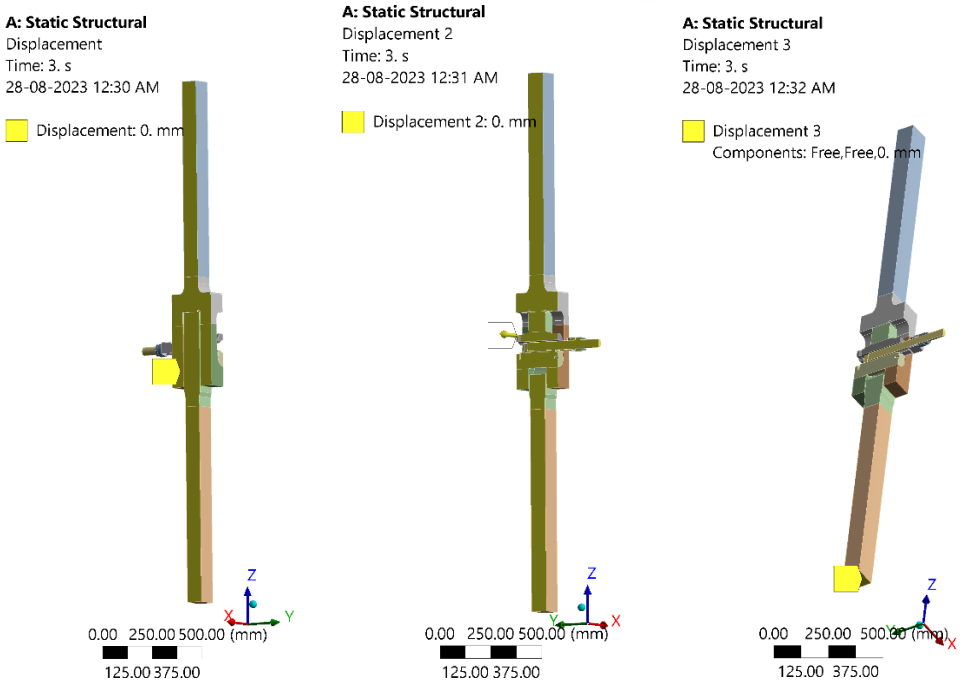

Figure 8.3: Boundary condition for C1 wedge half segment

8.4 Contacts

Frictional contacts are defined for interface, wedges to upper block and lower block, webs to lower block flange to upper block. Bonded contacts are defined for stud to nut and nut to outer wedge.

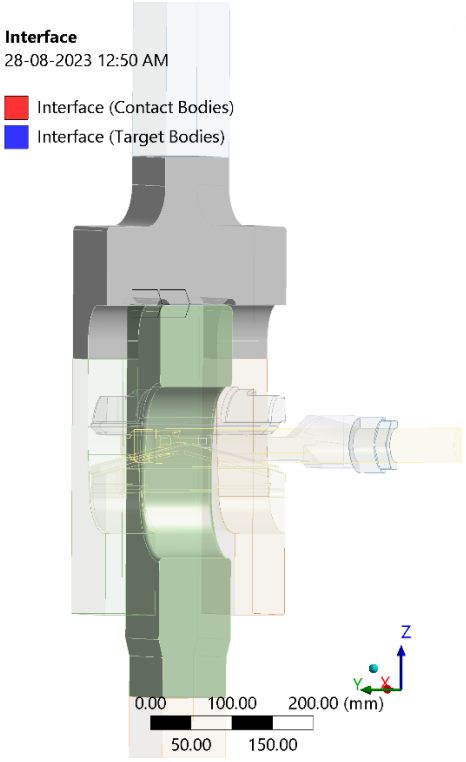

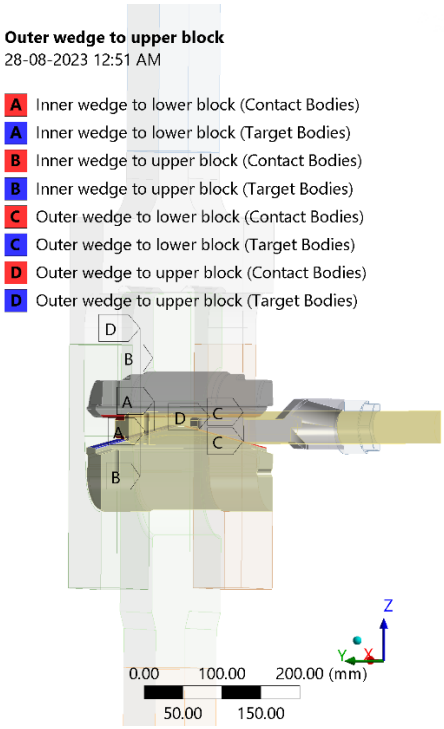

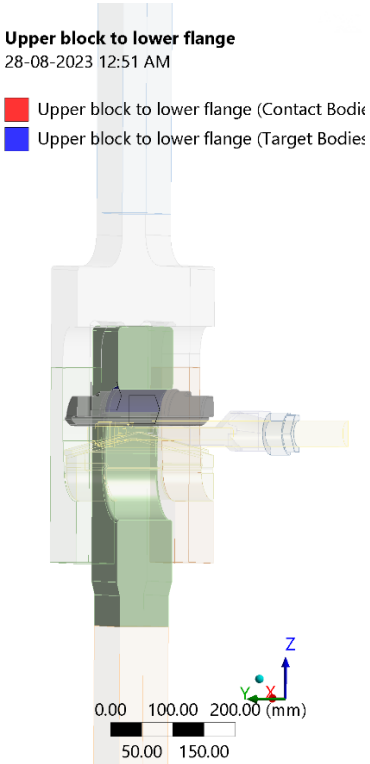

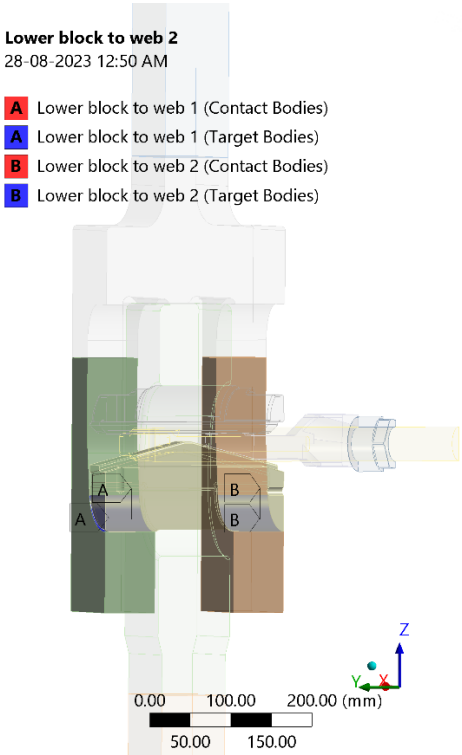

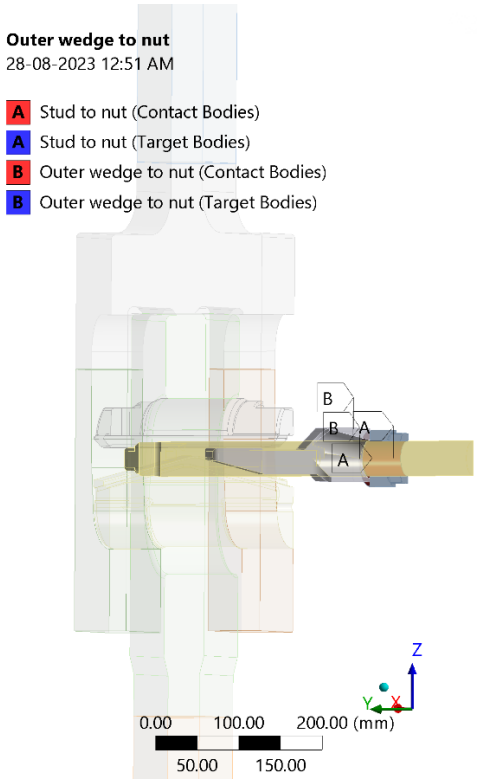

Contact surfaces identified, type of contact and friction coefficient are presented in Table 12.

Contact	Target	Type	μ
Upper Flange	Lower Flange	Frictional	0.4
Lower block	Web 1	Frictional	0.2
Lower block	Web 2	Frictional	0.2
Upper block	Lower flange	Frictional	0.2
Inner wedge	Lower block	Frictional	0.2
Inner wedge	Upper block	Frictional	0.2
Lower block	Outer wedge	Frictional	0.2
Lower block	Outer wedge	Frictional	0.2
Stud	Nut	Bonded	-
Outer wedge	Nut	Bonded	-

Table 12: Contacts definition

8.5 Preload and force

The preload is applied in the first substep to the stud in the longitudinal direction of the stud. Preload of 445kN as calculated in previous chapter is applied. The plot for the preload generated at the interface is presented in Figure 8.5. The preload generated at interface can be extracted at interface, reaction at contact of webs and lower block and contact at upper block and lower flange.

External load is applied in the second substep at the top of the shell as shown in Figure 8.4.

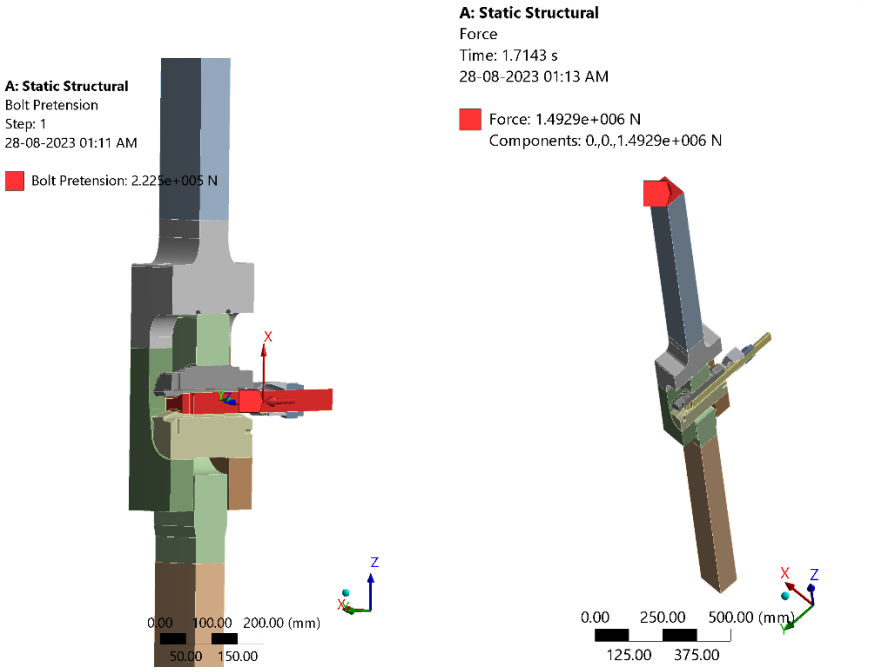

Figure 8.4: Stud pretension and force

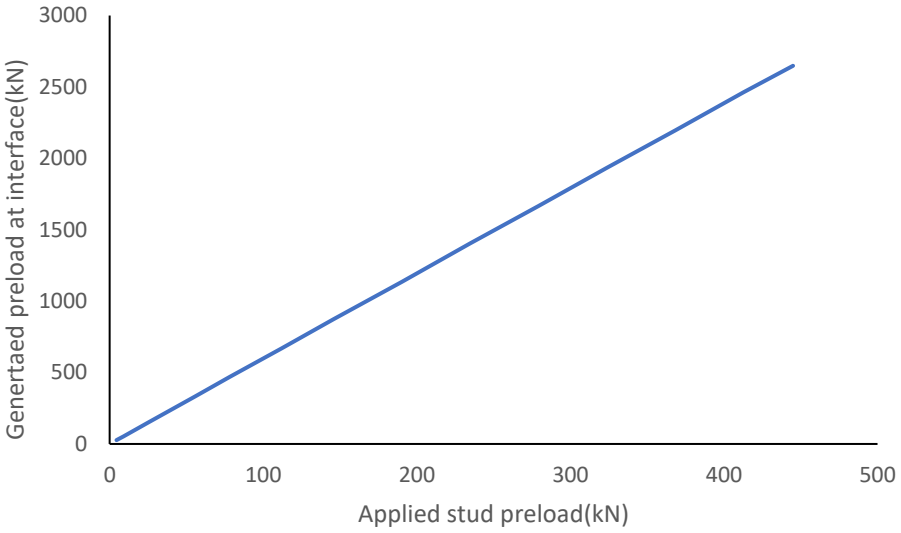

Figure 8.5: Generated preload at interface

The vertical preload is calculated at the interface between the upper flange and lower flange. It is seen that the vertical preload increases linearly with the horizontal load applied on the stud. The preload achieved is 2648kN compared to analytically calculated value of 2677kN. The variation in preload generated is 1.08% which is very low. The difference can be explained based on the movement of the flanges and webs and energy loss due to this movement.

8.6 Results

8.6.1 ULS resistance

ULS resistance is considered the load at which the lower flange of the connection reached 5% of plastic strain as per EN 1993-1-5[28] as shown in Figure 8.6. The load at 5% plastic strain is 3956kN(949MNm) which is 64% more than the design load of 2565kN.

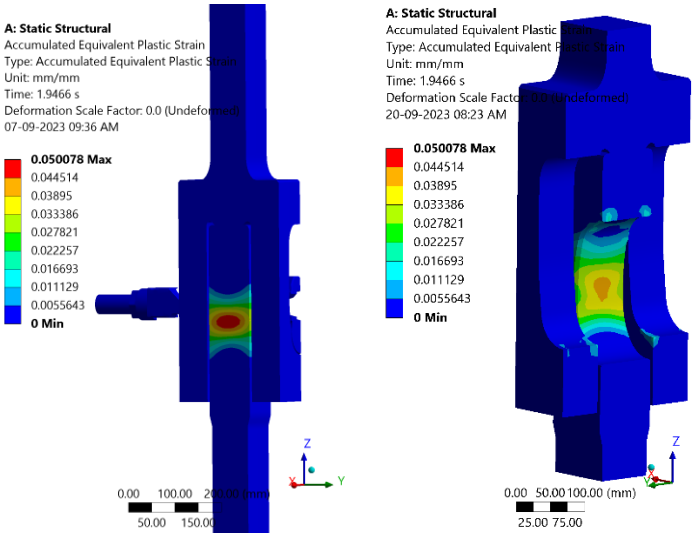

Figure 8.6: Plastic strain in lower flange

8.6.2 Load-displacement curve

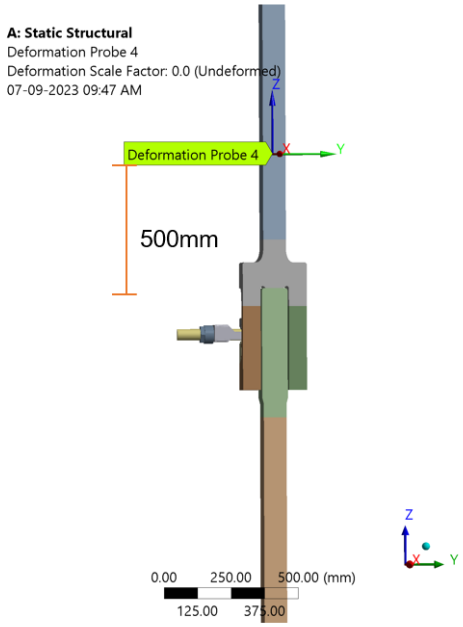

Figure 8.7: Deformation at top of shell

Deformation at 500mm above the interface of flanges is evaluated as shown Figure 8.7. Maximum deformation of around 7mm at ULS load of 3950kN is observed. Deformation till external applied of 3000kN is linearly proportional to applied load but the deformation increases rapidly for higher applied load. This change in load-displacement is indicative of plastic yielding and components reaching their stiffness peak. Deformation at 2565kN is around 2mm as shown in Figure 8.8.

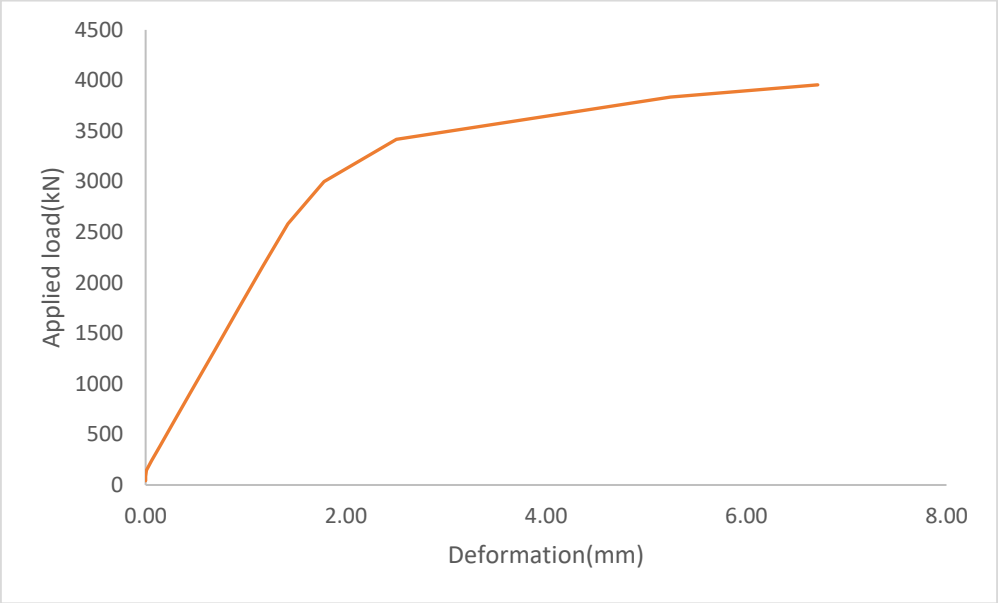

Figure 8.8: Load-displacement curve

8.6.3 Gap opening

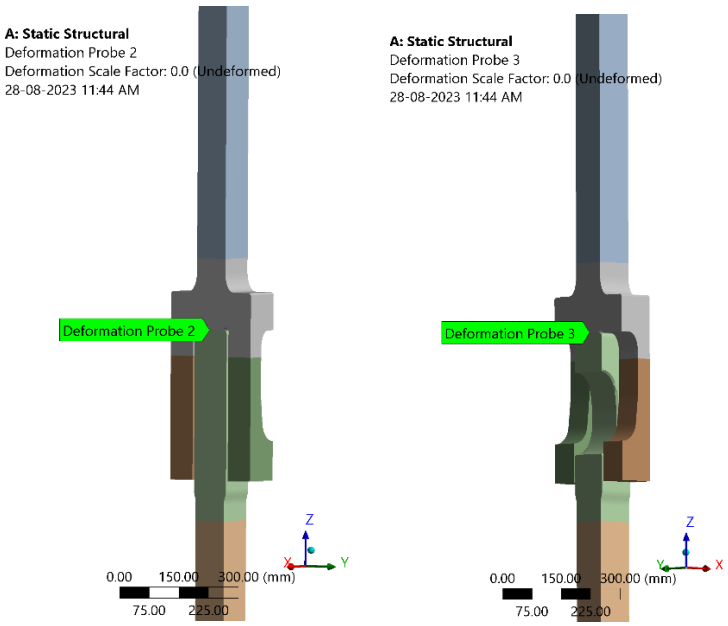

Figure 8.9: Deformation probes at interface

The opening of the connection can be inspected by measuring the gap between the upper flange and lower flange. This is measured in Ansys by evaluating the largest (minimum gap) and smallest (maximum gap) distance between contact surfaces. The results for the opening of the contact at interface is shown in Figure 8.10. The first gap opening is at 2165kN and full

opening is at 2582kN. The full opening can explained based on the preload generated at interface equal to 2628kN. At applied load of 2582kN, the preload at the interface is 0.

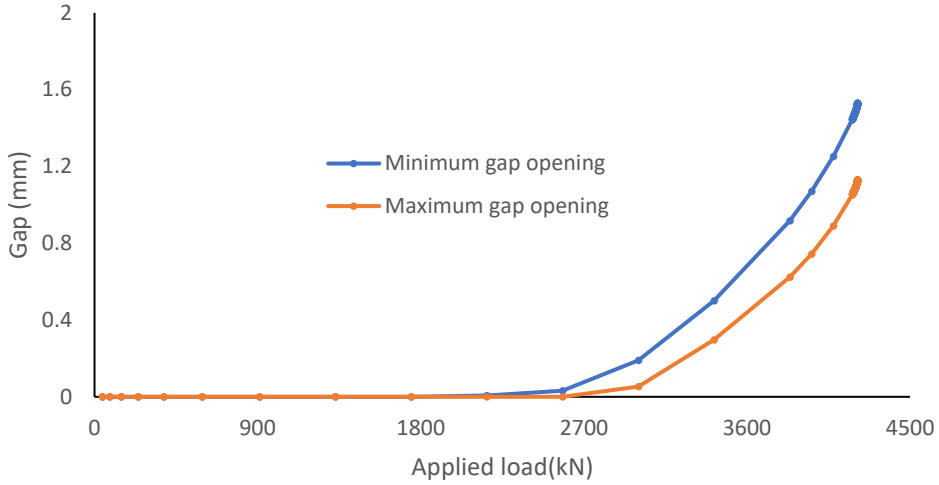

Figure 8.10: Minimum and maximum gap opening at interface

8.6.4 Mass of the connection

Mass of the C1 wedge connection mainly constitutes of mass of flange, upper crown and webs. Total weight of the connections is 28.8tonnes.

Description	Unit	
Upper flange crown as forged	Tonnes	11.6
Inner web	Tonnes	4
Outer web	Tonnes	4.2
Upper flange – total	Tonnes	19.8
Lower flange as rolled	Tonnes	9
Total weight	Tonnes	**28.8**

9 Optimization of C1 wedge connection

9.1 Optimization of webs

As discussed in previous chapter, the ULS resistance of C1 wedge connection is the failure of lower flange. To optimize the design the thickness of webs is reduced to allow almost equal net stress distribution in both flange and webs. For this, webs thickness have been reduced in 3 iterations from 67mm to 60mm, 53mm and 48mm respectively.

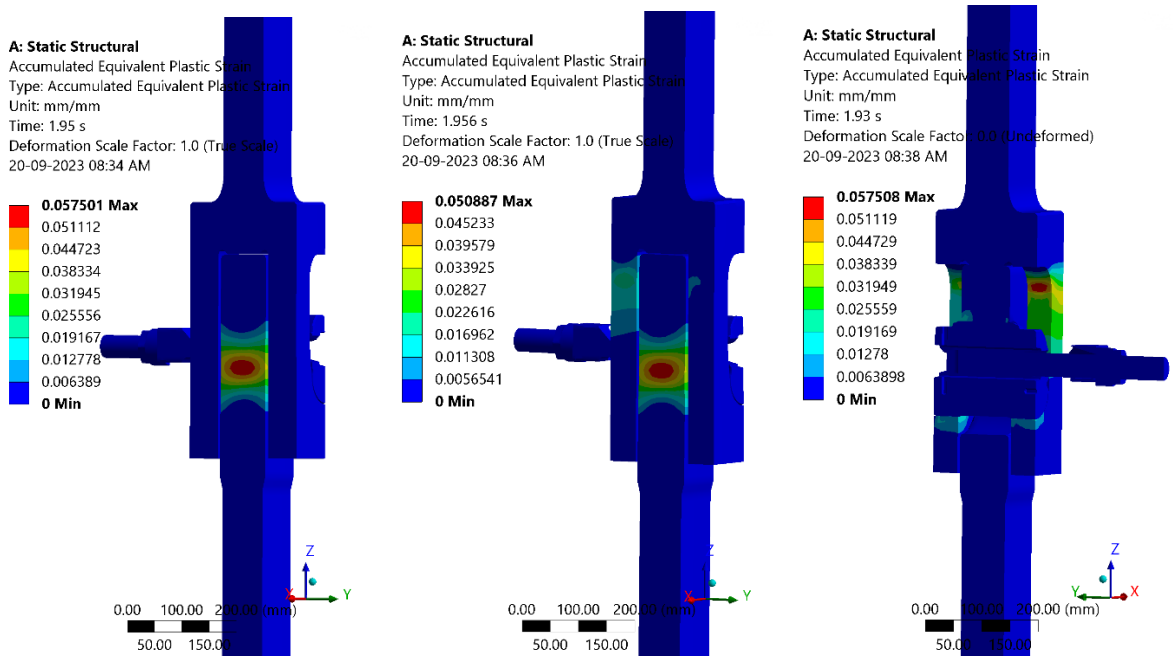

Figure 9.1: Plasticity in C1 wedge connection: 60mm(left), 53mm(middle) and 48mm(right)

As with 48mm of webs thickness, the net stress is equal analytically but in FEA the plasticity is highest in webs which could mean the failure of the webs before lower flange. This can be explained based on the bending of the webs. Therefore, the optimized design with 53mm thickness of webs is most appropriate. The ratio of web thickness to lower flange is 1.10.

		Web thickness			
Description	Unit	67mm	60mm	53mm	48mm
Upper flange crown as forged	Tonnes	11.6	10.6	9.9	9
Inner web	Tonnes	4	3.19	3.2	3
Outer web	Tonnes	4.2	3.77	3.3	3.1
Upper flange – total	Tonnes	19.8	17.56	16.2	15.1
Lower flange as rolled	Tonnes	9	8.9	8.8	8.8
Total weight	Tonnes	**28.8**	**26.5**	**25**	**23.9**

Table 13: Mass for C1 wedge connection

9.2 Optimization of flanges and webs

Further optimization carried out to design the connection for the ULS load as of the L-flange connection. L-flange segment had ULS resistance of 2506kN(787MNm) which is 30% higher than the design load of 1940kN(609MNm). Therefore, the aim is to reduce the dimensions of the C1 wedge connection to get the ULS strength 30% higher than the design load.

Optimized design is based on reducing the thickness of flange to reduce the net stress in the flange and the thickness of webs equal 1.1 times flange thickness as discussed in previous section. Hence,

Thickness of flange = 82mm
Thickness of webs = 45mm

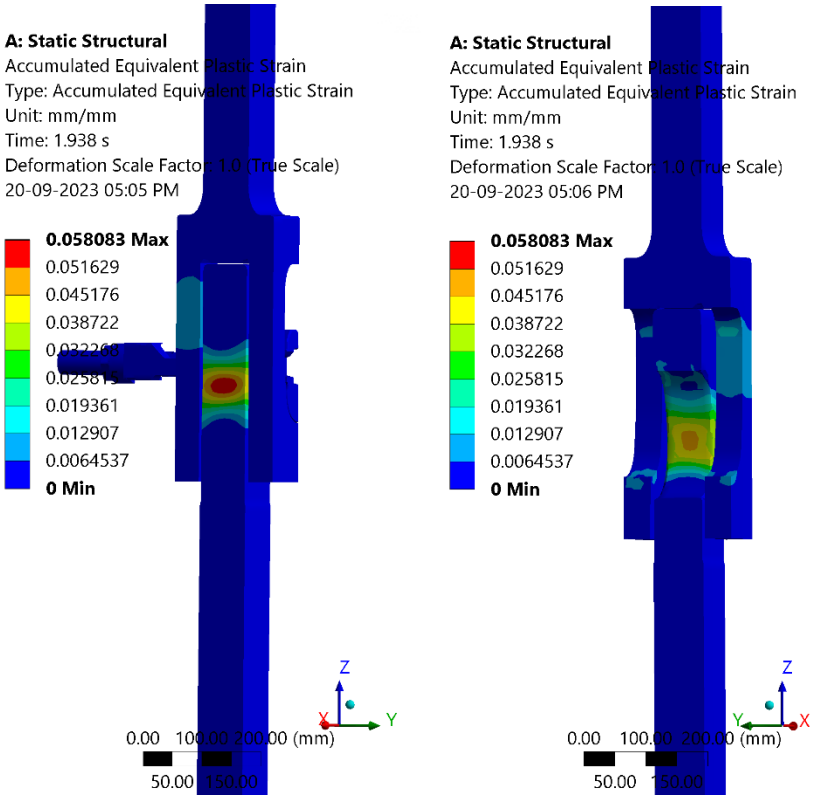

Figure 9.2: Plastic strain in optimized C1 wedge connection design

ULS resistance of the optimized connection is 3352kN(804MNm) which is almost equal to the L-flange ULS resistance. The corresponding mass:

		Web thickness	
Description	Unit	67mm	**45mm**
Upper flange crown- as forged	mt	11.6	**7.5**
Inner web	mt	4.0	**2.8**
Outer web	mt	4.2	**2.9**
Upper flange - Total	mt	19.8	**13.2**
Lower flange as rolled/forged	mt	9.0	**7.6**
Total weight	mt	28.8	**20.8**

10 Fatigue verification

The fatigue assessment is carried out for same design of tower and connections are designed for overturning moment. The design overturning moment is 609MNm and the diameter of the shell is 8m.

The critical components of L-flange connection are:

- Bolts
- Neck of the flange
- Circumferential(butt) welds

The critical components for C1 wedge connection are:

- Lower flange
- Circumferential(butt) welds

The welds in the upper flange webs are not critical as the fatigue loading is within the limit of preloading at the interface. Therefore, there are little stresses developed within that load spectrum. Also, the bolt force in the stud remains constant after preloading as the load transfer is through the crown of upper flange to lower flange through the interface.

10.1 Methodology

The fatigue assessment is carried out using Markov matrix. The fatigue life may be calculated based on the S-N fatigue approach under the assumption of linear cumulative damage (Palmgren-Miner rule) [2.2.1 DNV-RP-C203].

$$D = \sum_{i=1}^{k} \frac{n_i}{N_i} = \frac{1}{\bar{a}} \sum_{i=1}^{k} n_i (\Delta\sigma)^m \leq \eta = \frac{1}{DFF}$$

where:

D = accumulated fatigue damage

$\bar{a}$ = intercept of the design S-N curve with the log N axis

m = negative inverse slope of the S-N curve

k = number of stress blocks

n_i = number of stress cycles in stress block i

N_i = number of cycles to failure at constant stress range Δσi

η = usage factor

DFF = design fatigue factor

The Markov matrix is provided by C1 connections as presented in Table 14. The markov matrix consists of mean bending moment on the connection, moment range and their associated cycles for fatigue damage. The matrix is based on 10 million cycles and ULS moment of 748983kNm.

	Mean Moment [kNm]	Moment Range [kNm]	Cycles
0	-456470.00	12848.00	290.06
1	-431770.00	12848.00	1139.90
2	-407060.00	12848.00	5141.40
3	-382350.00	12848.00	98348.00
4	-357640.00	12848.00	470350.00
5	-332930.00	12848.00	1884000.00
…	…	…	…
448	334180.00	115630.00	5175.80
449	334180.00	141330.00	5376.20
450	358880.00	12848.00	775960.00
451	358880.00	38544.00	878.78
452	383590.00	12848.00	84653.00
453	408300.00	12848.00	3985.60

Table 14: Markov matrix

This matrix was scaled down to ULS moment of 609000kNm by multiplying the mean moment and moment range by the ratio:

(609000/748983)=0.813

The scaled matrix is provided in Table 15.

	Mean Moment [kNm]	Moment Range [kNm]	Cycles
0	-371157.07	10446.75	290.06
1	-351073.43	10446.75	1139.90
2	-330981.66	10446.75	5141.40
3	-310889.89	10446.75	98348.00
4	-290798.11	10446.75	470350.00
5	-270706.34	10446.75	1884000.00
…	…	…	…
448	271722.72	94019.09	5175.80
449	271722.72	114915.83	5376.20
450	291806.36	10446.75	775960.00
451	291806.36	31340.24	878.78
452	311898.13	10446.75	84653.00
453	331989.91	10446.75	3985.60

Table 15: Scaled Markov matrix

10.2 Results

The fatigue damage for respective components of L-flange and C1 wedge connection are presented in Table 16.

Description	Fatigue damage(%)	Governing fatigue damage
L-flange		
Bolt	5.9	**134.4**
Neck of the flange	14.2	
Circumferential welds	134.4	
C1 wedge connection		

Lower flange (nominal design)	76.6	**76.6**
Circumferential welds	38.6	
Lower flange (optimized design)	321.3%	**321.3%**

Table 16: Comparison of fatigue damage

Detailed calculations are presented in Appendix B.

10.3 Stress concentration factors(SCF)

Butt welds have higher fatigue damage as compared to other components. Tensile residual stresses post welding increases the mean stress. Stress concentration factors for L-flange butt welds and C1 wedge butt welds for tensile loading is calculated based on nominal stress and stress extracted from FEA.

Highest SCF of 1.84 is observed for L-flange butt welds for tensile loading. For C1 wedge butt welds, the highest SCF is 1.21.

It can be concluded that tress distribution in C1 wedge connection is better than L-flange connection and the butt welds in C1 wedge connection provide better fatigue life.

11 Conclusion and recommendations

In this chapter, the findings from the study are discussed and concluded, that allows an answer to the main research question:

"How do the higher overturning moment influence the design of the traditional L-flange connection vs the C1 wedge connection?"

11.1 Conclusions

Based on the results obtained in the previous chapters, the following conclusions can be made for L-flange and C1 wedge connection:

- The design of the connections is primarily based on the ULS criterion with design load of 609MNm. The bolt is the governing failure component for L-flange connection and lower flange is the governing failure component for C1 wedge connection.
  The ULS resistance offered by L-flange connection is comparatively lower than the C1 wedge connection. C1 wedge connection has ULS resistance of 949MNm which is 55% higher than the design load whereas L-flange connection has ULS resistance of 787MNm which is only 30% higher ULS compared to the design load.

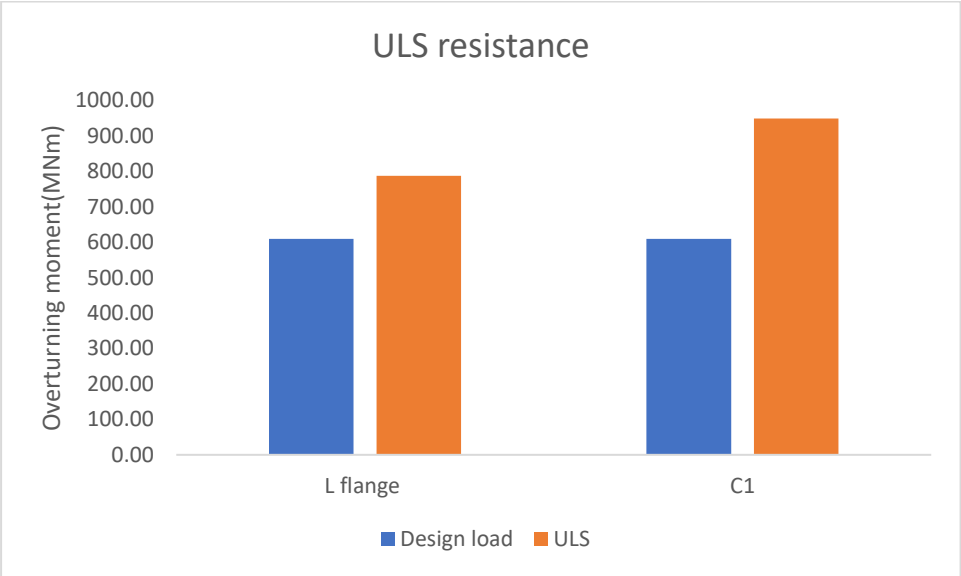

Figure 10.1: ULS resistance of L-flange and C1 wedge connection v/s design load

- C1 wedge connection used preload force in bolt more efficiently to generate higher contact force at the interface than compared to L-flange connection as L-flange connection is an eccentric connection. Load transfer in C1 wedge connection is through primary path till the interface opens.

- The gap opening at the interface for C1 wedge connection is after the applied load has surpassed the contact force generated through preloading of stud whereas L-flange connection starts opening at the start of the tensile load application and sooner the secondary load path is activated.

- L-flange connection has higher deformation than C1 wedge connection at the same elevation in the shell of the tower. The deformation is inversely proportional to the stiffness of the structure. Therefore, the L-flange connections offers less stiffness as compared to the C1 wedge connection.

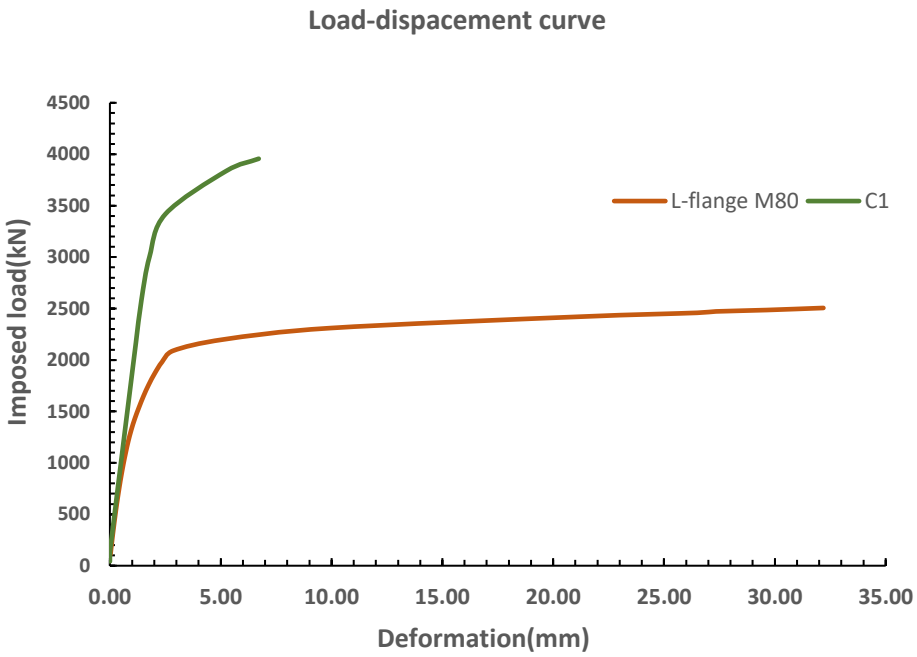

Figure 10.2: Displace curve for L-flange and C1 wedge connection at 500mm above the level of of interface of flanges

- L-flange connection has fatigue damage of 134.4% or service life of 22.32 years for the butt welds for which the shell thickness has to be increased. C1 wedge connection has fatigue damage of 76.6% or service life of 39.1 years for the lower flange. This impacts the thickness of the shell for the tower and leads to a reduction in mass and cost for the C1 wedge connection.

- Higher stress concentration factors are also observed at the location of circumferential butt welds in L-flange connection (1.84) than compared to the C1 wedge connection (1.21).

- Optimized C1 wedge connection for ULS criterion had fatigue damage of 321% or service life of 9.3 years as compared to fatigue damage of 134.4% or service life of 22.32 years for L-flange connection. Therefore, the optimized C1 wedge connection performs better for ULS criterion only.

- For the same design load of 609MNm, L-flange connection weights 53.72 tonnes and C1 wedge connection weighs 28.8 tonnes. C1 wedge connection has a comparable lower mass than that of L-flange connection.

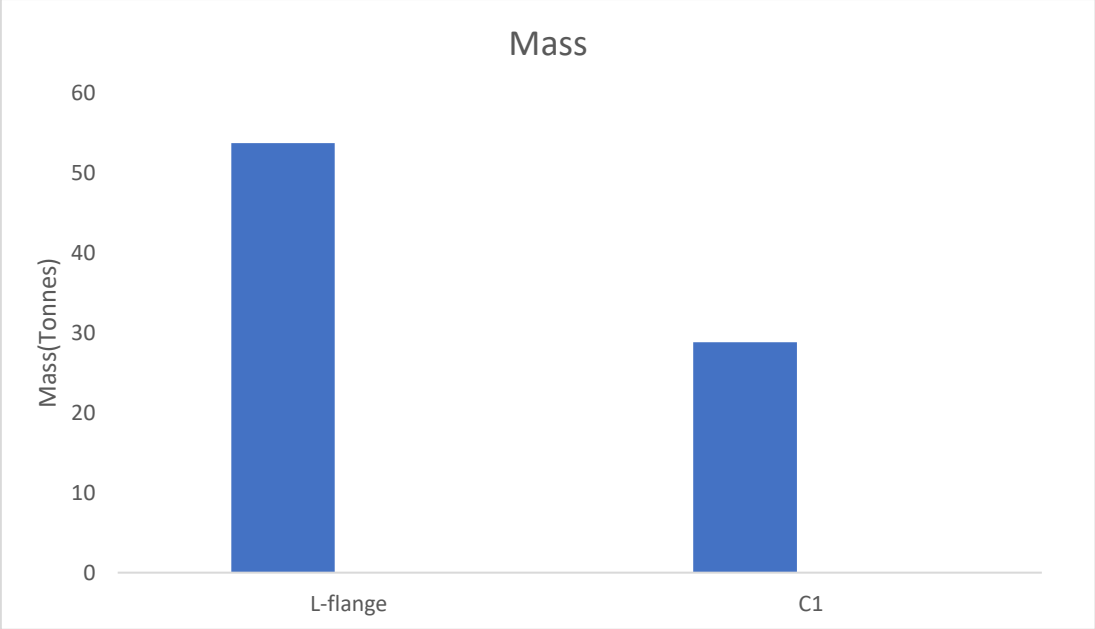

Figure 10.3: Mass of steel for L-flange and C1 wedge connection

It can be concluded that C1 wedge connection promises higher ULS and FLS capacity for the connections in offshore industry utilising the material used in a more efficient way.

11.2 Limitations

- The design of L-flange connection was translated to single segment which resembles well for ULS criteria but for fatigue criteria, it is almost impossible to fabricate/machine perfect components. Therefore, the imperfections play an important role which is not considered in this study.

- Mesh in FEA plays an important role. As the student license was used for the study which provides limited number of elements and nodes, the mesh was roughly spaced for few components and a mesh sensitivity analysis should be carried out.

- The design of the connection was based on the overturning moment which would be different for changing elevation of the tower. Therefore, the study should be done to automize the design of connection.

- Torque moment and self-weight of the tower and turbine is not considered in the study.

11.3 Future research recommendations

- In the thesis, the influence of imperfections/gap at the interface of flanges is not considered. The influence of imperfections would result in the additional bolt force to be generated in L-flange connection and higher stress in the lower flange of the C1 wedge connection. This would reduce the fatigue life of the connections. Therefore, it should be further investigated.

- The study is done for the diameter of the tower of 8m. However, with increasing wind turbine capacity, the diameter of the towers will increase up to 12m. Therefore, the design of the connections can be parametrized for the different dimensions of the towers.

- In this thesis, only overturning moment is considered. Torque moment and self-weight of the tower and wind turbine is neglected. Also, wave loads are neglected. It should be beneficial to study the behaviour of the connection considering all the loads at the connection level.

- The connection designed are assumed to be at a certain elevation on the tower. However, multiple connections are present at different levels of the tower. Therefore, it should be further investigated the effect of elevation of the tower for the design of the connections.

  .

References

1. Petersen, C., *Stahlbau: Grundlagen der Berechnung und baulichen Ausbildung von Stahlbauten*. 2012: Springer-Verlag.
2. Cheng, L., H. Xin, and M. Veljkovic, *Numerical analysis of ring flange connection with defined surface area.* ce/papers, 2021. **4**(2-4): p. 182-188.
3. WindEurope. *Financing and Investmentr Trends-the European Wind Industry in 2020*. 2021.
4. Selot, F., D. Fraile, and G. Brindley, *The european offshore wind industry-key trends and statistics 2018*. 2019, Tech. rep., WindEurope.
5. Weijtjens, W., et al., *Bolted ring flanges in offshore-wind support structures-in-situ validation of load-transfer behaviour.* Journal of Constructional Steel Research, 2021. **176**: p. 106361.
6. Schaumann, P. and R. Eichstädt. *Fatigue assessment of high-strength bolts with very large diameters in substructures for offshore wind turbines*. ISOPE.
7. Creusen, K.E.Y., et al., *Introducing the C1 wedge connection.* Steel Construction, 2022. **15**(1): p. 13-25.
8. Cheng, L., et al., *The C1 wedge connection in towers for wind turbine structures, tensile behaviour of a segment test.* Engineering Structures, 2023. **282**: p. 115799.
9. Gamesa, S. *Offshore Wind Turbines*. Available from: https://www.siemensgamesa.com/products-and-services/offshore.
10. Training, H.S. *Manual Handling Weight Limits: What are the Safe Lifting Guidelines and Techniques?* 2021.
11. Schaumann, P., R. Eichstädt, and A. Stang, *Advanced performance assessment methods for high-strength bolts in ring-flange connections.* Stahlbau, 2018. **87**(5): p. 446-455.
12. Gollub, P., et al., *Flanged foundation connection of the Offshore Wind Farm Amrumbank West–Concept, approval, design, tests and installation.* Stahlbau, 2014. **83**(8): p. 522-528.
13. Maljaars, J. and M. Euler, *Fatigue SN curves of bolts and bolted connections for application in civil engineering structures.* International Journal of Fatigue, 2021. **151**: p. 106355.
14. Creusen, K., *Design and analysis of a wedge connection for offshore foundations.* 2017.
15. Fric, N., et al. *Wind towers-design of flange ring connection*. in *Proceedings of the 14th international symposium of MASE*. 2011.
16. Seidel, M., *Zur Bemessung geschraubter Ringflanschverbindungen von Windenergieanlagen.* 2001.
17. Schaumann, P. and M. Seidel, *Fatigue loads of bolted ring flange connections in wind energy converters.* Stahlbau, 2002. **71**(3): p. 204-210.
18. Tobinaga, I. and T. Ishihara, *A study of action point correction factor for L-type flanges of wind turbine towers.* Wind Energy, 2018. **21**(9): p. 801-806.
19. *IEC 61400-6 Wind energy generation systems - Part 6: Tower and foundation design requirements.* 2020.
20. 1993-1-8:2005, E., *Eurocode 3: Design of steel structures - Part 1-8: Design of joints (Standard No. EN 1993-1-8).* 2005.
21. 1993-1-1, E., *Eurocode 3: Design of steel structures - Part 1-1: General rules and rules for buildings*. 2005.
22. Cheng, L., et al., *FE-assisted investigation for mechanical behaviour of connections in offshore wind turbine towers.* Engineering Structures, 2023. **285**: p. 116039.
23. Seidel, M., et al., *Full-scale validation of FE models for geometrically imperfect flange connections.* Journal of Constructional Steel Research, 2021. **187**: p. 106955.
24. Schaumann, P. and F. Marten. *Fatigue resistance of high strength bolts with large diameters*.
25. Technology, I.B., *Technical requirements for the use of bolt tensioning cylinders*.

26. ANSYS, *ANSYS Mechanical APDL Element Reference*. 2011.
27. DNV, *DNVGL-ST-0126: Support structures for wind turbines*. 2018.
28. *Eurocode 3 - Design of steel structures - pPart 1-5: Plated structural elements*. 2006.
29. C1Connections, *003-007 - ULS Test Report*. 2021.

Appendix A: Results from Cheng's[2] study

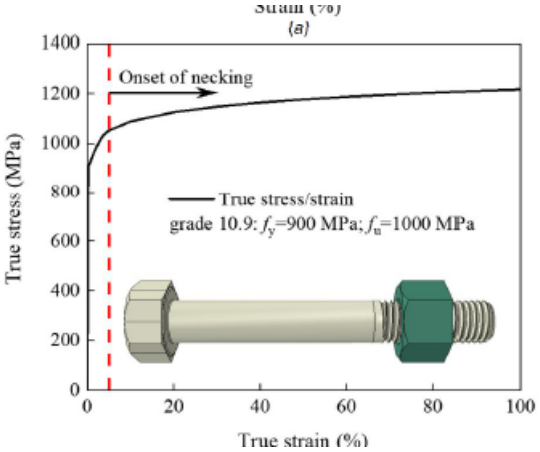

Figure A.1: Bolt material model

Case	Max. load (kN)	Max. bolt force (kN)	Displ.at max. load (mm)	Displ. at failure (mm)
RF-PT	915.5	1641.5	10.6	26.5
RFD-PT	917.1	1644.0	10.4	26.1
RF-FT	835.5	1474.3	15.7	46.6
RFD-FT	834.2	1476.1	17.6	46.8

Figure A.2: Displacement

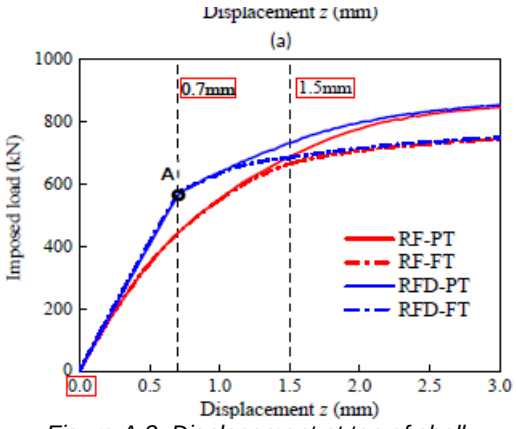

Figure A.3: Displacement at top of shell

Failure mode	Petersen's approach (kN)		FE results (kN)	
	$F_{t,Rd}=0.9f_{ub}A_s$	$F_{t,Rd}=f_{ub}A_s$	Case	F_U
$F_{U,A}$	1392	1546	RF-PT /RFD-PT	916
$F_{U,B}$	792	881	RF-FT/RFD-FT	835
$F_{U,C}$	801	801		

Figure A.4: ULS resistances

Appendix B: Detailed fatigue calculations

L-flange connection

The minimum and maximum of the force range spectrum is used as the load envelope for FE analysis.

$\max(F_{\max}) = 1394\ kN$ and $\min(F_{min}) = -1433kN$

Bolt

The critical location for bolt lies near the nut as shown in Figure B.. This is in order with results from Lu' results[22] .

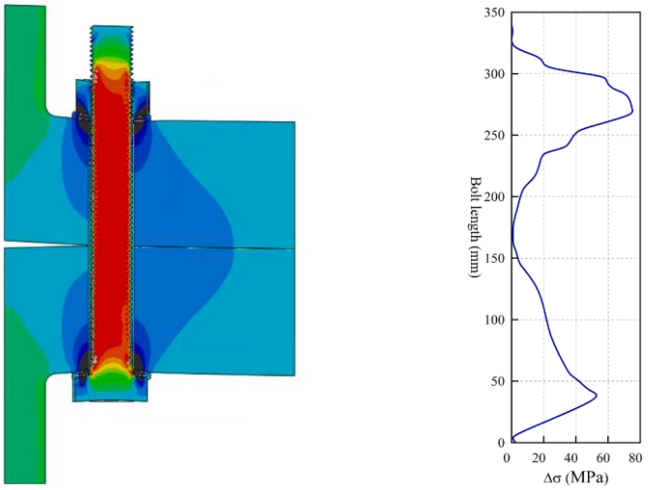

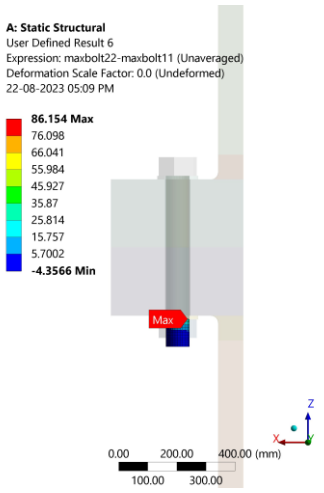

Figure B.1: Critical location for bolt

The M80 bolt is the L-flange connection is preloaded which makes it less susceptible to fatigue damage. The fatigue cracks could propagate at the threads which could be disastrous. Therefore, it is necessary to check the bolts for fatigue damage.

The fatigue damage in bolts is calculated using both normal stress method and peak stress method.

Normal stress is calculated as:

$$\Delta\sigma = F_b/A_s + M\ d_{bolt}/2.I_{bolt}$$

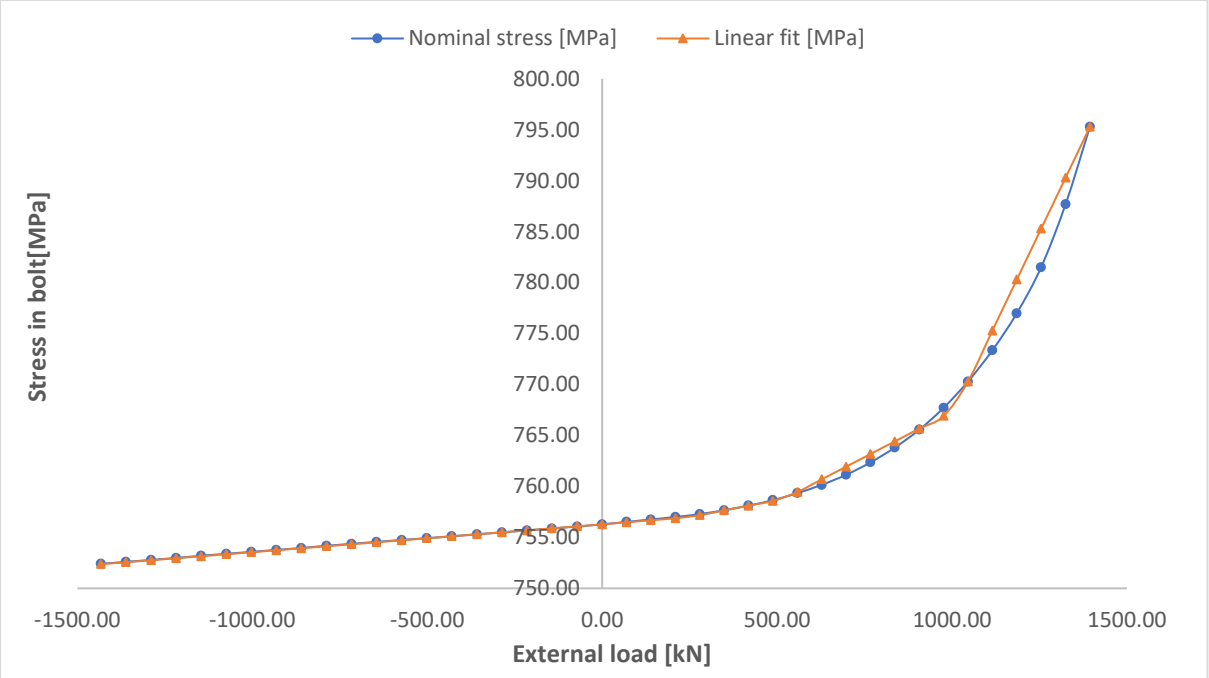

Peak stress is extracted from Ansys for the node that experiences the highest stress range and is plotted against applied external load as shown in **Error! Reference source not found.**. T he plot is then transformed using the fit transfer function to get the linear fit as shown in Table 17.

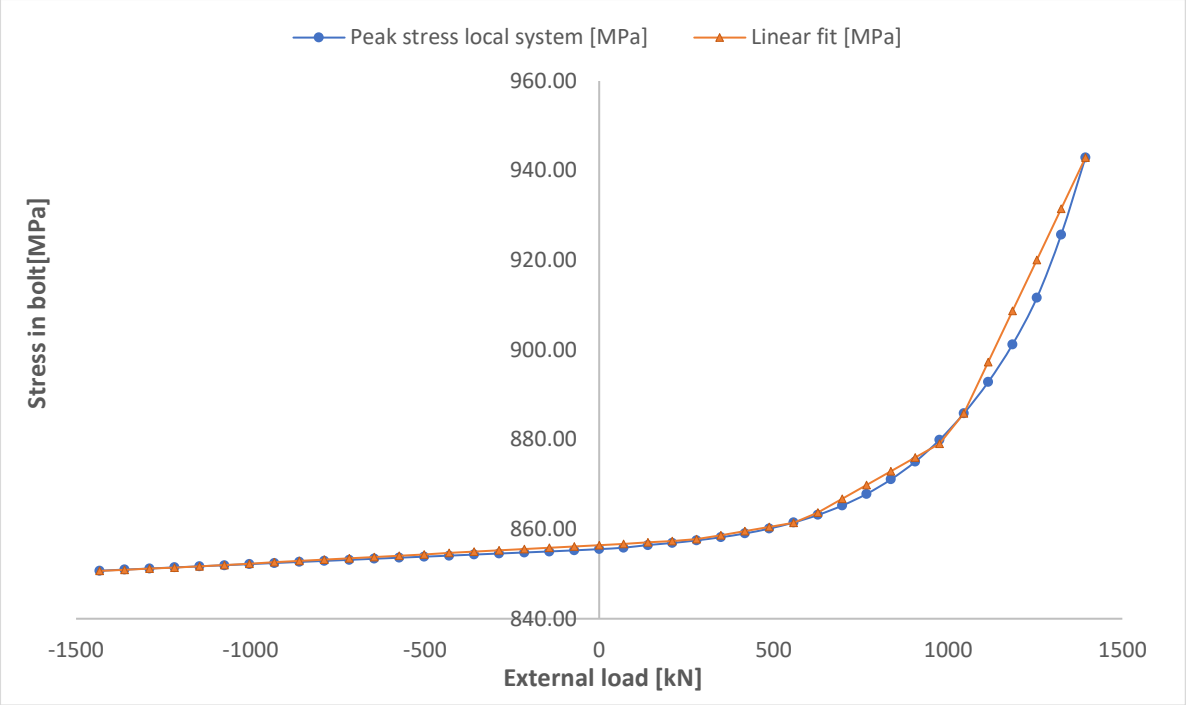

Fit transfer function			
	Nominal stress	Peak stress	Units
slope1 b1 Intercept1	0.003 756.3 0	0.00 855.53 -1212.72	[MPa/kN] MPa kN
Slope2 b2 intercept2	0.003 756.3 253.8	0.00 856.44 263.05	[MPa/kN] MPa kN
Slope3 b3 Intercept3	0.0067 755.3 521.85	0.01 854.08 582.84	[MPa/kN] MPa kN
Slope4 B4 Intercept4	0.017 750 1006.1	0.04 836.00 1015.01	[MPa/kN] MPa kN
Slope5 B6	0.072 695.3	0.164 714.5	[MPa/kN] MPa

Table 17: Fit transfer function for bolt stress

Using this fit transfer function(nominal stress), the stress range at every external load in the Markov matrix is calculated.

	F_{max} [kN]	**σ_{max} [MPa]**	**F_{min} [kN]**	**σ_{min} [MPa]**
0	-1309.95	752.70	-1347.34	752.60
1	-1238.05	752.90	-1275.45	752.80
2	-1166.13	753.10	-1203.53	752.99
3	-1094.21	753.29	-1131.60	753.19
4	-1022.28	753.49	-1059.68	753.39
5	-950.36	753.69	-987.76	753.58

…	…	…	…	…
448	1140.98	777.12	804.41	763.85
449	1178.38	779.81	767.01	763.18
450	1063.29	771.55	1025.89	768.87
451	1100.69	774.24	988.50	767.13
452	1135.21	776.71	1097.82	774.03
453	1207.14	781.87	1169.74	779.19

The basic design S-N curve is given as:

$$\log N = \log \bar{a} - m \log \Delta\sigma \left(\frac{t}{t_{ref}} \right)^k$$

Where:

N = predicted number of cycles to failure for stress range Δσ

$\Delta\sigma$ = stress range [MPa]

m = negative inverse slope of S-N curve

$\log \bar{a}$ = intercept of the design S-N curve with the log N-axis by S-N curve

K = 0.25 (for bolts)

The calculation procedure for entry 2 using S-N curve G is shown below:

The stress range:

$$\Delta\sigma = \sigma_{max} - \sigma_{min} = 0.11MPa$$

For N ≤ 10^6 cycles, m_1=3 and $\log \bar{a}$ =11.398:

$$\log N = 11.398 - 3 * \log (0.11 * 1.338)$$

$$N = 9.806 * 10^{13} > 10^6$$

For N ≥ 10^6 cycles, m_2 =5 and $\log \bar{a}$ =14.33

$$\log N = 14.33 - 5 * \log(0.11 * 1.338)$$

$$N = 4.49 * 10^{18}\ cycles$$

The fatigue damage under this stress range is:

$$\frac{n_i}{N_i} = 1.14 * 10^{-15}$$

The same procedure is carried out for all the entries in the Markov Matrix. The total fatigue damage can be calculated:

$$D = \sum_{i=1}^{k} \frac{n_i}{N_i} = 0.00329 \leq \eta = \frac{1}{DFF}$$

The design fatigue damage (using nominal stress approach)

$$D * DFF = 0.00329 * 3 = 0.0098 = 1\%$$

The same procedure is applied for peak stress method and the design fatigue damage:

$$D * DFF = 0.0196 * 3 = 0.059 = 5.9\%$$

Hence, it can be concluded that peak stress method gives more accurate fatigue damage.

Neck of the flange

The critical location for the neck of the flange is found in Ansys with maximum stress range as shown in Figure. Maximum and minimum principal stresses are extracted at this node for applied external load and plotted.

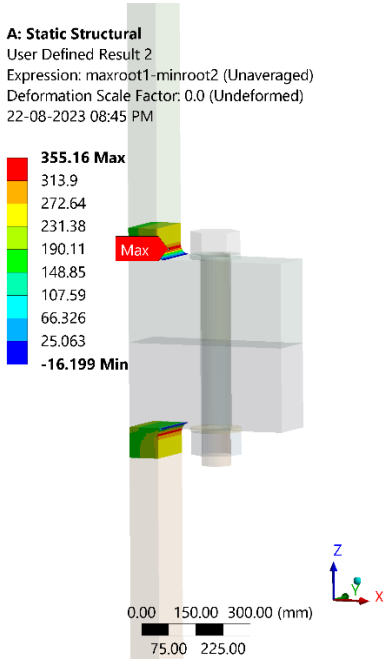

Figure B.2: Location of maximum stress range for neck of the flange

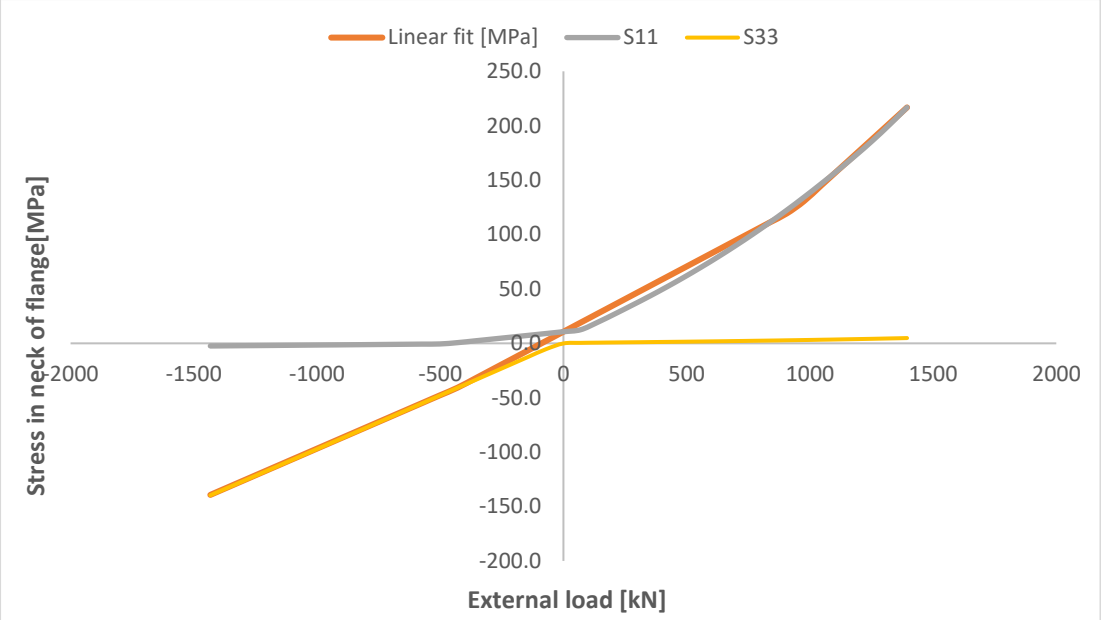

Fit transfer function		
Slope1	0.098	[MPa/kN]
b1	1.4	MPa
Intercept1	-424.7	kN
Slope2	0.120	[MPa/kN]
b2	10.7	MPa
intercept2	942.5	kN
Slope3	0.206	[MPa/kN]
b3	-70.5	MPa

Using this fit transfer function, the stress range at every external load in the Markov matrix is calculated.

	F_{max} [kN]	**σ_{max} [MPa]**	**F_{min} [kN]**	**σ_{min} [MPa]**
0	-1309.95	-127.21	-1347.34	-130.89
1	-1238.05	-120.15	-1275.45	-123.83
2	-1166.13	-113.09	-1203.53	-116.76
3	-1094.21	-106.02	-1131.60	-109.70
4	-1022.28	-98.96	-1059.68	-102.63
5	-950.36	-91.90	-987.76	-95.57
…	…	…	…	…
448	1140.98	164.61	804.41	107.16
449	1178.38	172.32	767.01	102.67
450	1063.29	148.61	1025.89	140.90
451	1100.69	156.31	988.50	133.20
452	1135.21	163.43	1097.82	155.72
453	1207.14	178.25	1169.74	170.54

DNV-RP-C203 states that for fatigue analysis of regions in base material not significantly affected by residual stresses due to welding or cold-forming, the stress range can be reduced if part of the cycle is in compression using the following reduction factor:

$$f_m = \frac{\sigma_t + 0.6|\sigma_c|}{\sigma_t + |\sigma_c|}$$

where:

σ_t= maximum tension stress where tension is defined as positive

σ_c = maximum compression stress where compression is defined as negative

fm is 1.0 when the material is in tension during the entire stress cycle, 0.8 when it is subject to zero-mean stress, and 0.0 when it is in compression during the entire stress cycle.

The basic design S-N curve is given as:

$$\log N = \log \bar{a} - m \log \Delta\sigma$$

Where:

N = predicted number of cycles to failure for stress range Δσ

$\Delta\sigma$ = stress range [MPa]

m = negative inverse slope of S-N curve

$\log \bar{a}$ = intercept of the design S-N curve with the log N-axis by S-N curve

The calculation procedure for entry 450 using S-N curve B1 is shown below:

The reduction factor:

$$f_m = 1.0$$

The stress range:

$$\Delta\sigma = \sigma_{max} - \sigma_{min} = 7.705MPa$$

For N ≤ 10^6 cycles, m_1=4 and $\log \bar{a}$ =15.117:

$$\log N = 15.117 - 4 * \log(7.705)$$

$$N = 3.713 * 10^{11} > 10^6$$

For N ≥ 10^6 cycles, m_2 =5 and $\log \bar{a}$ =17.146

$$\log N = 17.146 - 5 * \log(7.705)$$

$$N = 5.15 * 10^{12}\ cycles$$

The fatigue damage under this stress range is:

$$\frac{n_i}{N_i} = 1.51 * 10^{-07}$$

The same procedure is carried out for all the entries in the Markov Matrix. The total fatigue damage can be calculated:

$$D = \sum_{i=1}^{k} \frac{n_i}{N_i} = 0.047 \leq \eta = \frac{1}{DFF}$$

The design fatigue damage :

$$D * DFF = 0.047 * 3 = 0.142 = 14.2\%$$

Circumferential(butt) welds

The critical location for the welds is found in Ansys with maximum stress range as shown in Figure. Maximum and minimum principal stresses are extracted at this node for applied external load and plotted.

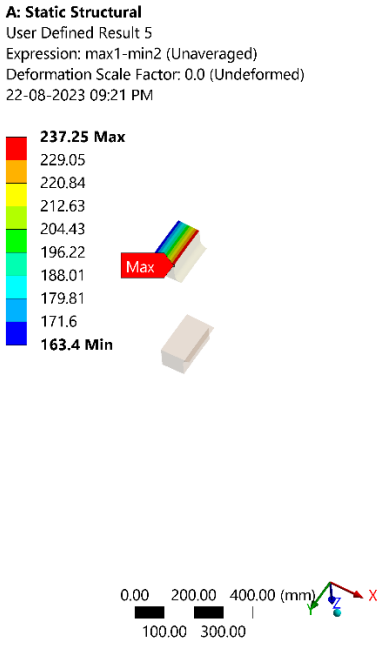

Figure B.3: location of maximum stress range for butt welds

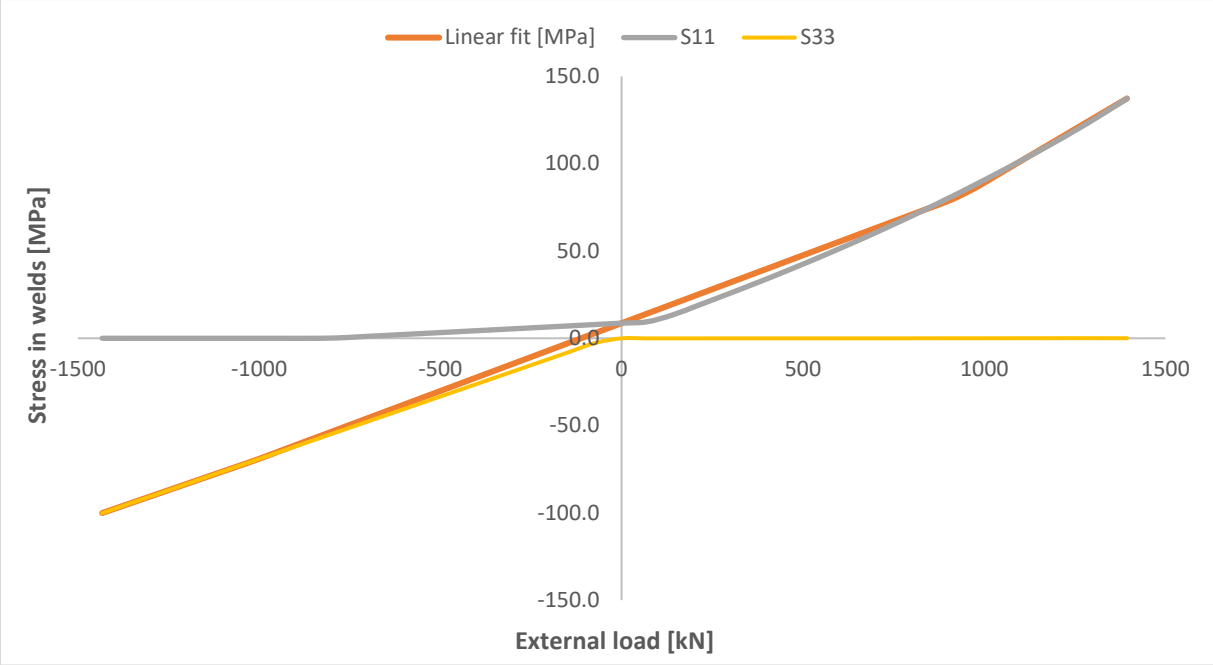

Fit transfer function		
Slope1	0.072	[MPa/kN]
b1	2.4	MPa
Intercept1	-1010.9	kN
Slope2	0.078	[MPa/kN]
b2	8.6	MPa
intercept2	0.122	kN
Slope3	-33.3	[MPa/kN]
b3	-70.5	MPa

Using this fit transfer function, the stress range at every external load in the Markov matrix is calculated.

	F_{max} [kN]	σ_{max} [MPa]	F_{min} [kN]	σ_{min} [MPa]
0	-1309.95	-91.29	-1347.34	-93.97
1	-1238.05	-86.15	-1275.45	-88.82
2	-1166.13	-81.00	-1203.53	-83.68
3	-1094.21	-75.85	-1131.60	-78.53
4	-1022.28	-70.71	-1059.68	-73.38
5	-950.36	-65.19	-987.76	-68.09
…	…	…	…	…
448	1140.98	106.35	804.41	71.15
449	1178.38	110.93	767.01	68.24
450	1063.29	96.84	1025.89	92.27
451	1100.69	101.42	988.50	87.69
452	1135.21	105.65	1097.82	101.07
453	1207.14	114.45	1169.74	109.87

DNV-RP-C203 states that for fatigue analysis of regions in welded structural details which have been subject to post weld heat treatment or where correspondingly low residual stresses

can be documented, the stress ranges may be reduced prior to the fatigue analysis depending on whether part of the stress range is tensile stress or compressive stress. The reduction factor can be derived from the following equation:

$$f_m = \frac{\sigma_t + 0.8|\sigma_c|}{\sigma_t + |\sigma_c|}$$

where:

σ_t= maximum tension stress where tension is defined as positive

σ_c = maximum compression stress where compression is defined as negative

fm is 1.0 when the material is in tension during the entire stress cycle, 0.8 when it is subject to zero-mean stress, and 0.0 when it is in compression during the entire stress cycle.

DNV RP C203 states that the reduction in fatigue strength for surfaces with Ra values larger than 3.2μm can be included in the design analysis by increasing the stress range at the considered hot spot by the following factor:

$$\psi = \frac{1 - 0.28\log\left({}^{R_m}/_{200}\right)}{1 - 0.22\log(6R_a)\log\left({}^{R_m}/_{200}\right)} = 1.085$$

Where:

R_a = 12.8 μm

R_m = 630MPa

The basic design S-N curve is given as:

$$\log N = \log \bar{a} - m \log \Delta\sigma$$

Where:

N = predicted number of cycles to failure for stress range Δσ

$\Delta\sigma$ = stress range [MPa]

m = negative inverse slope of S-N curve

$\log \bar{a}$ = intercept of the design S-N curve with the log N-axis by S-N curve

The calculation procedure for entry 450 using S-N curve C1 is shown below:

The reduction factor:

$$f_m = 1.0$$

The stress range:

$$\Delta\sigma = \sigma_{max} - \sigma_{min} = 4.57MPa$$

For N ≤ 10^6 cycles, m_1=3and $\log \bar{a}$ =12.449:

$$\log N = 12.449 - 3 * \log(4.57)$$

$$N = 10 * 10^{98} > 10^6$$

For N ≥ 10^6 cycles, m_2 =5 and $\log \bar{a}$ =16.081

$$\log N = 16.081 - 5 * \log(7.705)$$

$$N = 1.8 * 10^{12}\ cycles$$

The fatigue damage under this stress range is:

$$\frac{n_i}{N_i} = 4.3 * 10^{-07}$$

The same procedure is carried out for all the entries in the Markov Matrix. The total fatigue damage can be calculated:

$$D = \sum_{i=1}^{k} \frac{n_i}{N_i} = 0.448 \leq \eta = \frac{1}{DFF}$$

The design fatigue damage:

$$D * DFF = 0.448 * 3 = 1.34 = 134\%$$

C1 wedge connection

The minimum and maximum of the force range spectrum is used as the load envelope for FE analysis.

$\max(F_{\max}) = 1640\ kN$ and $\min(F_{min}) = -1686kN$

Lower flange(nominal design)

The critical location for the lower flange is found in Ansys with maximum stress range as shown in Figure. Maximum and minimum principal stresses are extracted at this node for applied external load and plotted. Peak stress in local coordinate system that was generated along the curved path is also plotted.

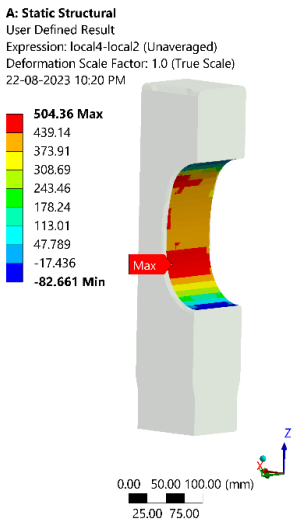

Figure B.4: location of maximum stress range

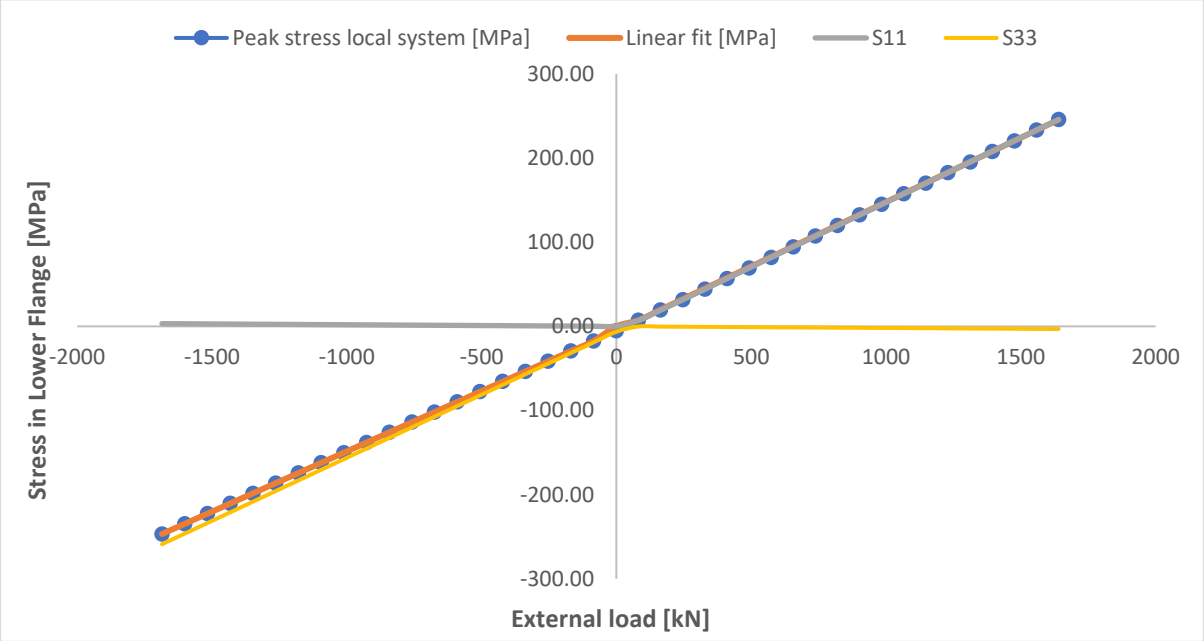

Fit transfer function		
Slope1	0.143	[MPa/kN]
b1	-5.2	MPa
Intercept1	-0.2	kN
Slope2	0.153	[MPa/kN]
b2	-5.2	MPa

Using this fit transfer function, the stress range at every external load in the Markov matrix is calculated.

	F_{max} [kN]	**σ_{max} [MPa]**	**F_{min} [kN]**	**σ_{min} [MPa]**

0	-1541.10	-226.06	-1585.09	-232.37
1	-1456.52	-213.94	-1500.51	-220.25
2	-1371.90	-201.82	-1415.90	-208.12
3	-1287.29	-189.70	-1331.28	-196.00
4	-1202.67	-177.57	-1246.67	-183.88
5	-1118.06	-165.45	-1162.05	-171.75
…	…	…	…	…
448	1342.31	199.99	946.36	139.45
449	1386.32	206.72	902.36	132.72
450	1250.91	186.02	1206.92	179.29
451	1294.91	192.75	1162.92	172.57
452	1335.53	198.96	1291.53	192.23
453	1420.14	211.89	1376.15	205.17

DNV-RP-C203 states that for fatigue analysis of regions in base material not significantly affected by residual stresses due to welding or cold-forming, the stress range can be reduced if part of the cycle is in compression using the following reduction factor:

$$f_m = \frac{\sigma_t + 0.6|\sigma_c|}{\sigma_t + |\sigma_c|}$$

where:

σ_t= maximum tension stress where tension is defined as positive

σ_c = maximum compression stress where compression is defined as negative

fm is 1.0 when the material is in tension during the entire stress cycle, 0.8 when it is subject to zero-mean stress, and 0.0 when it is in compression during the entire stress cycle.

The basic design S-N curve is given as:

$$\log N = \log \bar{a} - m \log \Delta\sigma$$

Where:

N = predicted number of cycles to failure for stress range Δσ

$\Delta\sigma$ = stress range [MPa]

m = negative inverse slope of S-N curve

$\log \bar{a}$ = intercept of the design S-N curve with the log N-axis by S-N curve

The calculation procedure for entry 450 using S-N curve B1 is shown below:

The reduction factor:

$$f_m = 1.0$$

The stress range:

$$\Delta\sigma = \sigma_{max} - \sigma_{min} = 6.73MPa$$

For N ≤ 10^6 cycles, m_1=4and $\log \bar{a}$ =15.117:

$$\log N = 15.117 - 4 * \log(6.73)$$

$$N = 6.39 * 10^{11} > 10^6$$

For N ≥ 10^6 cycles, m_2 =5 and $\log \bar{a}$ =17.146

$$\log N = 17.146 - 5 * \log(6.73)$$

$$N = 1.02 * 10^{13}\ cycles$$

The fatigue damage under this stress range is:

$$\frac{n_i}{N_i} = 7.64 * 10^{-08}$$

The same procedure is carried out for all the entries in the Markov Matrix. The total fatigue damage can be calculated:

$$D = \sum_{i=1}^{k} \frac{n_i}{N_i} = 0.255 \leq \eta = \frac{1}{DFF}$$

The design fatigue damage:

$$D * DFF = 0.255 * 3 = 0.766 = 76.6\%$$

Lower flange(optimized design)

The critical location for the lower flange is found in Ansys with maximum stress range as shown in Figure. Maximum and minimum principal stresses are extracted at this node for applied external load and plotted. Peak stress in local coordinate system that was generated along the curved path is also plotted.

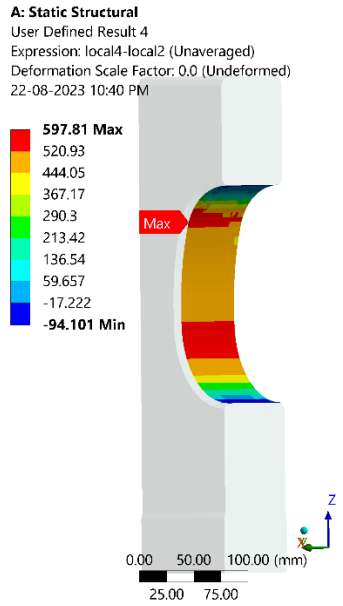

Figure B.5: location of maximum stress range

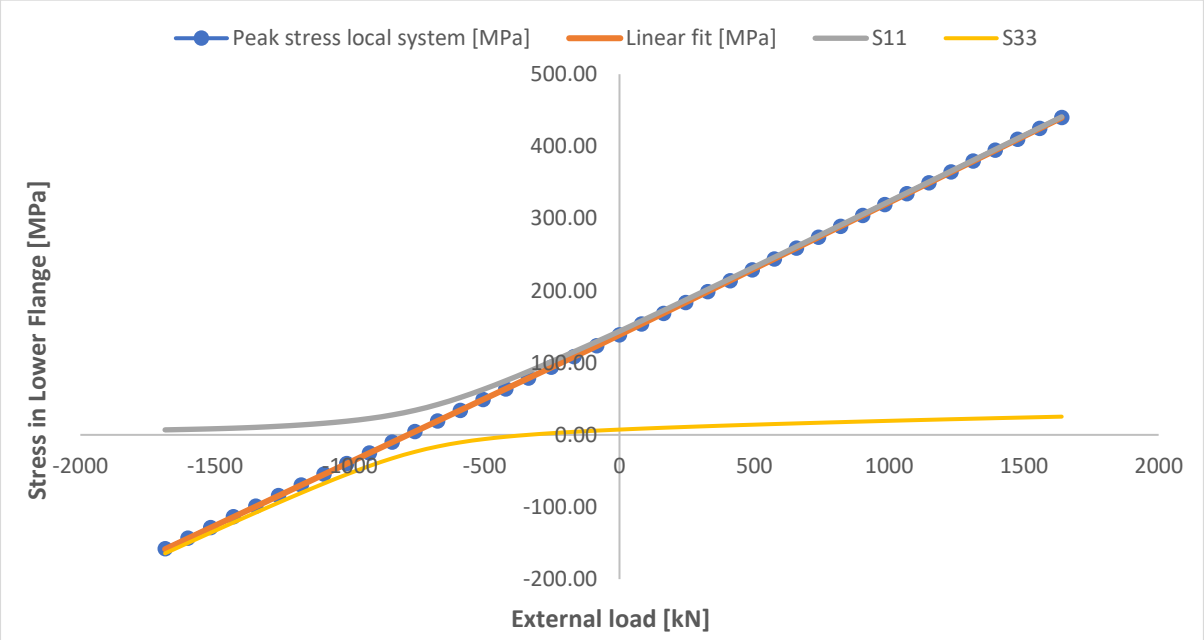

Fit transfer function		
Slope1	0.176	[MPa/kN]
b1	138.0	MPa
Intercept1	-87.0	kN
Slope2	0.184	[MPa/kN]
b2	138.7	MPa
intercept2	2537.7	kN
Slope3	0.184	[MPa/kN]
b3	0.184	MPa

Using this fit transfer function, the stress range at every external load in the Markov matrix is calculated.

	F_{max} [kN]	σ_{max} [MPa]	F_{min} [kN]	σ_{min} [MPa]
0	-1541.10	-133.065	-1585.09	-140.803
1	-1456.52	-118.189	-1500.51	-125.927
2	-1371.90	-103.307	-1415.90	-111.045
3	-1287.29	-88.4247	-1331.28	-96.1626
4	-1202.67	-73.5426	-1246.67	-81.2806
5	-1118.06	-58.6605	-1162.05	-66.3985
…	…	…	…	…
448	1342.31	385.0138	946.36	312.3419
449	1386.32	393.0899	902.36	304.2658
450	1250.91	368.2389	1206.92	360.1641
451	1294.91	376.3137	1162.92	352.0893
452	1335.53	383.7688	1291.53	375.694
453	1420.14	399.2987	1376.15	391.2239

DNV-RP-C203 states that for fatigue analysis of regions in base material not significantly affected by residual stresses due to welding or cold-forming, the stress range can be reduced if part of the cycle is in compression using the following reduction factor:

$$f_m = \frac{\sigma_t + 0.6|\sigma_c|}{\sigma_t + |\sigma_c|}$$

where:

σ_t= maximum tension stress where tension is defined as positive

σ_c = maximum compression stress where compression is defined as negative

fm is 1.0 when the material is in tension during the entire stress cycle, 0.8 when it is subject to zero-mean stress, and 0.0 when it is in compression during the entire stress cycle.

The basic design S-N curve is given as:

$$\log N = \log \bar{a} - m \log \Delta\sigma$$

Where:

N = predicted number of cycles to failure for stress range Δσ

$\Delta\sigma$ = stress range [MPa]

m = negative inverse slope of S-N curve

$\log \bar{a}$ = intercept of the design S-N curve with the log N-axis by S-N curve

The calculation procedure for entry 450 using S-N curve B1 is shown below:

The reduction factor:

$$f_m = 1.0$$

The stress range:

$$\Delta\sigma = \sigma_{max} - \sigma_{min} = 8.07MPa$$

For N ≤ 10^6 cycles, m_1=4and $\log \bar{a}$ =15.117:

$$\log N = 15.117 - 4 * \log(8.07)$$

$$N = 3.08 * 10^{11} > 10^6$$

For N ≥ 10^6 cycles, m_2 =5 and $\log \bar{a}$ =17.146

$$\log N = 17.146 - 5 * \log(8.07)$$

$$N = 4.08 * 10^{12}\ cycles$$

The fatigue damage under this stress range is:

$$\frac{n_i}{N_i} = 1.90 * 10^{-08}$$

The same procedure is carried out for all the entries in the Markov Matrix. The total fatigue damage can be calculated:

$$D = \sum_{i=1}^{k} \frac{n_i}{N_i} = 1.07 \leq \eta = \frac{1}{DFF}$$

The design fatigue damage:

$$D * DFF = 1.07 * 3 = 3.21 = 321.3\%$$

As the fatigue damage is beyond the allowable limits, the optimized design for ULS criteria cannot be provided for a safe design.

Circumferential(butt) welds

The critical location for the welds is found in Ansys with maximum stress range as shown in Figure. Maximum and minimum principal stresses are extracted at this node for applied external load and plotted. Peak stress in local coordinate system that was generated along the curved path is also plotted

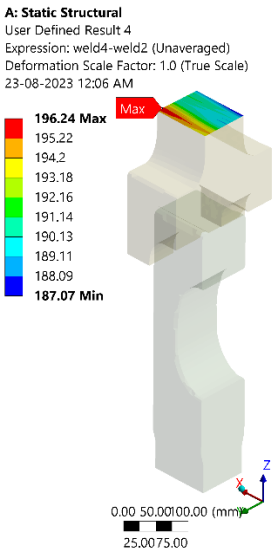

Figure B.6: location for maximum stress range

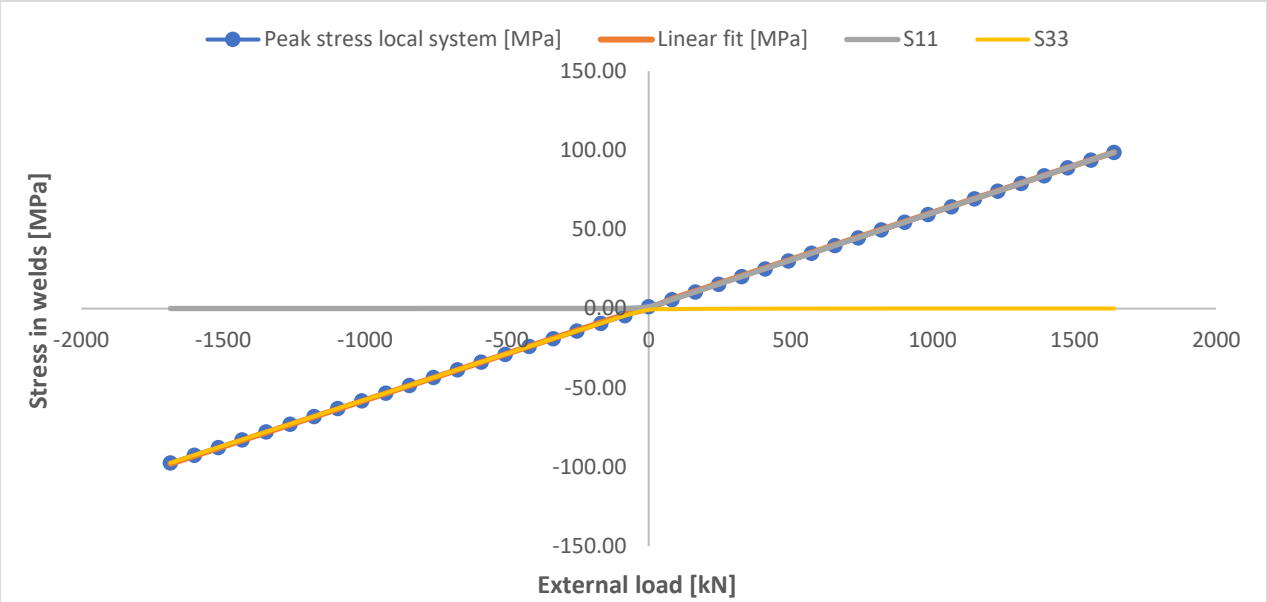

Fit transfer function		
Slope1	0.059	[MPa/kN]
b1	0.7	MPa
Intercept1	-558.5	kN
Slope2	0.059	[MPa/kN]
b2	1.2	MPa

Using this fit transfer function, the stress range at every external load in the Markov matrix is calculated.

	F_{max} [kN]	**σ_{max} [MPa]**	**F_{min} [kN]**	**σ_{min} [MPa]**
0	-1541.10	-89.5506	-1585.09	-92.1272

1	-1456.52	-84.5972	-1500.51	-87.1738
2	-1371.90	-79.6419	-1415.90	-82.2184
3	-1287.29	-74.6865	-1331.28	-77.2631
4	-1202.67	-69.7311	-1246.67	-72.3077
5	-1118.06	-64.7758	-1162.05	-67.3523
…	…	…	…	…
448	1342.31	80.9897	946.36	57.45191
449	1386.32	83.60547	902.36	54.83615
450	1250.91	75.55645	1206.92	72.94109
451	1294.91	78.1718	1162.92	70.32574
452	1335.53	80.58645	1291.53	77.97109
453	1420.14	85.61645	1376.15	83.00109

DNV-RP-C203 states that for fatigue analysis of regions in welded structural details which have been subject to post weld heat treatment or where correspondingly low residual stresses can be documented, the stress ranges may be reduced prior to the fatigue analysis depending on whether part of the stress range is tensile stress or compressive stress. The reduction factor can be derived from the following equation:

$$f_m = \frac{\sigma_t + 0.8|\sigma_c|}{\sigma_t + |\sigma_c|}$$

where:

σ_t= maximum tension stress where tension is defined as positive

σ_c = maximum compression stress where compression is defined as negative

fm is 1.0 when the material is in tension during the entire stress cycle, 0.8 when it is subject to zero-mean stress, and 0.0 when it is in compression during the entire stress cycle.

DNV RP C203 states that the reduction in fatigue strength for surfaces with Ra values larger than 3.2μm can be included in the design analysis by increasing the stress range at the considered hot spot by the following factor:

$$\psi = \frac{1 - 0.28\log\left({R_m}/{200}\right)}{1 - 0.22\log\left(6R_a\right)\log\left({R_m}/{200}\right)} = 1.085$$

Where:

R_a = 12.8 μm

R_m = 630MPa

The basic design S-N curve is given as:

$$\log N = \log \bar{a} - m \log \Delta\sigma$$

Where:

N = predicted number of cycles to failure for stress range Δσ

$\Delta\sigma$ = stress range [MPa]

m = negative inverse slope of S-N curve

$\log \bar{a}$ = intercept of the design S-N curve with the log N-axis by S-N curve

The calculation procedure for entry 450 using S-N curve C1 is shown below:

The reduction factor:

$$f_m = 1.0$$

The stress range:

$$\Delta\sigma = \sigma_{max} - \sigma_{min} = 2.62MPa$$

For N ≤ 10^6 cycles, m_1=3and $\log \bar{a}$ =12.449:

$$\log N = 12.449 - 3 * \log(2.62)$$

$$N = 7.44 * 10^{10} > 10^6$$

For N ≥ 10^6 cycles, m_2 =5 and $\log \bar{a}$ =16.081

$$\log N = 16.081 - 5 * \log(2.62)$$

$$N = 2.83 * 10^{13}\ cycles$$

The fatigue damage under this stress range is:

$$\frac{n_i}{N_i} = 2.74 * 10^{-08}$$

The same procedure is carried out for all the entries in the Markov Matrix. The total fatigue damage can be calculated:

$$D = \sum_{i=1}^{k} \frac{n_i}{N_i} = 0.129 \leq \eta = \frac{1}{DFF}$$

The design fatigue damage:

$$D * DFF = 0.129 * 3 = 0.386 = 38.6\%$$